STUDY OF POCOFOAM AS A HEAT EXCHANGER ELEMENT IN CRYOGENIC APPLICATIONS

A Thesis Presented to
The Academic Faculty

By

Noelle Joy Keltner

In Partial Fulfillment
Of the Requirements for the Degree
Master of Science in Mechanical Engineering

Georgia Institute of Technology

May 2014

STUDY OF POCOFOAM AS A HEAT EXCHANGER ELEMENT IN CRYOGENIC APPLICATIONS

Approved by:

Dr. S. Mostafa Ghiaasiaan, PE, Advisor
School of Mechanical Engineering
Georgia Institute of Technology

Dr. Prateen V. Desai
School of Mechanical Engineering
Georgia Institute of Technology

Dr. Sheldon M. Jeter
School of Mechanical Engineering
Georgia Institute of Technology

Dr. Akif Gurun
Product Service, GE Power & Water
General Electric

ACKNOWLEDGEMENTS

Pursuing a graduate degree in engineering has taught me many things. Beyond the essentials of differential equations and parametric studies, finer skills like time management and knowledge of self have developed.

I'd like to first thank Dr. Mostafa Ghiaasiaan at the Georgia Institute of Technology for working with me as my advisor. The distance study program makes a thesis option degree a challenge, but Dr. Ghiaasiaan helped me work through those challenges. Equally integral in facing the challenges of working as a distance student was Tom Mulcahey at the Georgia Institute of Technology. Finally, I could not have completed my thesis without the participation of my committee members – Doctors Sheldon Jeter and Prateen Desai of the Georgia Institute of Technology, and Dr. Akif Gurun of General Electric.

My managers at General Electric were likewise indispensable. My thanks goes to Edward Reed, formerly of General Electric, for helping me obtain the necessary approval at GE to pursue the graduate program. Appreciation is due also to Matt Jun at GE for his assistance navigating the tuition assistance programs.

Lastly, my acknowledgements would not be complete without thanking my various friends and family who have helped me maintain my sanity throughout my graduate degree. Jill Cassavant, Laura Florez and Kelsey Beach have helped me maintain my cultural balance throughout grad school by attending events all over Atlanta with me. My brother's annual pilgrimage to attend DragonCon with me has also provided invaluable respite. My heartfelt appreciation goes also to Edgar Marin-Ruiz, for encouraging me to go to grad school in the first place, and for all the good times and life lessons we shared together. And thanks to Warren

Wendell, for being generally awesome and accompanying me on many distracting adventures which have always reminded me to get out and enjoy the world around me.

Table of Contents

LIST OF TABLES

LIST OF FIGURES

LIST OF SYMBOLS

A_{foam}	Contact area of cryogenic cooler with foam heat exchanger (m^2)
A_{helix}	Contact area of cryogenic cooler with helical heat exchanger (m^2)
C	Inertial Flow resistance
c_f	Forscheimer's coefficient
c_p	Specific Heat (J/kg-K)
CFD	Computational Fluid Dynamics
D	Viscous flow resistance (m^{-1})
D_e	Equivalent diameter (m)
E	Energy (J)
E_t	Fluid energy (J)
E_s	Solid energy (J)
F	External body forces (N)
F_r	Radial component of force (N)
F_x	Axial component of force (N)
g	Acceleration of gravity (m/s^2)
$\hat{h}$	Local specific enthalpy (J/kg)
h_{in}	Specific enthalpy at inlet (J/kg)
h_{out}	Specific enthalpy at outlet (J/kg)
$h_{coldtip}$	Enthalpy at temperature of cryogenic cooler (J/kg)
I	Identity tensor

k	Thermal conductivity (W/m^2-K)
k_t	Turbulent thermal conductivity (W/m^2-K)
k_{eff}	Effective thermal conductivity (W/m^2-K)
$\hat{k}$	Overall thermal conductivity (W/m^2-K)
$\hat{k}_s$	Solid zone thermal conductivity (W/m^2-K)
$\hat{k}_{eff}$	Effective fluid zone thermal conductivity (W/m^2-K)
l	Length (m)
$\dot{m}$	Mass flow rate (kg/s)
OFHC	Oxygen-free high thermal conductivity
p	Pressure (Pa)
r	Radius (m)
R	Gas constant
Re	Reynolds number
Re_K	Porous Reynolds number
S	Source term
t	Time (s)
T	Temperature (K)
v	Velocity (m/s)
v_r	Radial component of velocity (m/s)
v_x	Axial component of velocity (m/s)
x	Axial spatial coordinate (m)
Greek Symbols	
β	Permeability
ε	Porosity

ε	Heat exchanger effectiveness (%)
ρ	Density (kg/m^3)
μ	Dynamic viscosity (Pa-s)
τ	Stress tensor
ν	Kinematic viscosity (m^2/s)

SUMMARY

Superconductors present great potential for weight reduction and increased power delivery when compared to traditional copper power delivery systems, but current systems require cryogenic cooling systems. Traditional superconductor cooling systems consist of helium cooled by helical heat exchangers made of Oxygen Free High thermal Conductivity (OFHC) copper tube. The helium is cooled by bulky heat exchangers consisting of OFHC copper coils wrapped around a cryogenic cooler heat sink for heat transfer into the working fluid. Metal foams have recently been studied in a variety of heat transfer applications, and could greatly reduce the weight of heat exchanger modules in superconductor cooling systems while simultaneously providing increased heat transfer effectiveness. Aluminum and Copper foams have been available for several years, but more recently, graphite foams, such as PocoFoam™, have been developed which have particularly good heat transfer characteristics. Using Computational Fluid Dynamics (CFD) to model a cryogenic heat exchanger application, this study examines the effectiveness and pressure drop of several metal foam heat exchangers, and compares their performance with the traditional helical coil design for superconductor cooling applications. The CFD simulation results show that a heat exchanger with the same heat sink contact area as existing helical heat exchangers weighs up to 95 percent less and can be up to 25 percent more effective, depending on system conditions such as pressure, cryogenic cooler temperature and helium inlet temperature. Aluminum and copper foam heat exchangers had comparable weight to the PocoFoam heat exchanger, but were significantly less effective than the helical or PocoFoam heat exchanger models.

CHAPTER 1

1.1 Introduction

Cryogenic processes have been significantly developed over the last 50 years and play an increasingly important role in a variety of industries, including production of liquefied natural gas (LNG), rocket propulsion, food processing, metal tempering, biomedical applications, and cooling for superconductors. As these industries begin to rely increasingly on cryogenic fluids, the reduction of costs and improvement in heat exchanger effectiveness associated with cryogenic processes becomes increasingly important.

Cost reduction in cryogenic processes will be intrinsically linked to the efficiency and weight of components in the cryogenic process, particularly heat exchangers. Superconductor research has indicated a large potential weight savings by replacing heavier traditional copper conductors with superconducting materials. However, superconductors require a cryogenic cooling system to maintain conductor integrity. Traditional heat exchangers for superconductor applications rely on contact between a copper cold core and helical copper tubing containing the working fluid wrapped around the cold core, as illustrated in Figure 1. These traditional heat exchangers operate around 70% effectiveness and are bulky [1]. The low effectiveness results in the need for significant power input to the cryogenic cooler system to obtain desired levels of cooling. Since superconductors have potential applications in both small scale electronics applications, such as computer processors as well as large scale projects

like transmission lines, power input and heat exchanger effectiveness are considerable challenges for macro scale applications.

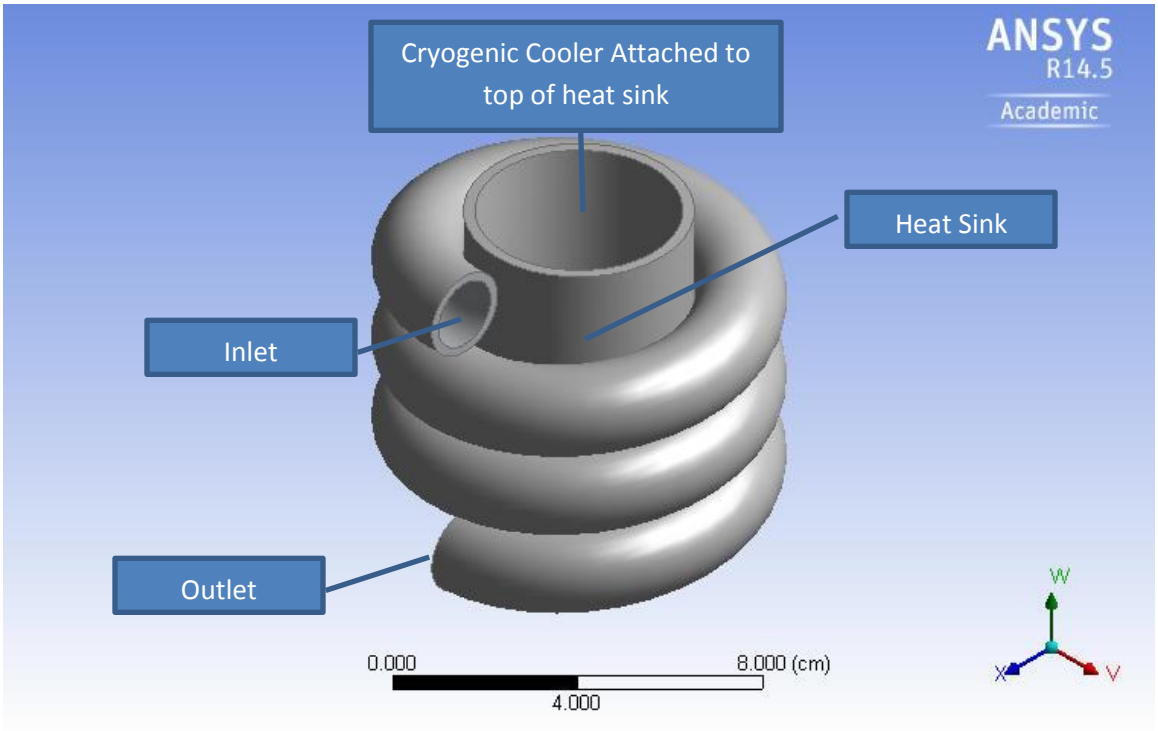

Figure 1: Helical cryogenic cooler

Recent research has examined the application of various low weight metal foams with high heat conductivity in automotive and electronics cooling applications. However, their application in the cryogenic temperature range has not been largely studied. Metal foams may be attractive alternatives for the traditional helical coil heat exchanger in many superconductor cooling applications. Aluminum and copper foams have been widely studied, and more recently, graphite-foams, such as PocoFoam, have shown promise for many heat exchange applications. Graphite based foams have out-of-plane heat conductivities up to ten times greater than aluminum and copper foams, and preliminary research has shown potential for high efficiency heat exchange with

significant reductions in size and weight, as compared to traditional helical coil designs. However, many of the documented properties of graphite and metal foams are valid near ambient conditions, and their cryogenic properties have not been widely studied.

This study examines the potential application of two metal foams and one graphite foam (PocoFoam) as a heat exchanger elements in a superconductor cooling applications. Using ANSYS 14.5, various models were created to study the feasibility of using metal foams in superconductor cooling applications. Two metal foam heat exchangers, one PocoFoam heat exchanger, and one traditional helical heat exchanger were modeled. The geometry of the helical heat exchanger is shown in Figure 1, and a section view of the geometry for the three foam heat exchangers is shown in Figure 2. Each metal foam heat exchanger consisted of a two-centimeter diameter pipe with a cryogenic cooler attached perpendicularly to the system. Adjacent to the cryogenic cooler, a metal foam insert was situated inside the pipe, measuring three centimeters in length. The three models of this configuration differed only in the type of foam used as an insert: aluminum, copper or graphite PocoFoam. Each system was simulated for a variety of inlet and cryogenic cooler temperatures. The effectiveness and pressure drop incurred by each system was then compared. Finally, the weight of the helical system was compared to the weight of the metal foam heat exchanger systems.

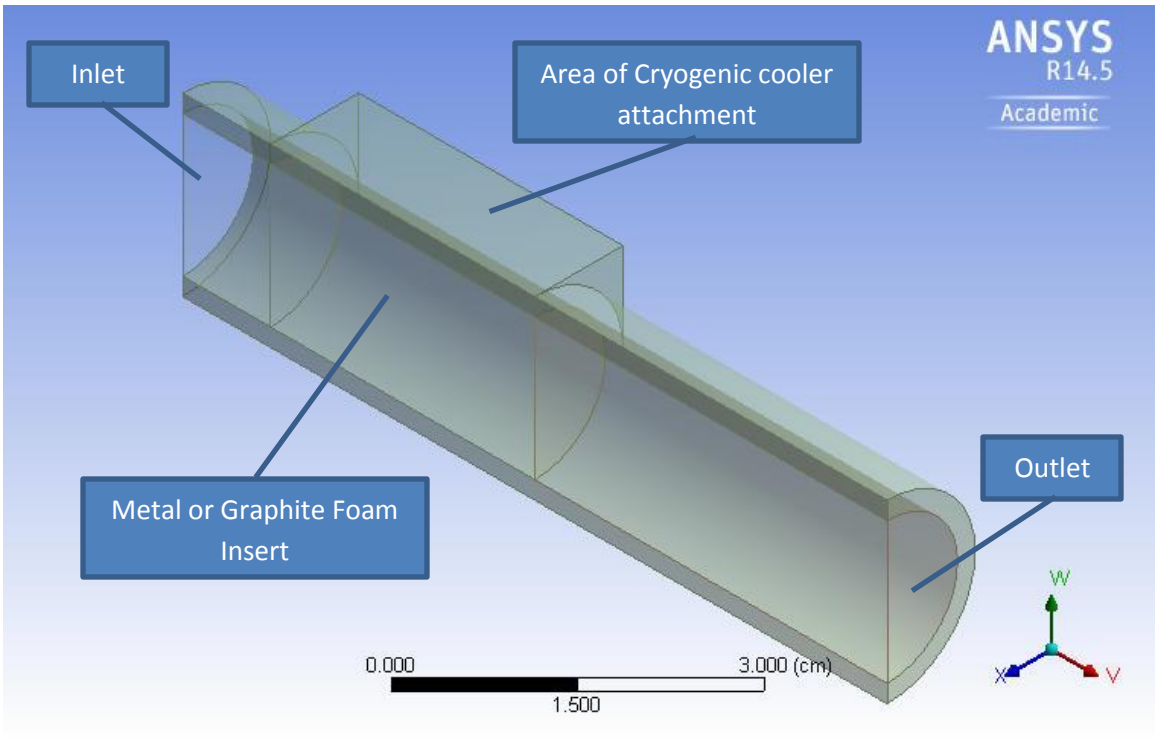

Figure 2: PocoFoam Heat Exchanger Model

1.2 Background

PocoFoam shows exemplary heat transfer characteristics and has recently been studied in a variety of applications. The thermal conductivity of PocoFoam is directional, with 35 W/mK conductivity in plane and 135 W/mK out of plane, which is up to 10 times the thermal conductivity of comparable metal foams [2]. The properties of PocoFoam have been documented, and applications in air and water in several electronics and automotive applications [3] [4] [5] [6]. The application of metal foams in cryogenic applications is largely unstudied.

1.2.1 Properties

Metal foams intrinsically possess characteristics that are challenging to define and consistently model. Pore diameter, specific surface area, density, and even height of a sample during the manufacturing process can each lead to subtle variations in metal foam properties. Several researchers have studied these parameters in attempts to better understand and classify various metal foams.

Foams can be characterized by many properties, including relative density and specific surface area [7]. Relative density is defined as the ratio of foam density to the density of a solid sample of the parent material [8]. Effective thermal conductivity of a foam is dependent on its relative density, conductivity of the base material, and the geometry of the conductive pathways through the porous material [9] [10]. The relative conductivity of a foam can be classified as a function of its relative density and the base metal conductivity.

In addition to describing key characteristics, Han et al. observed that foams with high relative density have higher thermal conductivities, but poor convective heat transfer. Foams that are more ‘open’ are better for convective heat transfer and reduced pressure drop but have lower thermal conductivity, so a balance must be found based on design needs [7].

The method for mechanical contact between a metal foam and intended heat transfer surface has also been found to have an impact on effectiveness and longevity of the heat exchanger. Epoxy, simple mechanical contact, medium and high temperature brazing, wire-arc spray coating and vacuum furnace brazing are among the methods that have been studied to obtain thermal contact between foams and their surrounding materials. Some methods are more effective than others. Howard and Korinko

examined several high temperature brazing methods on porous foams, but found such brazes to lead to excessive creep damage and corrosion in various metal foams. Their best mechanical interfaces are achieved with moderate temperature brazes [11]. Wire-arc spray coating methods have been shown to result in a thin layer of metal covering the top of the foam, proving good contact with the foam [12]. Epoxy bonds, even when using epoxy with high thermal conductivity, results in decreased thermal performance when compared with brazing methods of mechanical contact [13].

Little research has been done to assess the impact of fouling on foam heat exchangers. Pressure drop is inherently a concern even in clean heat exchangers, and fouling may decrease system performance and increase the pressure required to pass a working fluid through a metal foam heat exchanger [7]. Some researchers have proposed the use of channels, holes, gaps, or finned structures in the foam material to reduce pressure drop [14] [15] [16]. Others have examined parallel flow applications where the cooling fluid does not significantly penetrate the foam but rather skims its surface as a means of reducing the power required to achieve convective heat transfer in metal foam system [17] [18].

Characterization of the surface area of foams presents another challenge. Some researchers have used optical microscopy combined with image processing software algorithms to estimate the surface area of a foam, but these techniques can lead to large uncertainties. Since the effective surface area is critical for the calculation of other parameters, such as the Nusselt number, much of the existing research shows a large variation in experimental flow characteristic data. Current manufacturing processes are not optimized to allow the level of control over foam porosity and surface area that would allow the mechanical characteristics of a foam, such as Nusselt number, to be calculated in advance [19].

Because of the difficulty presented in measuring the surface area of a foam, some researchers have instead tried to take a numerical modeling approach to characterizing flow parameters. Several studies have been published using different geometric models for foams (cubic, dodecahedron, interconnected hexagonal cells, and others) to predict parameters such as pressure drop [20] [21] [22], effective thermal conductivity [20] [23] [24] [10], heat transfer rate [25] [26], or foam mechanical properties [27]. Further research in this area may lead to advances that could allow the geometry of the foam to be optimized [7].

Singh and Kasana developed a resistor model for predicting effective thermal conductivity of porous metal foams based on available experimental data. Experimental data from aluminum and reticulated vitreous carbon (RVC) foam samples was used. Both air and water were used in different experiments. They developed a resistor model that strongly correlated thermal conductivity to porosity and the ratio of thermal conductivity of the constituents [28].

Straatman et al [29] investigated the effect of porosity and pore diameter on the Nusselt number and Reynolds number for PocoFoam. Their research involved impinging a flow of water across a block of PocoFoam material at a variety of velocities to determine its flow characteristics. The procedure was repeated with two other commercially available metal foam blocks to generate a comparison of the characteristics of each material. The Nusselt and Reynolds numbers for each foam were determined experimentally using the heat transfer and flow measurements from the experimental set-up, and the importance of geometry in the determination of these figures was discussed. Of the materials compared, PocoFoam had nearly twice the out-of-plane thermal conductivity and a

comparable porosity and effective area. PocoFoam had a slightly lower pressure drop than the other materials, similar thermal resistance, and similar Nusselt and Reynolds numbers.

Lin noted that graphite foams possess high thermal conductivity, low density and high specific surface area [5]. However, thermal conductivity is directional, and pressure drop can be high. High pressure drops lead to large pumping power to push a cooling media through the foam, leading to a low coefficient of performance (COP – ratio of removed heat to input pumping power). Due to directionality and pressure drop, the configuration of a foam is very important.

Graphite foams often have inferior mechanical properties, such as tensile strength, when compared to metal foams. Mixing graphite foams with epoxy resins can significantly improve the mechanical properties, but at the expense of thermal properties [5].

1.2.2 Applications

Straatman et al studied heat transfer from a heated surface bonded to a flat layer of PocoFoam cooled by a parallel flow of air [17]. Gravity affects the foaming process, resulting in a porosity gradient when foams are formed. Straatman's experiments attempted to characterize the difference in performance of foams from the top, bottom and middle of a given foam lot. This experiment also attempted to determine the optimal thickness of a foam for parallel flow by starting with a sample 10 mm thick, then gradually reducing thickness to evaluate the resultant changes in performance.

Since the foam provides a rough surface, turbulent flow exists even at relatively low Reynolds numbers (Re>200,000), where Re is the standard, rather than porous, Reynolds number for air flow across a sample of foam. Foam thicknesses of 10, 5, 3, and 1 mm were tested for airflows between 3 and 10 meters per second and heat flux ranges of 20 to 70 W/m^2. Among the thicknesses studied, 3 millimeters was found optimal, as the 5 and 10 millimeter samples showed negligible improvement in heat transfer. The results suggest that the foam temperature is effectively the same temperature as the base material, and that the penetration of air into the foam is relatively small for parallel flow. Data also showed that heat transfer enhancements were greater at lower air flow speeds and decreased as air velocity increased.

Straatman et al [17] explain the difference in heat transfer effectiveness with respect to air speed as a function of eddies of flow that develop at the surface of the foam. At lower velocities, the eddies have lower momentum, but a significant amount of air flow penetrates the foam as opposed to flowing across the foam. At higher air velocities, the eddies have more energy, but the amount of air penetrating the foam is smaller compared to the amount of air flowing across the foam.

Foams with larger pore diameter have rougher surface areas and therefore better heat transfer enhancements for the parallel flow applications that Straatman studied. The rough surface area facilitated air penetration into the foam. For parallel flow, foam “openness” must be balanced to obtain the optimum mix of heat conduction and convective resistance.

Using weight reduction in motherboard heat sink applications as motivation, Kuang examined Cu foam heat exchangers with axial cooling flow provided by a fan [30]. Their research found that foam height must be optimized to find the best balance of heat

transfer surface area with cooling flow resistance. They were able to replace a traditional heat sink with a copper foam with one-tenth the weight of traditional alternative heat sinks, and had half the volume for the same cooling area flow.

Lin et al characterized heat transfer properties of both solid and corrugated PocoFoam blocks of two profiles: 1x1x5 centimeters and 1x5x5 centimeters, as illustrated in Figures 3 and 4 [31]. Air was introduced into a 1x5 centimeter face in all cases. For the 1x5x5 blocks, heat transfer was comparable between solid and corrugated blocks at the same air flow speed, but the pressure drop for the corrugated block was significantly lower as air speed increased. The 1x5x5 corrugated block achieved over 500 W/m^{2}K at 1m/s air flow with about 0.5kPa pressure drop. The 1x1x5 corrugated block achieved over 1300 W/m^{2}K heat transfer at 1m/s air flow with about 0.3 kPa pressure drop.

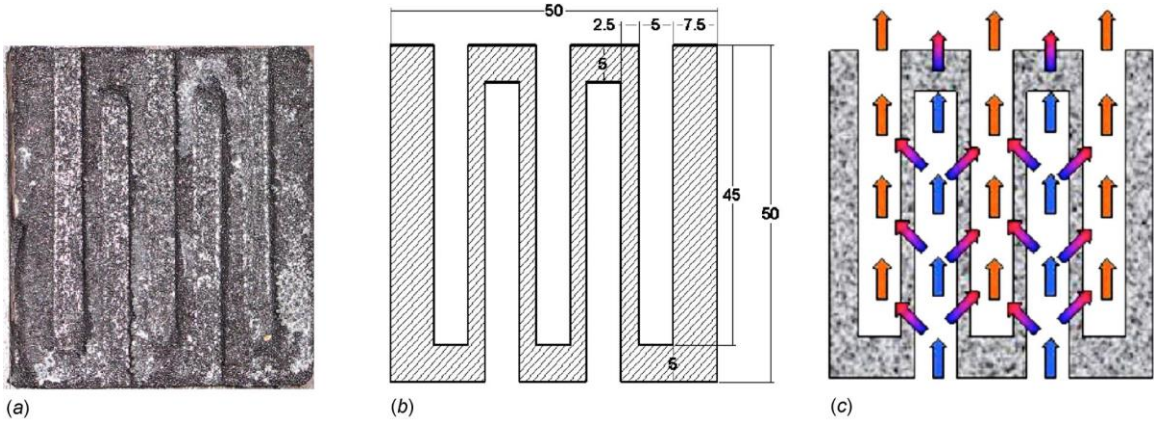

Figure 3: Corrugated PocoFoam block measuring 1x1x5 cm studied by Lin et. al. [31]

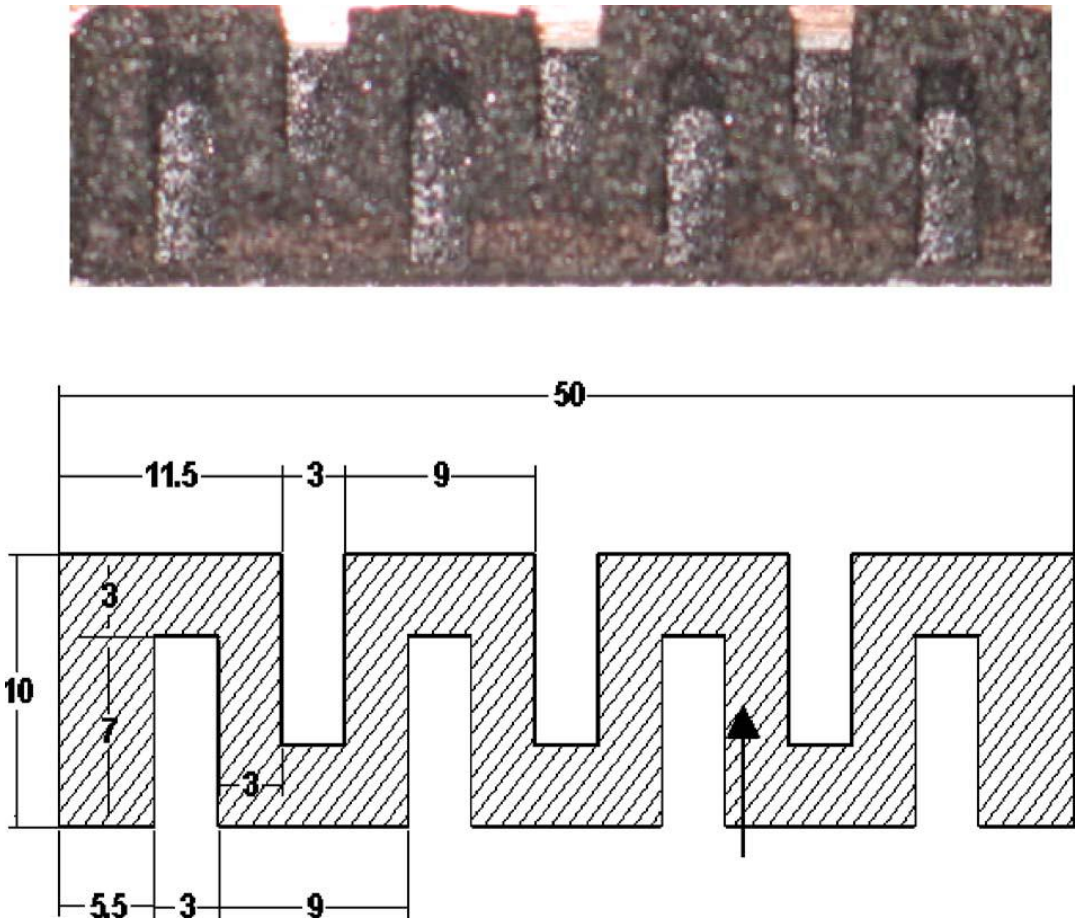

Figure 4: Corrugated PocoFoam block measuring 1x1x5 cm as studied by Lin et. al. [31]

Lin designed a heat exchanger using two parallel paths of four foam blocks each. Each foam block had a profile of 1x1.7x1 cm. The corrugated block configuration was found to have one-fifth the pressure drop of solid blocks in the same configuration and better heat transfer performance. The four-block configuration reached a heat transfer effectiveness of 0.85 with 0.25 m/s flow. The effectiveness decreased as flow rate increased.

The work of Lin et al. [31] illustrates that heat transfer surface area must be balanced with pressure drop, and also illustrates the inverse relationship between flow rate on heat transfer effectiveness. Although heat transfer improved as air flow increased in

single-block applications, the author found that heat transfer effectiveness decreased with increasing air flow for the 4-block arrangement.

Motivated by electronics cooling applications, Haskell examined PocoFoam heat sink applications with perpendicular flow [6]. Foam heat sinks of different materials were soldered to aluminum or copper carrier plates to examine heat transfer characteristics. Haskell compared thermal performance of geometrically identical heat sinks of different materials. The heat sink materials compared in this study were aluminum, copper, and two types of graphite foams.

The carrier plate was clamped to a heat source. Haskell's experiments suggest that lower thermal conductivity foams exhibit reduced thermal performance and high flow velocities when compared to traditional aluminum and copper heat sinks. Haskell's results indicate that foam heat exchangers are best suited for lower flow applications.

Recent research has investigated the use of materials with a high latent heat of melting as heat dissipation devices for electronics applications. Graphite foams infiltrated with paraffin have recently been studied [32]. Paraffin infiltration of over 92% of the open volume of graphite foams was achieved. The thermal diffusivities of the composite wax/graphite structure was greatly improved over paraffin alone. Characteristics of the composite depended on cell sizes, foam structure, and thermal conductivity of the foam [3].

Elayiaraja et. Al. studied the heat transfer characteristics of a copper metal foam used as a heat sink in an electronic cooling application. The performance of a copper foam heat sink was compared with that of a typical aluminum heat sink, and the pressure drop across the foam was measured to experimentally determine the permeability of the

copper foam. This study showed that the copper foam heat sink performed 35-40% better than the aluminum block heat sink [33].

Sertkaya, Altinisik, and Dincer experimentally compared the performance of an aluminum finned heat exchanger with an aluminum foam heat exchanger. Their study evaluated finned heat exchangers with three different fin spacings, and three foam heat exchangers each with a different number of pores per inch (PPI). The foam heat exchangers consisted of aluminum foam on the exterior of the heat exchanger tubes in place of aluminum fins. Each design was submitted to air flow of 0.5 to 7 m/s. In all cases studied, the aluminum foam heat exchangers were less effective, and had higher pressure drops. The most effective fin heat exchanger was nearly 25% more effective than the most effective aluminum foam heat exchanger [34]. Their results indicate that metal foams are not always the best choice of heat exchanger material, and the application parameters should be considered against prior experiments to determine if a metal foam will be a suitable heat exchanging material.

Garrity, Klausner, and Mei studied the performance of an aluminum louvered fin heat exchanger against the performance of similar heat exchangers where the louvered fins were replaced with either aluminum or graphite foams. For each foam, three different PPI foams were studied. In this study, the 10 PPI aluminum foam had the highest volumetric heat transfer coefficient and the lowest pressure drop of all the foams studied. The graphite foam heat exchangers removed more heat per unit volume, but had much higher system pressure drops. The best coefficient of performance (COP) and power density were obtained by the louvered fin model, leading the authors to conclude that in this application, foams provide advantages if heat exchanger volume is a driving factor, but the louvered fin model was better when weight or COP were more important design factors [4].

Klett and Conway studied a graphite foam in both electronics cooling and automotive cooling applications. In the electronics heat sink application, a heater was used to simulate the heat load of a commercially available computer processor. Using a finned foam heat sink in place of the commercially available aluminum finned heat sink, the steady state temperature of the heater was 3 degrees cooler. The finned foam heat sink weighed over 80% less than the aluminum heat sink. The automotive application studied demonstrated that graphite foam could increase the heat transfer coefficient and reduce system weight, but would incur large pressure drops, leading the Klett and Conway to conclude that graphite foams should not be used as direct substitutes for existing heat exchanger elements, but rather should be designed to take advantage of their unique structure and heat transfer properties [35].

Mancin et. Al. considered copper forms with 5, 10, 20, and 40 PPI in a forced convection application with mass flow rates that varied between 0.0055 kg/s to 0.0125 kg/s. Two 10 PPI samples with different relative densities were studied, where relative density is defined as the density of the foam with respect to the density of the base material. These experiments indicated that pressure drop increases with the pore density of the foam sample. The best heat transfer coefficient was obtained with the 5 PPI copper foam sample, and heat transfer coefficient decreased as PPI increased [36].

Lu, Zhao and Tassou studied metal foam filled pipes as heat exchangers. Using numerical analysis, their study examined the heat transfer characteristics of pipes filled with copper and steel alloy foams of different porosities and pore sizes (PPI). Compared to heat transfer in a pipe without foam, heat transfer could be enhanced up to 40 times, but with significant pressure drop [37].

Aluminum and copper foams were studied in a convective heat transfer application with vertical airflow by Kamath, Balaji, and Venkateshan. In their experiments, the heat transfer coefficient increased as inlet air velocity increased, and the metal foams increased heat transfer by a factor of 2.6 to 3.8 when compared to open channel air flow. Kamath et. al. found that the performance of the copper foam was 4% greater than the aluminum foam [38].

Zhao et. al. considered a concentric tube heat exchanger using metal foam as a heat exchange element as shown in Figure 5. The study showed that heat transfer capacity increased as the pore density or porosity increased. Zhao et. al. also found that the amount of heat transfer was a function of the ratio of flow cross sectional areas [39].

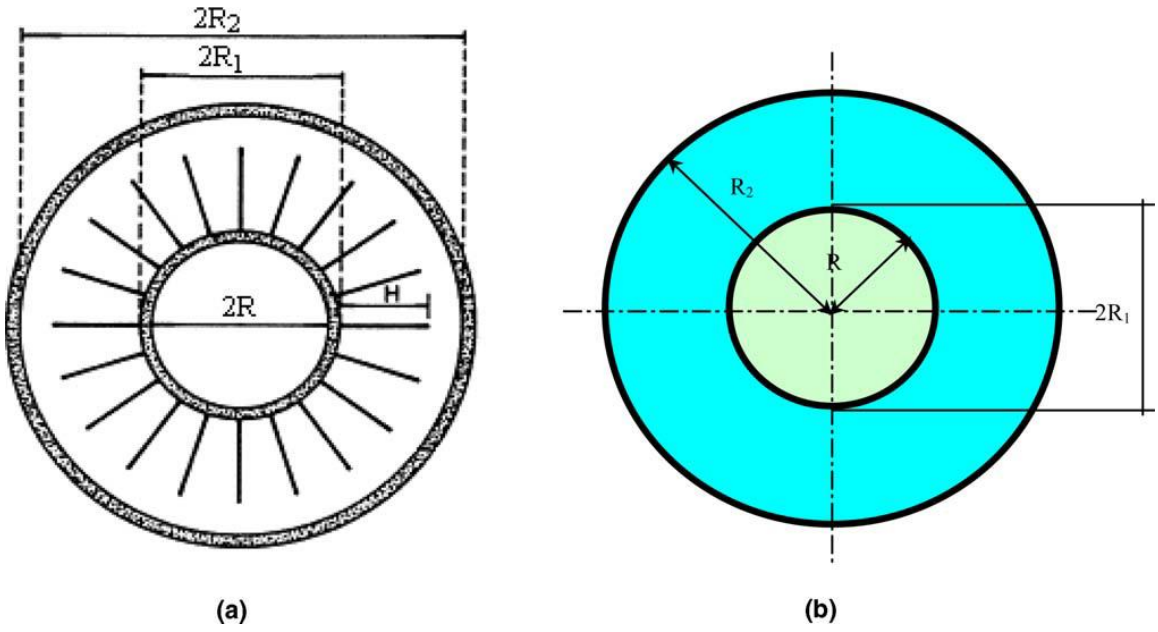

Figure 5: Geometry of (a) conventional finned tube heat exchanger and (b) metal foam heat exchanger studied by Zhao et. al. [39]

The applications examined in the above studies all involved heat transfer at or above ambient conditions. Cryogenic applications, such as those studied in the present study, present many unique challenges. Heat exchangers can represent a large amount of the investment costs for some processes including LNG plants and cryogenics. When heat exchanger performance is low, the power input for the process must be increased to support the process. Traditional heat exchanger models assume constant fluid properties. For high efficiency heat exchangers used in cryogenics, additional effects need to be considered – including changes in fluid properties, heat exchange with the surroundings, and flow maldistribution caused by fouling, poor fabrication tolerances, and changes in fluid properties such as viscosity or density [40].

Lumped parameter models assume no heat transfer with surroundings, negligible longitudinal heat conduction, constant heat transfer coefficients, and constant heat capacity. These assumptions are often not valid in cryogenic applications due to large temperature differences between the working fluid and the environment, and operation near the critical point for the working fluid.

1.3 Review of Patents

The Georgia Tech Research Corporation (GTRC) holds a patent utilizing a porous heat exchange element and force augmentation device to realize effective heat exchange in an automotive application [3]. In this application, the high pressure drop across the porous region was leveraged to improve aerodynamic stability of the vehicle. Also, given the high surface area and effectiveness of porous materials, efficient heat transfer

was obtained even at low or zero velocity, which could reduce or eliminate the need to induce a forced flow across the heat exchanger and pull engine load in the process.

A patent for graphite foams and production methods is held by Philip Theriault [41]. Previous processes for creating graphite foams involved manipulating the temperature of a mixture of inert gas and pitch material in order to convert it to graphite, then changing the pressure in the system to cause bubbles to form. This method would yield pore sizes greater than 10 microns. In order to form a foam with pore sizes less than 10 microns that would also have enough mechanical strength to allow machining, a new process was developed.

The patented graphite foam fabrication process involves mixing curled graphite fibers. The curl is believed to contribute to the mechanical strength of the material. A graphite forming resin or pitch is added, and the mixture is compressed to reduce volume and increase strength of the material. Heat is applied to cause the mixture to carbonize, but no temperature or pressure adjustments are required to form the foam structure, as in other foam production methods. This structure of this foam is formed during the process of mixing carbon fibers with resin and compressing the mixture. The foam is then subjected to a second heating process to induce graphitization.

As a result of the method described above, a graphite foam is created in which the fibers are around 25-250 microns in diameter, have an ordered molecular structure, and a porosity of 95-98%.

CHAPTER 2

2.1 Motivation and Problem Definition

In this study, the existing literature was used as a foundation for further study of metal foams as heat exchanger elements in cryogenics applications, motivated by superconductor cooling applications. Traditional superconductor cooling applications consist of a conductor contained within a helium cooled conduit. Helium is periodically cooled by a helical coil heat exchanger as seen in Figure 6, which consists of a cryogenic cooler surrounded by several turns of copper pipe. Helium gas is circulated through the copper pipe and acts as the coolant for the system. The geometry of the helical model created for this study is shown in Figure 1. For computational simplicity, the heat sink to which the cryogenic cooler would be mounted was modeled as a thin cylinder to reduce the number of nodes and thus computational time. In a real system, this cylinder would be solid. When weight comparisons are made in the results chapter, the cylinder weight will be calculated assuming the heat sink is a solid cylinder.

The proposed metal foam heat exchanger system would replace the helical cryogenic cooler with a metal foam heat exchanger. Several metal foams have been developed in recent years. This project will compare the effectiveness and pressure drop for graphite foam, aluminum foam and copper foam, and compare the performance of these systems with the traditional helical heat exchanger. Helium was chosen as the working fluid based on its use in traditional superconductor cooling system. It has excellent heat transfer characteristics, is electrically inert, and disperses readily in air, minimizing risks in the event of a system rupture.

A foam heat exchanger was modeled in ANSYS Fluent consisting of a half pipe symmetric geometry with a foam insert in the helium flow path. The pipe is made of OFHC (Oxygen Free High thermal Conductivity) copper and measures two centimeters in diameter, with a 2 mm wall thickness. The inlet region is one centimeter in length and leads into a three centimeter length foam insert, followed by a 4 cm long exit region. A cryogenic cooler tip is situated above the foam region, with a contact region that mates exactly with one-half of the pipe geometry and measures three centimeters long. The half-pipe geometry was chosen to reduce nodes and computation time required to obtain a convergent solution.

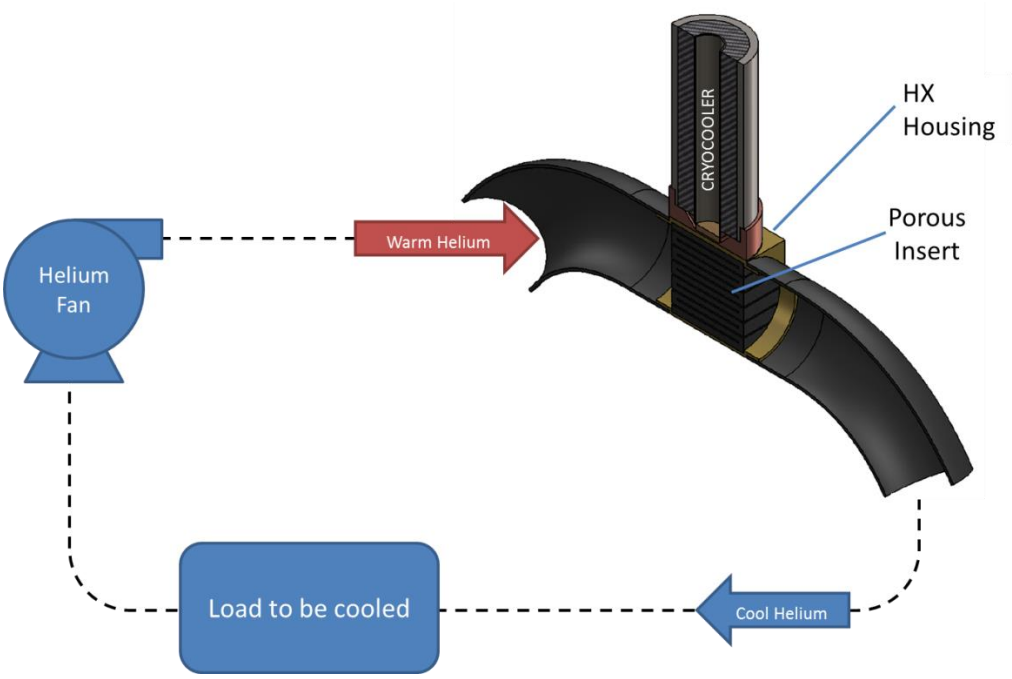

Figure 6: Proposed Superconductor Cooling System Arrangement [1]

Graphite foam has recently been studied in a variety of ambient and elevated temperature applications, but there are not many published studies on its application in

cryogenic ranges. Aluminum and copper foams have also been studied in a variety of heat exchanger applications, but their results have not been compared to graphite foam performance. In this study, the same metal foam model will be used to study each of these foams. The same inlet temperature, cryogenic cooler temperature, mass flow rate, and system pressures will be examined for each foam. The same FLUENT model was used for each foam, differing only in the properties of the foam.

2.2 Materials and Boundary Conditions

The pipe walls and cryogenic cooler application tip were modeled as OFHC copper, and the characteristics published by NIST [42] were input into the Fluent model. Thermal conductivity and heat capacity for OFHC copper are highly temperature dependent in the cryogenic range considered in this study. The equations below govern the specific heat and thermal conductivity of OFHC copper at cryogenic ranges. The thermal conductivity values for RRR=50 were used from the NIST publication. For simplicity, these equations were used to obtain seven discrete points over the temperature range considered in the study, and a seven-point piecewise linear representation of these properties was entered into the material definition parameters in Fluent. The exact values used in this study are shown in Table 2 below.

$$\log(k) = \frac{\left(a + cT^{0.5} + gT^{1.5} + iT^{2}\right)}{\left(dT^{0.5} + dT + fT^{1.5} + hT^{2} + 1\right)} \quad (1)$$

Where k is thermal conductivity, T is temperature in Kelvin, and a, b, c, d, f, g, h, and i are constants.

$$C_p = 10^{a+b\log(T)+c(\log(T))^2+d\log(T)^3+e\log(T)^4+f\log(T)^5+g\log(T)^6+h\log(T)^7+i\log(T)^8} \quad (2)$$

Where C_p is specific heat, T is temperature in Kelvin, and a, b, c, d, e, f, g, h and i are constants. The values for the constants used in Equations 1 and 2 above are shown in Table 1.

The aluminum foam studied in this application is made from a base material of 6061-T6 Aluminum. NIST publishes values for thermal conductivity and specific heat of 6061 aluminum at cryogenic temperatures using the same equations (1 and 2) listed above, but using different constants. The constants used to calculate thermal conductivity and specific heat for 6061 are listed in Table 1 below.

Table 1: Coefficients for OFHC Copper and 6061-T6 Aluminum for Equations 1 and 2 [42] [43]

	OFHC Copper		6061-T6 Aluminum	
	k	C_p	k	C_p
a	1.8743	-1.91844	0.07918	46.6467
b	-0.41538	-0.15973	1.0957	-314.292
c	-0.6018	8.61013	-0.07277	866.662
d	0.13294	-18.996	0.08084	-1298.3
e	0.26426	21.9661	0.02803	1162.27
f	-0.0219	-12.7328	-0.09464	-637.795
g	-0.051276	3.54322	0.04179	210.351
h	0.0014871	-0.3797	-0.00571	-38.3094
i	0.003723	0	0	2.96344

Table 2: Properties for OFHC Copper Used in CFD Model

	10K	20K	30K	50K	70K	90K	100K
Specific Heat [J/kg-K]	0.099	7.506	26.474	96.269	135.879	205.1	255.3
Thermal Conductivity [W/mK]	320.4	1368	1444.4	863.56	670.02	500.3	443.9
Density [kg/m^3]				8941			

Table 3: Properties for 6061-T6 Aluminum used in CFD model

	10K	20K	30K	50K	70K	90K	100K
Specific Heat [J/kg-K]	14.204	28.428	41.098	62.048	78.548	91.914	97.701
Thermal Conductivity [W/mK]	1.573	8.854	33.445	18.838	298.295	433.334	492.198
Density [kg/m^3]				2700			

The values in Table 2 above were used for both the material properties of the pipe, but also for the copper foam. For porous regions, ANSYS Fluent modifies the density and thermal conductivity to account for porosity using the Equations 3 and 4 below.

$$\hat{k} = \varepsilon \hat{k}_f + (1-\varepsilon)\hat{k}_s \quad (3)$$

Equations 3 represents the effective thermal conductivity of a porous region, where ε is the porosity of the medium, $\hat{k}_s$ is the solid medium thermal conductivity, and $\hat{k}_f$ is the fluid thermal conductivity.

$$\hat{\rho} = \varepsilon \hat{\rho}_f + (1-\varepsilon)\hat{\rho}_s \quad (4)$$

Equation 4 details the calculation for effective density of a porous region, where ε is the porosity of the medium, $\hat{\rho}_s$ is the density of the solid medium, and $\hat{\rho}_f$ is the density of the fluid.

The ANSYS Fluent package is equipped to simulate porous regions in fluid flow using viscous and internal resistance values. In order to represent aluminum, copper and Poco foams properly in the CFD model, porosity, flow resistance, thermal conductivity, density and heat capacity had to be entered for each material.

For PocoFoam, density, heat capacity and thermal conductivity valid at ambient conditions have been published by PocoGraphite [2]. The literature surveyed for this study made no reference to dependency of these properties on temperature, and no data on thermal characteristics at cryogenic temperature ranges is available. Since ANSYS Fluent scales thermal conductivity based on porosity, as indicated in Equation 3, the published thermal conductivity and porosity were used to back-calculate an equivalent bulk material thermal conductivity. This value is reflected in Table 4 below.

Viscous and inertial resistance values for PocoFoam were not readily available in the literature. For each foam, permeability and Forcheimer coefficients are available in the published literature. Permeability, porosity, and the Forcheimer coefficient can be used in combination with the Ergun equations to calculate values for viscous and inertial flow resistance

The viscous resistance (detailed in **Error! Reference source not found.**) and inertial esistance (as calculated by **Error! Reference source not found.**) were calculated using published values for porosity and average pore diameter.

$$D = \frac{\varepsilon}{\beta} \tag{5}$$

$$C = \frac{2\varepsilon^2 c_f}{\sqrt{\beta}} \tag{6}$$

where β is the calculated permeability, ε is the porosity, and c_f is Forchheimer's inertial coefficient.

Aluminum and Copper foams are often compressed to maximize their effectiveness in heat transfer applications. Boomsma [24] documented the flow characteristics of 6061-T6 aluminum, and how compression affected the flow characteristics. Boomsma's reported for 95 percent porosity aluminum foam compressed by a factor of 6 were used to calculate the permeability and viscous resistance shown in Table 4. Since both 6061-T6 aluminum foam and OFHC copper foam are manufactured by ERG [44] [45], it was assumed that their flow characteristics would be similar. In the ANSYS model, the same flow characteristics were used for both foams, and only the thermal characteristics and density differed.

Table 4: Metal Foam Material Properties Used in CFD Analysis

Property	Poco Foam	Aluminum Foam	Copper Foam
Permeability [m^2]	$6.13x10^{-10}$ [29]	$2.48x10^{-10}$ *	$2.48x10^{-10}$
Forcheimer coefficient	$4.46x10^{-1}$ [29]		
Viscous Resistance [$1/m^2$]	$1.34x10^{9}$**	$2.44x10^{9}$ *	$2.44x10^{9}$
Inertial resistance [1/m]	$2.42x10^{4}$**	8701 [24]	8701
Porosity	0.82 [29]	0.60 [24]	0.60

*calculated from values reported by Boomsma [24]

**calculated from values reported by Poco Graphite, Inc. [2]

The working fluid used in the heat exchanger simulation was helium and the NIST real gas model was enabled in Fluent to ensure proper helium properties were referenced for the flow calculations [46]. Inlet mass flow rates were specified such that flows would remain in the laminar range.

2.3 Mesh Dependency Study

The first step in the study was to set up a mesh and obtain mesh independence to ensure solution results were not affected by mesh resolution. In order to ensure proper calculation of heat transfer between the pipe wall and the fluid within, the fluid and solid domains were modeled as a multi-component part. The fluid region was meshed with a few layers of inflation to obtain better results at the interface between the wall and fluid.

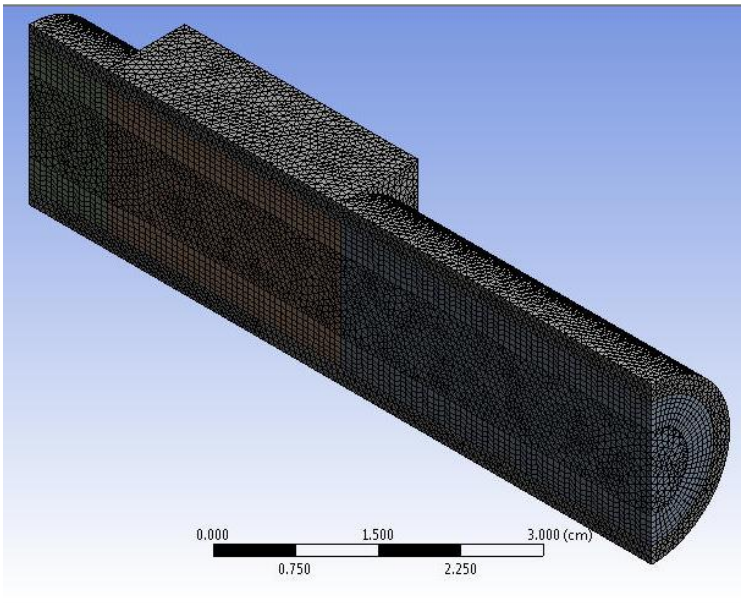

Figure 7: Mesh 5 Isometric View

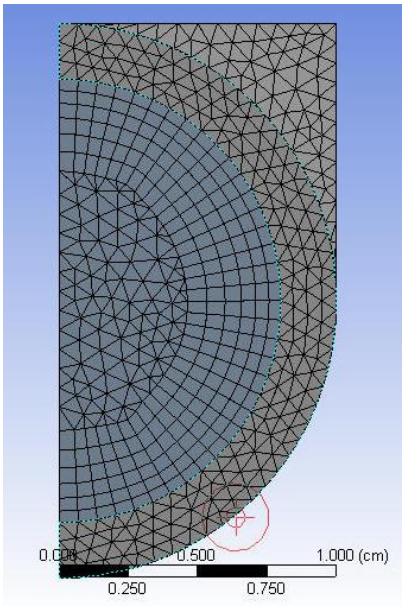

Figure 8: Mesh 5 end view detailing inflation layers

For the mesh dependency study, the heat exchanger was modeled with a three-centimeter long porous region, an inlet temperature of 80K, a cold tip temperature of 40K, a mass flow rate of 0.001 kilograms per second for a half-shell geometry (or 0.002 kilograms per second for a full pipe), and the solution was calculated. The mesh density was then increased and the solution calculated again. This iterative process was repeated until a mesh was generated that no longer produced a change in the calculated system results.

Table 5: Mesh Dependency Study Results

	Nodes	Elements	System dP (Pa)	Cryocooler Heat Flux (W)	New enthalpy flow (W)
Mesh 1	17087	56909	657	-19.416	19.302
Mesh 2	26998	95840	656	-19.420	19.316
Mesh 3	24792	127834	655	-19.422	19.312
Mesh 4	40192	149050	655	-19.423	19.313
Mesh 5	54559	209830	654	-19.423	19.317
Mesh 6	68543	226430	654	-19.426	19.320
Mesh 7	85323	287120	654	-19.425	19.319

As indicated in Table 5, meshes 6 and 7 showed no decrease in error over mesh 5, therefore, mesh 5 was chosen as the optimized mesh for the 2 cm system due to its accuracy and computational efficiency compared to meshes 6 and 7.

2.4 Solution Methods

The system was then simulated in Fluent for a variety of cases, each case involving a distinct combination of inlet temperature, system pressure, mass flow rate, and cold tip temperature. The same cases were simulated for copper foam, aluminum foam, PocoFoam, and the traditional helical heat exchanger design. Momentum calculations in the x, y, and z direction were performed to a convergence of 10^{-6} and energy to a level of 10^{-8}. ANSYS Fluent includes a variety of solver methods for each of the major parameters of the system. Solver methods could be independently selected for pressure, density, momentum, turbulent kinetic energy, energy, gradient and overall solution scheme. For each model, several trial runs were performed, varying the solver methods on each run, until a combination of solution methods that yielded consistently converging results was obtained. The solution methods used for each model are summarized in Table 6.

Table 6: Solution Methods

	Helical	**PocoFoam**	**Copper Foam**	**Aluminum Foam**
Scheme	Coupled	PISO	Coupled	Coupled
Gradient	Least Squares Cell Based	Least Squares Cell Based	Least Squares Cell Based	Least Squares Cell Based
Pressure	Standard	Standard	PRESTO!	Standard
Density	Second Order Upwind	Third-order MUSCL	Third-order MUSCL	Third-order MUSCL
Momentum	Third-order MUSCL	Power Law	Power Law	Power Law
Turbulent Kinetic Energy	Power Law	First Order Upwind	First Order Upwind	First Order Upwind
Energy	Second Order Upwind	Power Law	Power Law	Power Law

For comparison, a standard helical heat exchanger was also modeled. In order to produce results that were directly comparable, the helical heat exchanger was modeled to have the same cryogenic cooler contact area as the foam models, however, this led to a model with significantly greater axial contact length, even though the overall contact area was the same. The contact area of the cryogenic cooler with the foam model was calculated from:

$$A_{foam} = (\pi r)l \tag{7}$$

Where πr is one half the circumference of the pipe, and l is the length of the cryogenic cooler contact area.

For simplicity, the helical heat exchanger was modeled such that for every turn of the helical coil, a 0.1 centimeter width of the helical pipe was in direct contact with the cryogenic cooler core. Since there are three turns of pipe in the helical cryogenic cooler system, the appropriate diameter cryogenic cooler core was chosen by selecting a dimension such that the contact area over three turns of pipe would be identical to the contact area of the foam system using the following equation:

$$A_{helix} = (3)(0.1)(2\pi r) \tag{8}$$

The same inlet temperature, system pressure, mass flow rate, and cryogenic cooler temperature cases were repeated for the helical cryogenic cooler model. The results will be discussed in a later section.

2.5 Summary of Case Studies

Each of the four heat exchanger designs was simulated under 130 distinct system configurations. Flow rates of 9 milligrams per second, 2 grams per second and 5 grams per second were studied at 1, 2, 3 and 4 MPa of system pressure. Three cryogenic cooler temperatures were examined – 10K, 20K and 50K. For each cryogenic cooler temperature, inlet fluid temperatures of 2, 5, 10, and 50 digress above the cryogenic cooler temperature were studied.

The cases studied for 1MPa are outlined in Tables 5 through 7 below. The case studies for 2, 3, and 4MPa are included in Appendix F. For each case study, the Reynolds number, calculated at the temperature and pressure of the fluid at the inlet, is calculated. The standard Reynolds number characterizes both the helical model and the inlet zone of the porous heat exchanger designs, since both designs have the same diameter. The pore-based Reynolds number for each foam type is also included. Helium properties were obtained from an online database maintained by NIST [42]. The pore-based Reynolds numbers are proportional to the permeability of the foam. Thus, based on the values in Table 3, PocoFoam has the lowest pore-based Reynolds number because it has the lowest permeability.

Table 7: Summary of cases and Reynolds numbers for 1MPa, 9 mg/s flow

Inlet Temperature [K]	Cryogenic cooler temperature [K]	Re in open pipe	Re_K for PocoFoam	Re_K for Copper Foam	Re_K for Aluminum Foam
12	10	18061	356	226	226
15	10	16659	242	154	154
20	10	14568	151	96	96
60	10	7882	27	17	17
22	20	13876	130	83	83
25	20	12970	106	67	67
30	20	11742	79	51	51
70	20	7192	21	13	13
52	50	8574	33	21	21
55	50	8297	31	20	20
60	50	7882	27	17	17
100	50	5792	12	8	8

Table 8: Summary of cases and Reynolds number calculations for 1MPa, 2 g/s flow

Inlet Temperature [K]	Cryogenic cooler temperature [K]	Re in open pipe	Re_K for PocoFoam	Re_K for Copper Foam	Re_K for Aluminum Foam
12	10	40135	356	226	226
15	10	37019	242	154	154
20	10	32373	151	96	96
60	10	17516	27	17	17
22	20	30835	130	83	83
25	20	28823	106	67	67
30	20	26093	79	51	51
70	20	15981	21	13	13
52	50	19054	33	21	21
55	50	18438	32	20	20
60	50	17516	27	17	17
100	50	12871	12	8	8

Table 9: Summary of cases and Reynolds number calculations for 1MPa, 5 g/s flow

Inlet Temperature [K]	Cryogenic cooler temperature [K]	Re in open pipe	Re_K for PocoFoam	Re_K for Copper Foam	Re_K for Aluminum Foam
12	10	100337	356	226	226
15	10	92548	242	154	154
20	10	80933	151	96	96
60	10	43789	27	17	17
22	20	77088	130	83	83
25	20	72057	106	67	67
30	20	65233	79	51	51
70	20	39954	21	13	13
52	50	47635	33	21	21
55	50	46094	32	20	20
60	50	43789	27	17	17
100	50	32178	12	8	8

CHAPTER 3

3.1 Computational Fluid Dynamics (CFD)

Simulation and modeling of complex systems was historically time consuming and often impractical. The advent of the modern computer has revolutionized the academic community and introduced new methods for modeling and solving complex systems of equations that would have taken years by hand. Several software packages, collectively known as Computation Fluid Dynamics (CFD) packages, have been developed specifically to model fluid systems. One such CFD package is ANSYS Fluent [47], which contains individual software modules to build, mesh, and simulate a fluid system. The system geometry can be created in the ANSYS Design Modeler software package, then the completed geometry can be fed into the ANSYS Mesh Builder, where the desired characteristics of the mesh can be specified. Once the geometry and mesh have been created, ANSYS Fluent can be used to specify material and fluid properties, temperatures ranges, and boundary conditions to simulate the response of the system.

3.2 Modeling the Superconductor Cryogenic Cooling System

Four different models were created in ANSYS Fluent, version 14.5.7. Three models had identical geometry, differing only in the material selected for the metal foam insert used as a heat exchanger. The fourth model created was a helical coil cryogenic cooler which is the current standard technology used in many superconductor cooler applications.

Zero heat transfer to the surroundings was used in these models to simulate the vacuum jacket insulation that would be typical in this application. For all four heat exchanger

models, the cryogenic cooler contact areas were modeled as adiabatic surfaces. For a basis of comparison, the helical heat exchanger was modeled such that the contact area between the pipe and the heat sink is the same as the contact area between the heat sink and pipe for the foam heat exchanger models as described in section 2.4 above.

3.3 Governing Equations

Porous materials alter the flow characteristics of a medium. Reynolds numbers are calculated to classify whether the flow in a region is laminar, transitional, or turbulent. In standard pipe flow applications, the Reynolds number is a ratio of equivalent diameter, velocity and density to dynamic viscosity as shown below.

$$\mathrm{Re} = \frac{D_e v \rho}{\mu} \tag{9}$$

Where D_e is the equivalent diameter, v is the velocity, ρ is the density, and μ is the dynamic viscosity

For a porous region, the effect of permeability must be factored into the pore-based Reynolds number. Boomsma and Poulikakos discussed the factors that must be considered in calculating flow characteristics in porous regions [48]. The porous Reynolds number can be represented:

$$\mathrm{Re}_K = \frac{\rho\sqrt{K}}{\mu} \tag{10}$$

Where K is the permeability of the foam, ρ is the density, and μ is the dynamic viscosity.

Since the primary objective of this study is to understand the steady state response of the cryogenic cooler systems modeled, the system will be simulated by numerical solution of the conservation of mass and balance of momentum equations. In order to account for the heat transfer obtained by each system, the conservation of energy equation will also have to be solved.

The conservation of mass equation can be represented:

$$\frac{\partial \rho}{\partial t} + \nabla \bullet (\rho \vec{v}) = S \tag{11}$$

Where ρ is the density of the gas, $\vec{v}$ is the vectoral velocity of the gas, t is time, and S is the Source term, which is equal to zero in the absence of chemical reactions [47].

The balance of momentum equation is:

$$\frac{\partial}{\partial t}(\rho \vec{v}) + \nabla \bullet (\rho \vec{v} \vec{v}) = -\nabla p + \nabla \bullet \tau + \rho \vec{g} + \vec{F} \quad \text{[47]} \tag{12}$$

Where p is static pressure, τ is a stress tensor, $\vec{g}$ is the acceleration of gravity, $\vec{F}$ is the external body forces or source terms.

For a Newtonian fluid, the stress tensor term in the balance of momentum equation is:

$$\underline{\underline{\tau}} = \mu\left[\left(\nabla\vec{v} + \nabla\vec{v}^{T}\right) - \frac{2}{3}\nabla \bullet \vec{v}\underline{\underline{I}}\right] \quad (13)$$

Where I is the identity tensor and TP indicates a transposed matrix [47].

Conservation of Energy:

$$\frac{\partial}{\partial t}(\rho E) + \nabla \bullet \left(\vec{v}(\rho E + p)\right) = \nabla \bullet \left(k_{eff}\nabla T - \sum_{j} h_j \vec{\psi}_j + (\tau \bullet \vec{v})\right) + S \quad (14)$$

Where:

$$E = \hat{h} - \frac{p}{\rho} + \frac{v^2}{2}$$

$$\hat{h} = \int_{T1}^{T2} c_p dT$$

$$k_{eff} = k + k_t$$

Where k is the thermal conductivity of the gas, k_t is the turbulent thermal conductivity term, c_p is the specific heat of the gas, h is the local enthalpy, T is the temperature of the gas, v is the local velocity, $\vec{\psi}_j$ is the diffusion flux of species (when the fluid is multi-component), and S is the source term [47].

The above continuity, energy and momentum equations can be simplified given the geometrical constraints of the system modeled in this study. Since all three foam heat exchangers consist of a circular system, the simplifications below will be in two-dimensional polar coordinates.

In this study, the NIST real gas model was used in order to assure that the variations in helium properties such as compressibility, specific heat capacity, and van der Waals forces are accounted for in the cryogenic temperature range. FLUENT has several algorithms built in to model real gas behavior. For the purpose of the polar coordinate simplifications below, the ideal gas model will be used, though the model used for this study incorporates the real gas model.

For an ideal gas, the equation of state can be simplified to:

$$p = \rho RT \tag{15}$$

Where R is the gas constant, T is the temperature of the gas, and ρ is the density of the gas [49].

Assuming negligible effects from gravity and expanding in three dimensional Cartesian coordinates used to model the heat exchanger system, the continuity equation can be simplified to:

$$\frac{\partial \rho}{\partial t} + \frac{\partial}{\partial x}(\rho v_x) + \frac{\partial}{\partial y}(\rho v_y) + \frac{\partial}{\partial z}(\rho v_z) = 0 \tag{16}$$

Where x, y, and z are the directional coordinates, and v_x, v_y, and v_z are the directional components of velocity.

Expanding the momentum equation in three dimensional Cartesian coordinates and assuming body forces are negligible yields the following components for the x, y, and z directions :

$$\rho\left[\frac{\partial v_x}{\partial t}+v_x\frac{\partial v_x}{\partial x}+v_y\frac{\partial v_x}{\partial y}+v_z\frac{\partial v_x}{\partial z}\right]=-\frac{\partial p}{\partial x}+\left[\mu\left(\frac{\partial^2 v_x}{\partial x^2}+\frac{\partial^2 v_x}{\partial y^2}+\frac{\partial^2 v_x}{\partial z^2}\right)\right] \quad (17)$$

$$\rho\left[\frac{\partial v_y}{\partial t}+v_x\frac{\partial v_y}{\partial x}+v_y\frac{\partial v_y}{\partial y}+v_z\frac{\partial v_y}{\partial z}\right]=-\frac{\partial p}{\partial y}+\left[\mu\left(\frac{\partial^2 v_y}{\partial x^2}+\frac{\partial^2 v_y}{\partial y^2}+\frac{\partial^2 v_y}{\partial z^2}\right)\right] \quad (18)$$

$$\rho\left[\frac{\partial v_z}{\partial t}+v_x\frac{\partial v_z}{\partial x}+v_y\frac{\partial v_z}{\partial y}+v_z\frac{\partial v_z}{\partial z}\right]=-\frac{\partial p}{\partial z}+\left[\mu\left(\frac{\partial^2 v_z}{\partial x^2}+\frac{\partial^2 v_z}{\partial y^2}+\frac{\partial^2 v_z}{\partial z^2}\right)\right] \quad (19)$$

In Cartesian coordinates, the conservation of energy equation simplifies to:

$$\frac{\partial}{\partial t}(\rho E)+\frac{\partial v_x}{\partial x}(\rho E+p)=k_{eff}\frac{\partial^2 T}{\partial x^2}+\tau_x v_x \quad (20)$$

$$\frac{\partial}{\partial t}(\rho E)+\frac{\partial v_y}{\partial y}(\rho E+p)=k_{eff}\frac{\partial^2 T}{\partial y^2}+\tau_y v_y \quad (21)$$

$$\frac{\partial}{\partial t}(\rho E)+\frac{\partial v_z}{\partial z}(\rho E+p)=k_{eff}\frac{\partial^2 T}{\partial z^2}+\tau_z v_z \quad (22)$$

For the porous media, the conservation of mass and momentum equations must be modified to account for the flow obstruction presented by the metal foams. To account for the effects of porosity, the conservation of mass equation is multiplied by the porosity, ε.

$$\frac{\partial}{\partial t}(\varepsilon\rho)+\nabla\bullet(\varepsilon\rho\vec{v})=0 \quad (23)$$

The balance of momentum, Equation 10, had no specific force term, F, when simplified for the simple three dimensional area with no porous media as shown in Equations 15, 16, and 17. To represent conservation in the porous zone, a flow restriction force, F, must be added to

(15, 16, and 17. For the axial and radial directions, these forces can be represented:

$$F_x=-\left(\frac{\mu}{\beta_x}v_x+\frac{1}{2}C_x\rho|\vec{v}|v_x\right) \quad (24)$$

$$F_y=-\left(\frac{\mu}{\beta_y}v_y+\frac{1}{2}C_y\rho|\vec{v}|v_y\right) \quad (25)$$

$$F_z=-\left(\frac{\mu}{\beta_z}v_z+\frac{1}{2}C_z\rho|\vec{v}|v_z\right) \quad (26)$$

Where μ is the fluid molecular viscosity, β is the permeability of the foam, C is the inertial resistance factor, and v is the velocity.

Combining terms and simplifying, the porous-zone momentum equation becomes:

$$\rho\left[\frac{\partial v_x}{\partial t}+v_x\frac{\partial v_x}{\partial x}+v_y\frac{\partial v_x}{\partial y}+v_z\frac{\partial v_x}{\partial z}\right]= -\frac{\partial p}{\partial x}+\left[\mu\left(\frac{\partial^2 v_x}{\partial x^2}+\frac{\partial^2 v_x}{\partial y^2}+\frac{\partial^2 v_x}{\partial z^2}\right)\right]-\left(\frac{\mu}{\beta}v_x+\frac{1}{2}C\rho|\vec{v}|v_x\right) \quad (27)$$

$$\rho\left[\frac{\partial v_y}{\partial t}+v_x\frac{\partial v_y}{\partial x}+v_y\frac{\partial v_y}{\partial y}+v_z\frac{\partial v_y}{\partial z}\right]= -\frac{\partial p}{\partial y}+\left[\mu\left(\frac{\partial^2 v_y}{\partial x^2}+\frac{\partial^2 v_y}{\partial y^2}+\frac{\partial^2 v_y}{\partial z^2}\right)\right]-\left(\frac{\mu}{\beta}v_y+\frac{1}{2}C\rho|\vec{v}|v_y\right) \quad (28)$$

$$\rho\left[\frac{\partial v_z}{\partial t}+v_x\frac{\partial v_z}{\partial x}+v_y\frac{\partial v_z}{\partial y}+v_z\frac{\partial v_z}{\partial z}\right]= -\frac{\partial p}{\partial z}+\left[\mu\left(\frac{\partial^2 v_z}{\partial x^2}+\frac{\partial^2 v_z}{\partial y^2}+\frac{\partial^2 v_z}{\partial z^2}\right)\right]-\left(\frac{\mu}{\beta}v_z+\frac{1}{2}C\rho|\vec{v}|v_z\right) \quad (29)$$

The porous region will also affect the rate at which heat is transferred to the working fluid. The effect of the metal structure and flow resistance must be accounted for in the energy equation. Thus, in the porous zone, the energy equation becomes:

$$\frac{\partial}{\partial t}\left(\varepsilon\rho_t E_t+(1-\varepsilon)\rho_s E_s\right)+\frac{\partial v_x}{\partial x}\left(\rho_t E_t+P\right)=\hat{k}\frac{\partial^2 T}{\partial x^2}+\tau_x v_x \quad (30)$$

$$\frac{\partial}{\partial t}\left(\varepsilon\rho_t E_t+(1-\varepsilon)\rho_s E_s\right)+\frac{\partial v_y}{\partial y}\left(\rho_t E_t+P\right)=\hat{k}\frac{\partial^2 T}{\partial y^2}+\tau_y v_y \quad (31)$$

$$\frac{\partial}{\partial t}\left(\varepsilon\rho_t E_t + (1-\varepsilon)\rho_s E_s\right) + \frac{\partial v_z}{\partial z}\left(\rho_t E_t + P\right) = \hat{k}\frac{\partial^2 T}{\partial z^2} + \tau_z v_z \quad (32)$$

Where:

$$\hat{k} = \varepsilon\hat{k}_t + (1-\varepsilon)\hat{k}_s$$

where ε is the porosity of the medium, $\hat{k}_s$ is the solid medium thermal conductivity, and $\hat{k}_t$ is the fluid thermal conductivity.

CHAPTER 4

4.1 Results and Discussion

For each case study, pressure difference, outlet temperature and heat exchanger effectiveness were captured. The effectiveness was computed using the enthalpy at the inlet, outlet, and the enthalpy of helium evaluated at the cold tip temperature according to Equation 31.

$$\varepsilon = 100 * \frac{h_{in} - h_{out}}{h_{in} - h_{coldtip}} \quad (33)$$

where ε is effectiveness, h is enthalpy, and subscripts 'in', 'out' and 'coldtip' represent the inlet, outlet and cryogenic coolers, respectively.

In most cases, the effectiveness increased as the temperature difference between the helium at the inlet and the cryogenic cooler increased. Some cases exhibited a change in slope at lower temperature ranges. This phenomenon will be discussed in the case sections below.

Three flow rates were considered. Many existing cryogenically cooled superconductor systems have helium mass flow rates in the two to ten gram per second range, however the published literature on metal foams has indicated that due to the large viscous and inertial resistance of the foams, slower flow rates tend to be more effective at heat transfer without causing unreasonable pressure drops. A few cases were run at a variety of flow rates to see comparative results. Based on the results of these initial

cases, the published literature on metal foams and the typical flow rates of cryogenic cooling systems, the flow rates of nine milligrams per second, two grams per second and five grams per second were selected for additional study.

For the helical heat exchanger, nine milligrams, two and five grams per second were used directly since a full pipe geometry was modeled. For the metal foam models, a half pipe geometry with a symmetry condition was modeled. In order to model the same flow rates, 4.5 milligrams per second, 1 gram per second and 2.5 grams per second were modeled due to the half geometry.

4.1.1 Nine milligram per second case discussion

The nine milligram per second flow data showed the best effectiveness numbers for the copper and graphite foam heat exchangers. Several figures below plot the effectiveness of each heat exchanger system as a function of the temperature of the helium entering the system. Each line represents a different heat exchanger model and cryogenic cooler temperature.

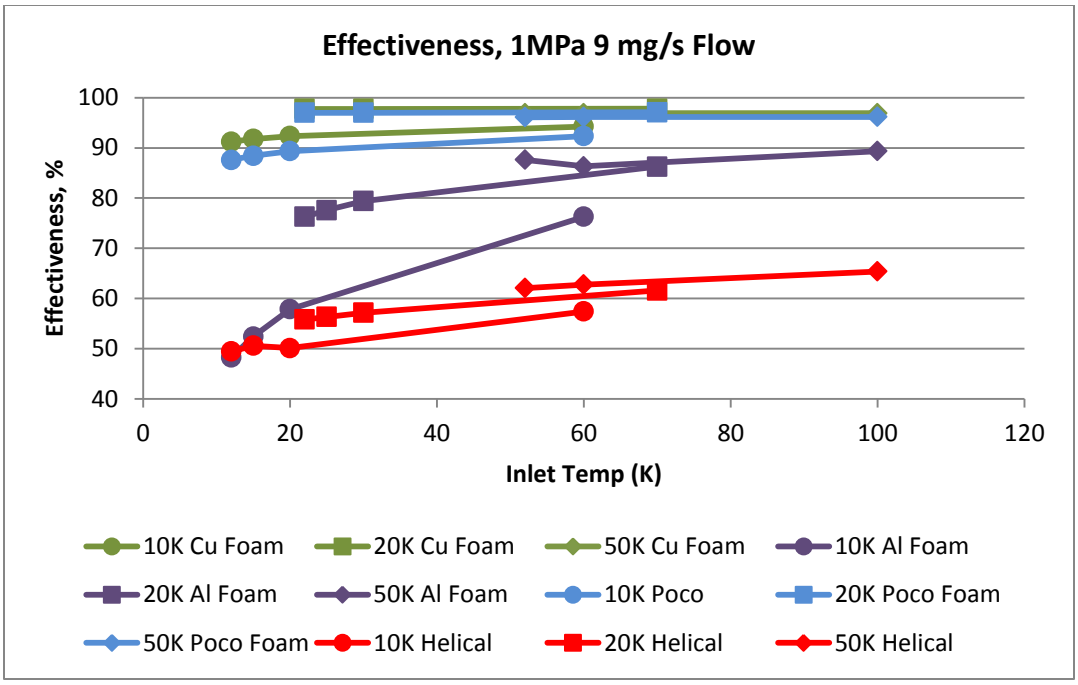

Figure 9: Heat exchanger effectiveness for 1MPa, 9 mg/s flow

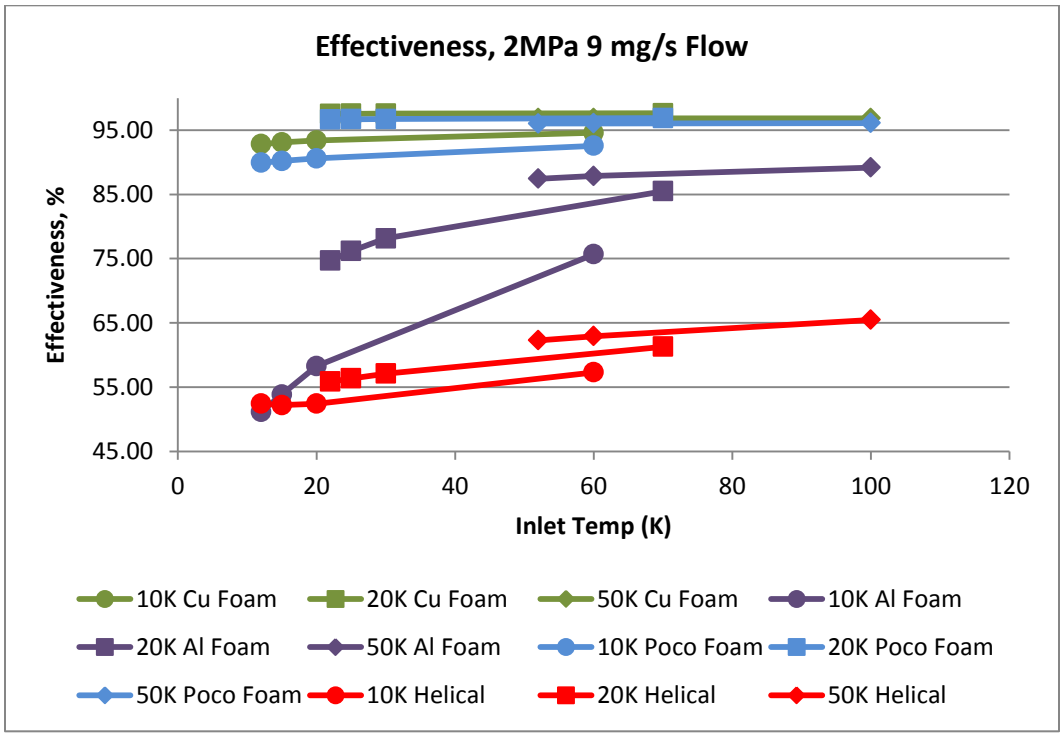

Figure 10: Heat exchanger effectiveness for 2MPa, 9 mg/s flow

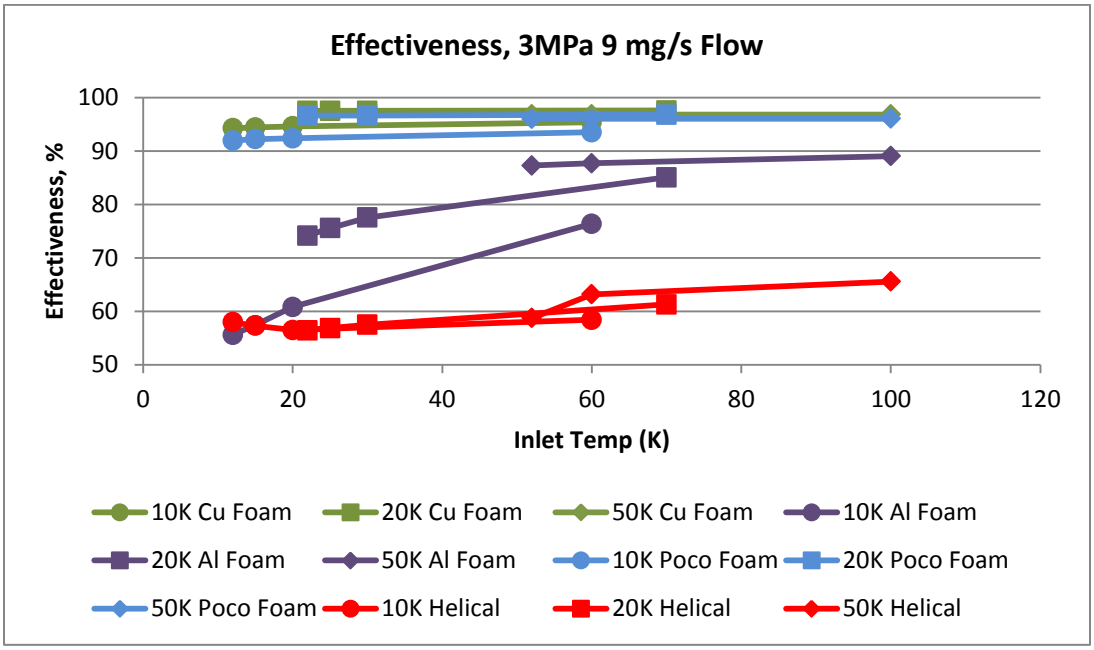

Figure 11: Heat exchanger effectiveness for 3MPa, 9 mg/s flow

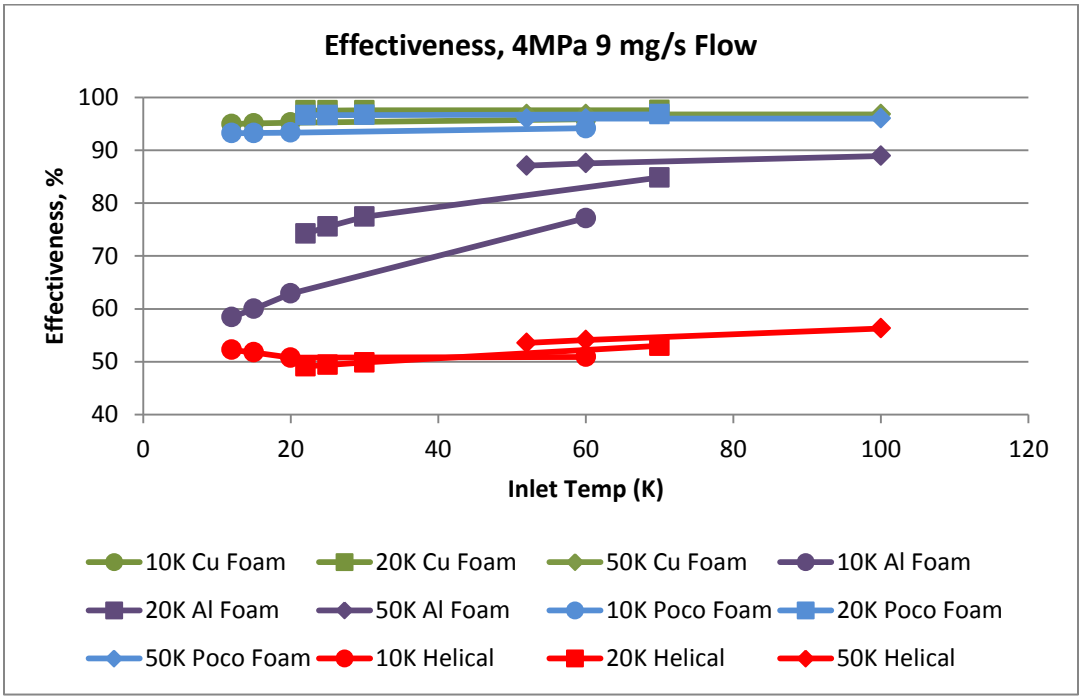

Figure 12: Heat exchanger effectiveness for 4MPa, 9 mg/s flow

As seen in Figures 9, 10, 11 and 12 below, the effectiveness of each system is highly affected by the changes in material properties over the temperature range considered. Graphite and copper foam heat exchangers performed the best in all cases. The helical heat exchanger had the poorest performance in all but the 12 K inlet temperature cases for 1, 2 and 3 MPa, where the helical model slightly out-performed the aluminum foam model.

For all system pressures, the copper foam heat exchanger was the most effective, increasing the effectiveness over a traditional helical heat exchanger by 34-47%. However, it is important to note that graphite foam properties have not been well documented at cryogenic temperatures, and since the calculated effectiveness of the graphite foam heat exchanger is within 2 percent of the copper foam model, graphite foam material properties at cryogenic temperatures merit additional study to better understand which heat exchanger would be the most efficient. Both aluminum and copper foams properties are highly non-linear at cryogenic temperatures, and constant properties that were measured near ambient temperature were used for the graphite foam because data on temperature dependency at cryogenic temperatures was not available.

The aluminum foam heat exchanger exhibited comparable effectiveness over the helical heat exchanger for the 10 K cryogenic cooler, but exhibited significant improvements for the 20 K and 50 K cryogenic coolers. This improvement in heat transfer can be attributed to the increase in thermal conductivity of 6061-T6 aluminum as seen in Figure 13.

For all heat exchangers considered, the greatest variation in effectiveness occurred for the 10 K cryogenic cooler. In the 10 to 20 K temperature range, the properties of helium change rapidly. In this range, the specific heat decreases at higher pressures, and the thermal conductivity increases as exhibited in Figures 14 and 15. These rapid changes in property correspond to the most non-linear progression of heat exchanger effectiveness.

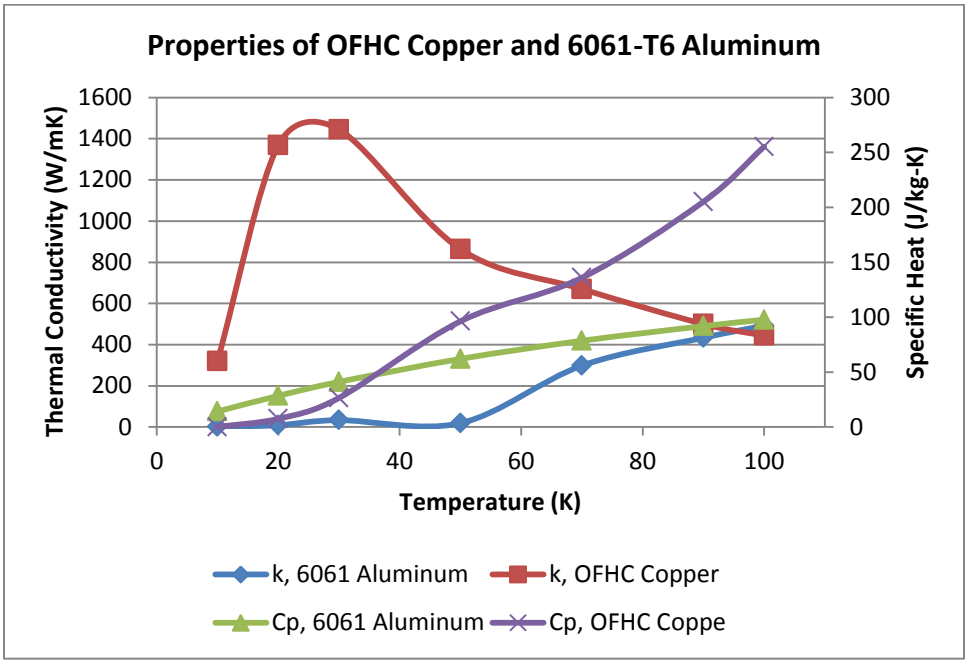

Figure 13: Properties of OFHC Copper and 6061-T6 Aluminum

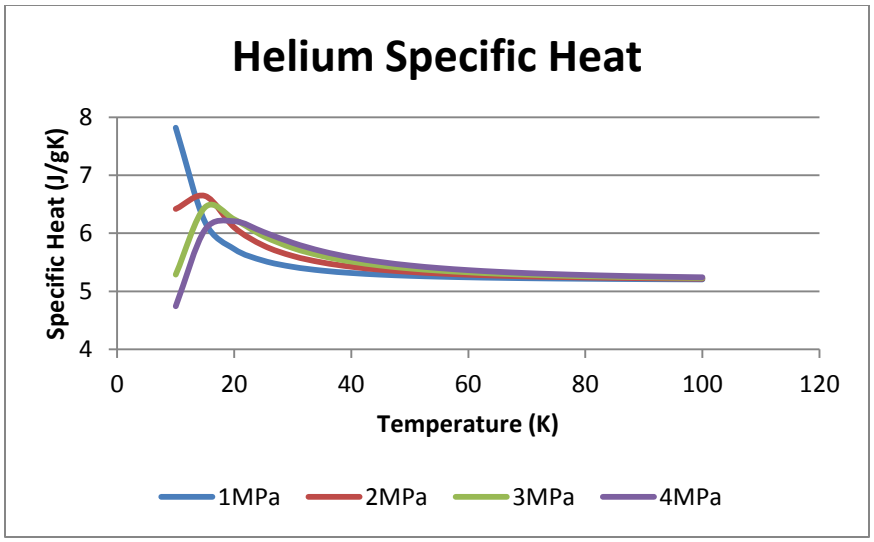

Figure 14: Helium Specific Heat

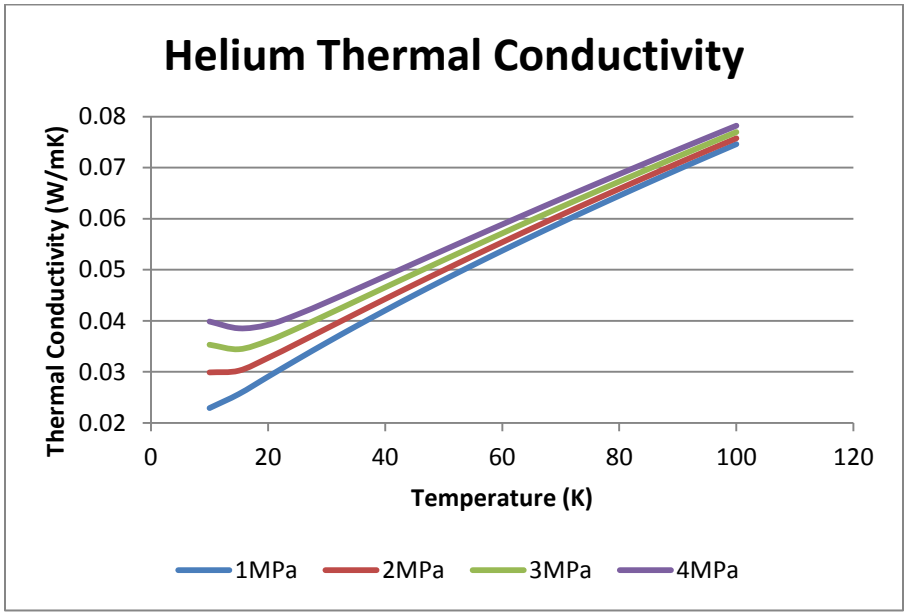

Figure 15: Helium Thermal Conductivity

Data was pulled from the NIST database for Helium and plotted to create Figures 14 and 15 [50]. As indicated in these figures, below around 20 K, Helium has a much lower specific heat and a slightly higher thermal conductivity at 3 and 4 MPa of pressure. The decreased specific heat results in a smaller energy input requirement to change the

temperature of the fluid in this temperature range, and the higher thermal conductivity results in more efficient heat conduction.

The non-conformity of thermal conductivity and specific heat of helium below 20 K also explains why trends for heat exchanger effectiveness deviated from trends in higher temperature ranges for the lowest temperature combinations considered in the study. At 10 K, the specific heat of helium decreases significantly as system pressure increases. The thermal conductivity of helium increases over this same range. The combination of these changes results in a reduction of system power input required to change the temperature of the helium, which in turn explains the increase in heat exchanger performance as system pressure increases for the lowest temperature cases examined.

Significant differences in temperature distribution can be observed between the PocoFoam heat exchanger and the aluminum and copper foam models. For simplicity of comparison, all temperature distribution visualizations in the following sections will represent the 22 K helium inlet, 20 K cryogenic cooler, 1 MPa case.

Because the low flow rate allowed the helium to spend significant residence time in the foam heat exchanger element, the temperature of the helium decreased throughout the flow profile for all of the copper and graphite foam heat exchangers as seen in Figures 16 and 17. Due to the lower thermal conductivity of the aluminum foam, the helium at the center of the heat exchanger was not cooled as effectively and temperature striations can be observed in Figure 18.

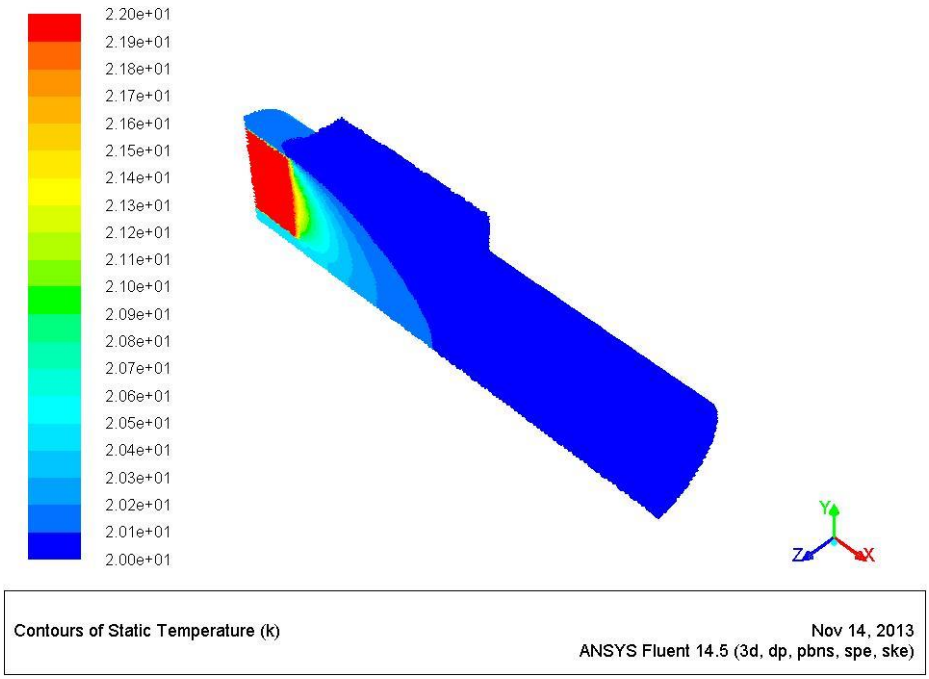

Figure 16: PocoFoam HX Temperature Profile for 22K/20K Temperature Differential and 1MPa System Pressure, 9 mg/s flow, Re=13876, Re_K=130

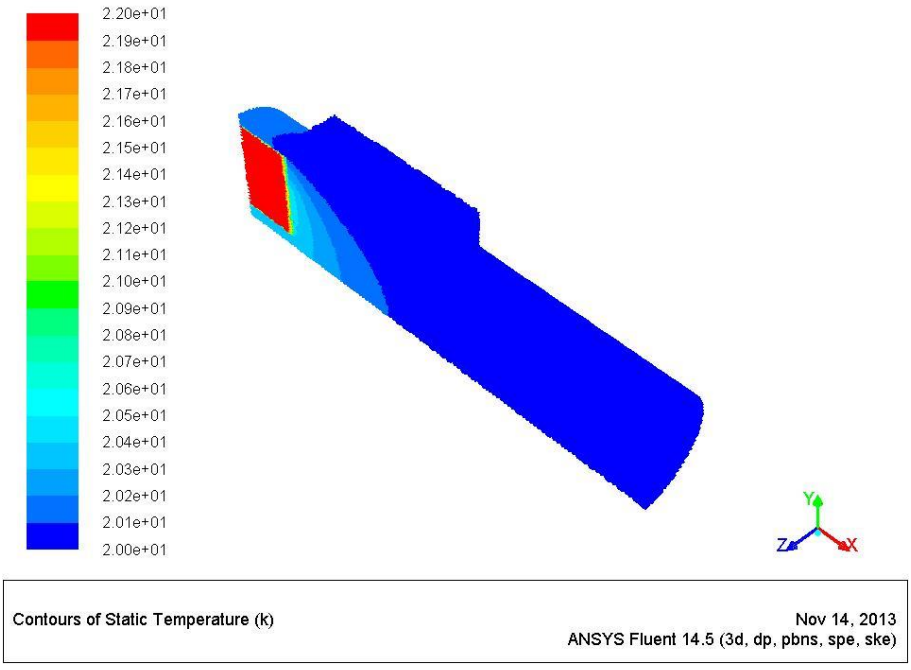

Figure 17: Copper Foam HX Temperature Profile for 22K/20K Temperature Differential and 1MPa System Pressure, 9 mg/s flow, Re=13876, Re_K=2611

The helical heat exchanger had the poorest performance, and the bulk temperature of the fluid was not as low as the other heat exchangers. In Figure 19, it can be observed that, similar to the aluminum foam heat exchanger, the helical heat exchanger was not able to effectively lower the temperature across the entire flow profile, and temperature striations can be observed.

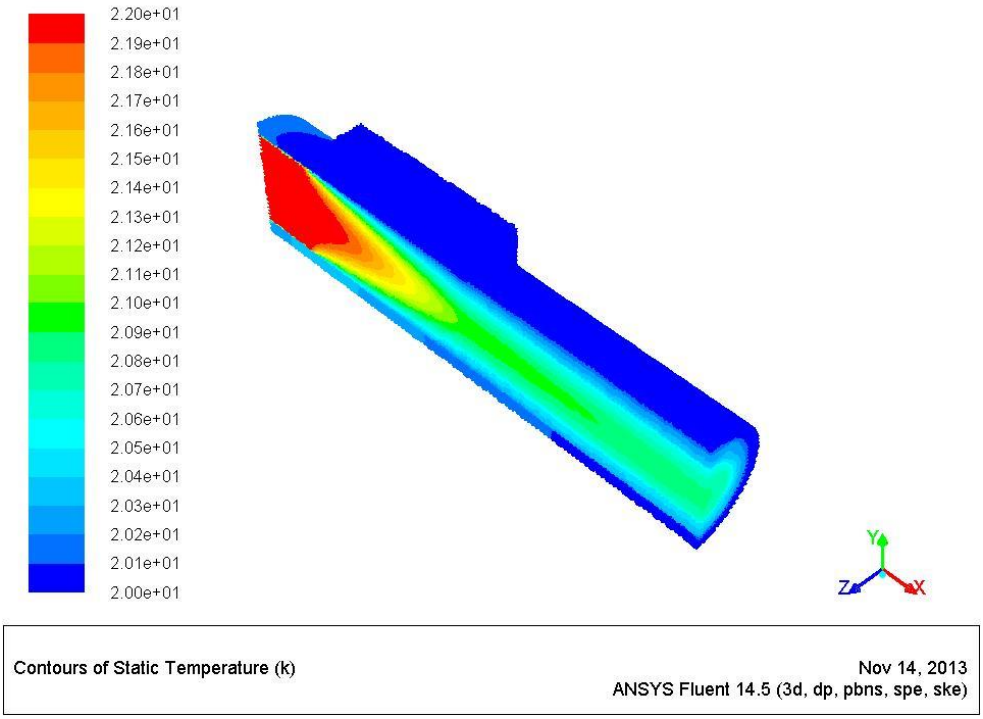

Figure 18: Aluminum Foam HX Temperature Profile for 22K/20K Temperature Differential and 1MPa System Pressure, 9 mg/s flow, Re=13876, Re_K=1633

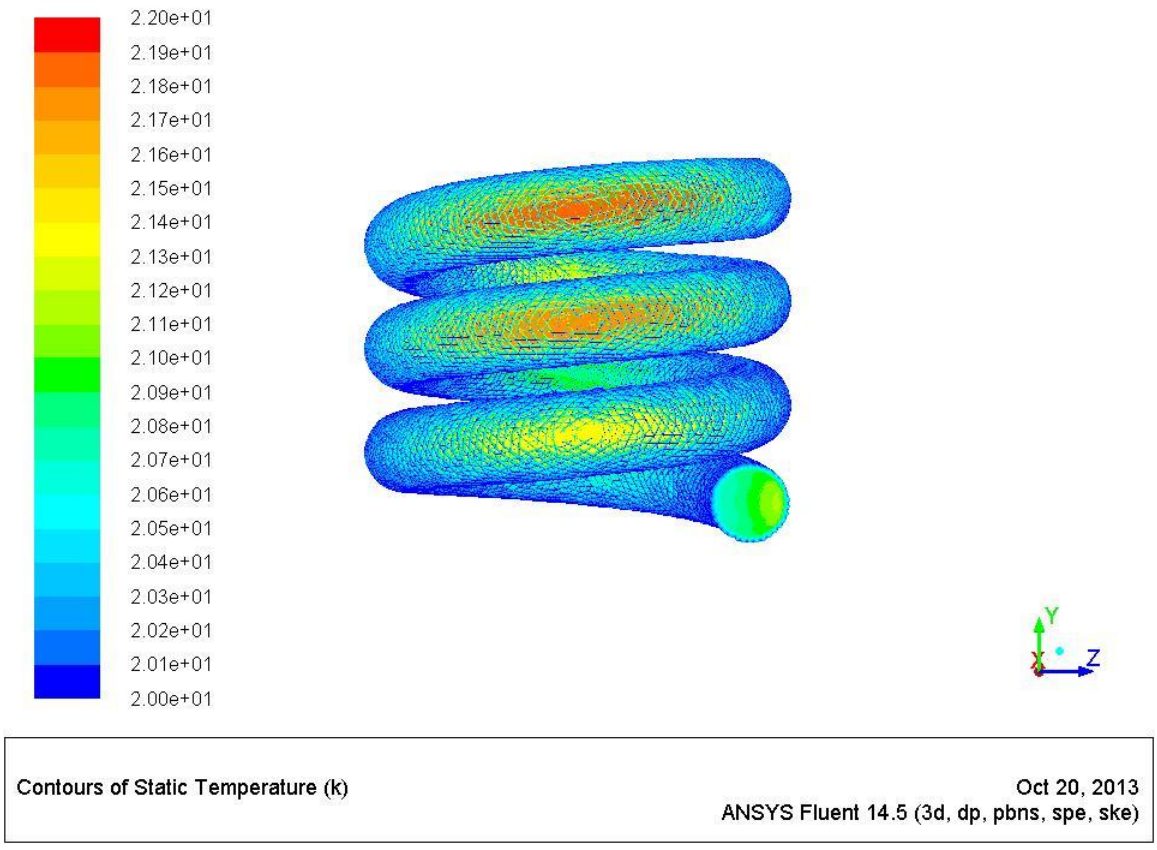

Figure 19: Helical HX Temperature Profile for 22K/20K Temperature Differential and 1MPa System Pressure, 9 mg/s flow, Re=13876

4.1.2 Two grams per second case discussion

When the system flow rate was increased to two grams per second, all models saw a drop in effectiveness. The graphite and copper foam heat exchanger effectiveness dropped approximately 5% and the difference in effectiveness between the copper and graphite foam models widened. The helical dropped nearly 8%, and the aluminum and copper foam systems dropped around 10%. This non-uniformity in performance drop can be attributed to the difference in pressure drop of the different models, and the subsequent effect that the pressure change has on helium properties.

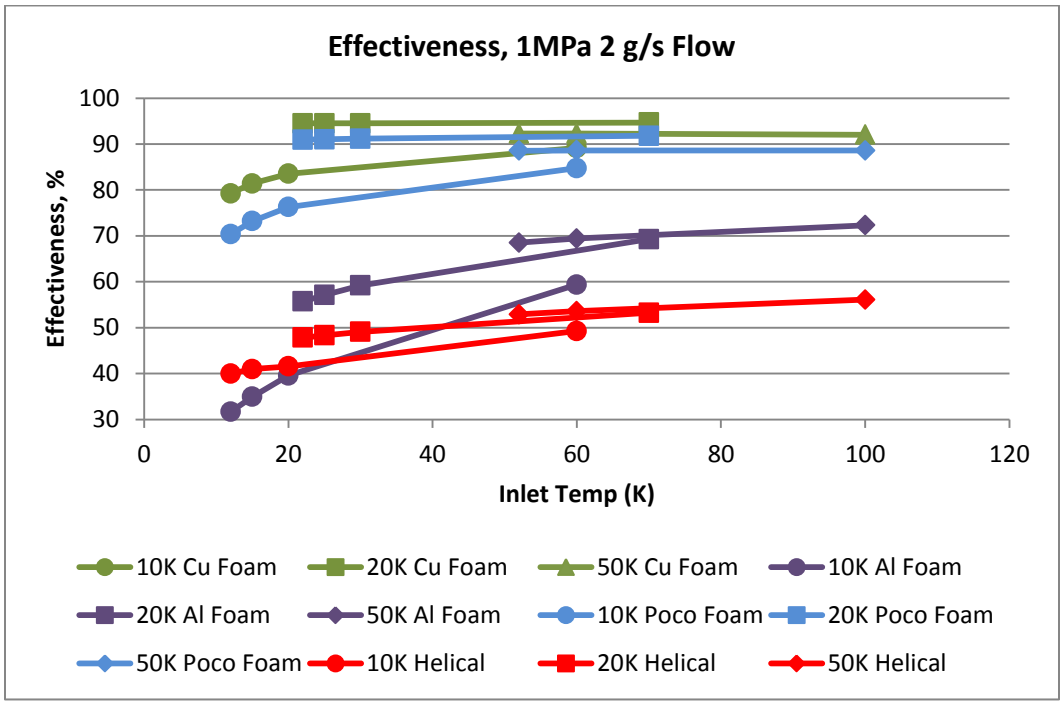

Figure 20: Heat exchanger effectiveness for 1MPa, 2 g/s flow

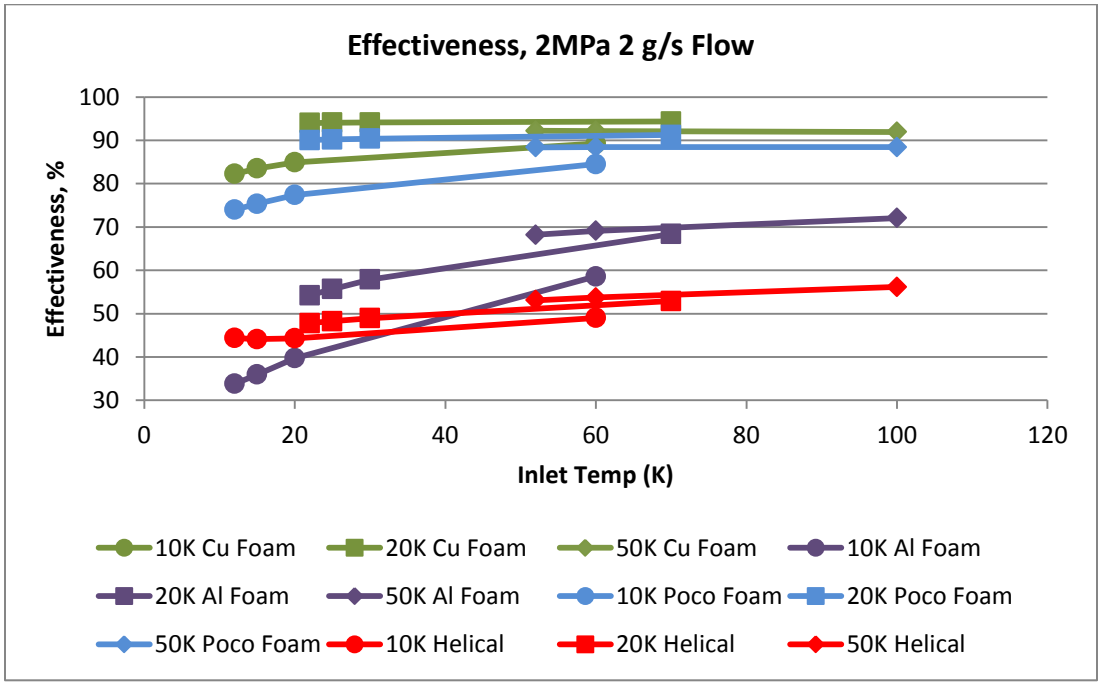

Figure 21: Heat exchanger effectiveness for 2MPa, 2 g/s flow

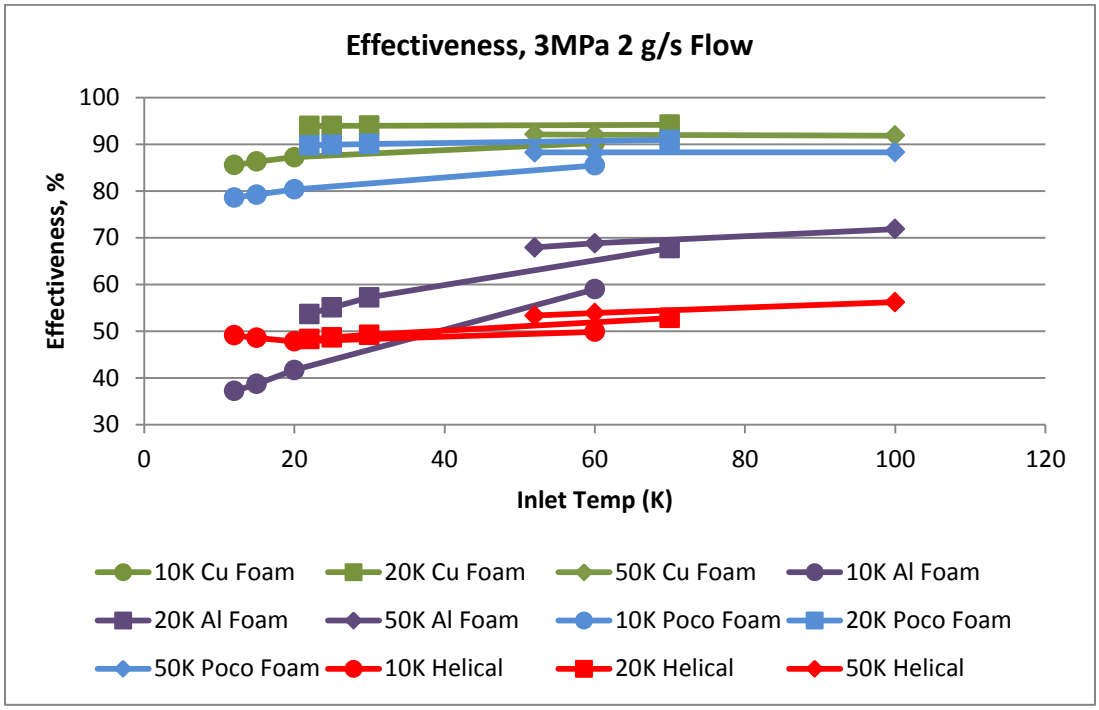

Figure 22: Heat exchanger effectiveness for 3MPa, 2 g/s flow

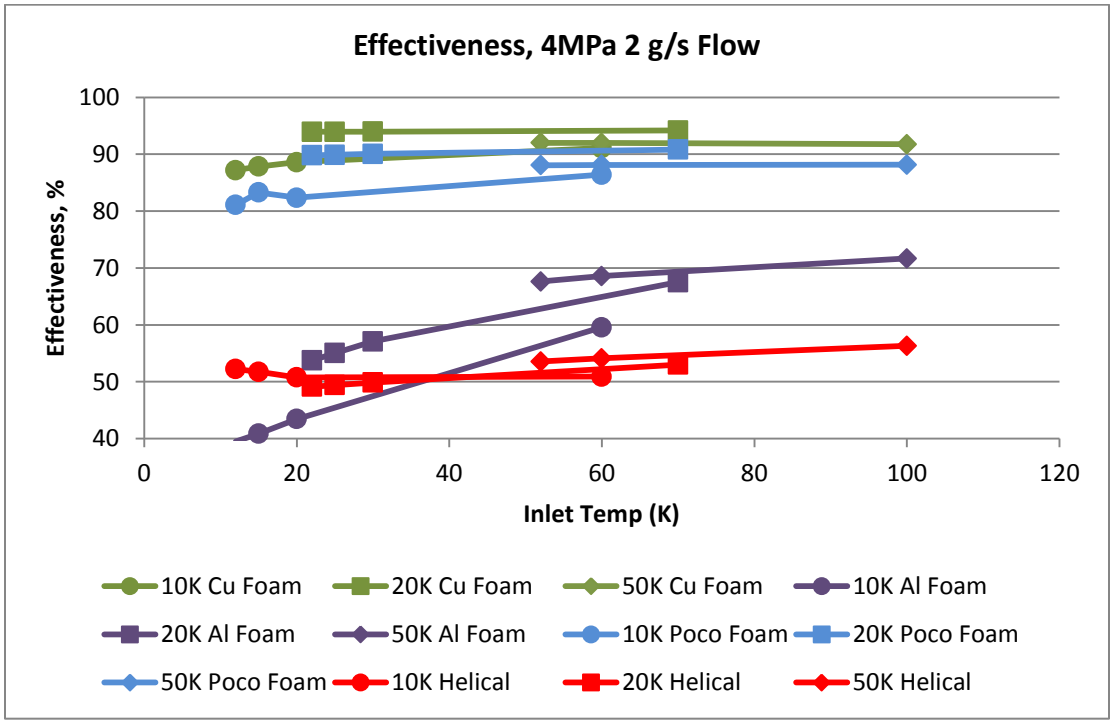

Figure 23: Heat exchanger effectiveness for 4MPa, 2 g/s flow

As noted in the 9 milligram per second flow case, the graphite and copper foam heat exchangers were much more effective at cooling the bulk of the working fluid, as seen in Figures 24 and 25 below. However, the effect that the decreased residence time in the foam element had on the temperature distribution can be easily observed. All three foam models exhibited a decrease in the radial depth of effective cooling as compared to the 9 milligram per second case.

Similar to the 9 milligram per second case, the copper and graphite foam heat exchangers outperformed the helical heat exchanger in terms of outlet temperature. The aluminum foam heat exchanger was the least effective at lowering the bulk fluid temperature at the very center of the pipe, while the helical exchanger was similarly ineffective at lowering the bulk temperature at the outer surface of the heat exchanger. The graphite and copper foam heat exchangers achieved temperatures nearly 0.8 degrees Kelvin lower at the wall surface than the helical heat exchanger did in its most effective regions.

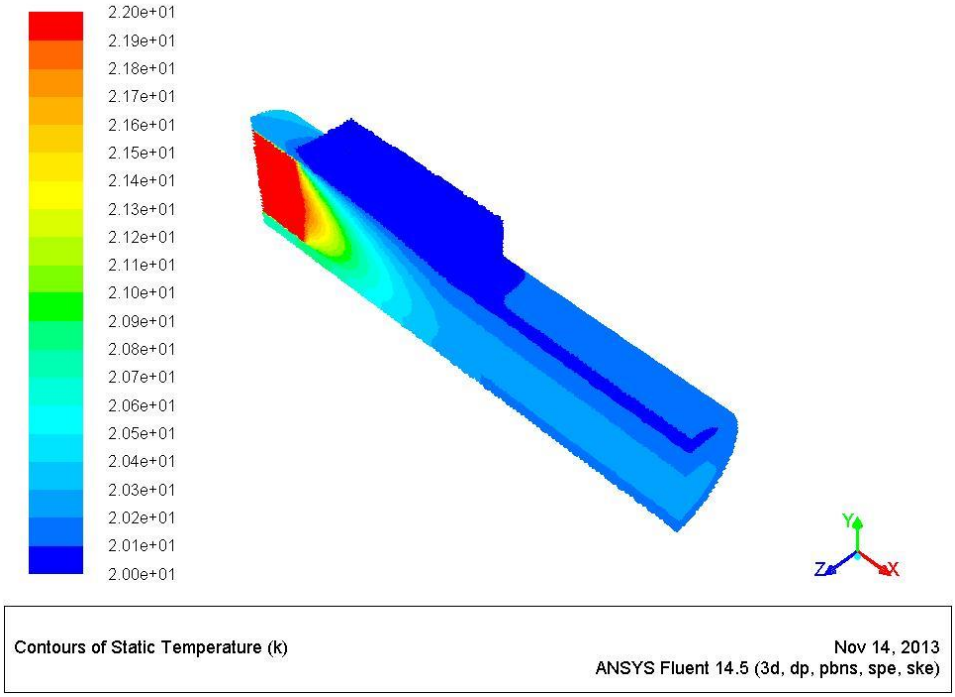

Figure 24: PocoFoam HX Temperature Profile for 22K/20K Temperature Differential and 1MPa System Pressure, 2 g/s flow, Re=30835, Re_K=130

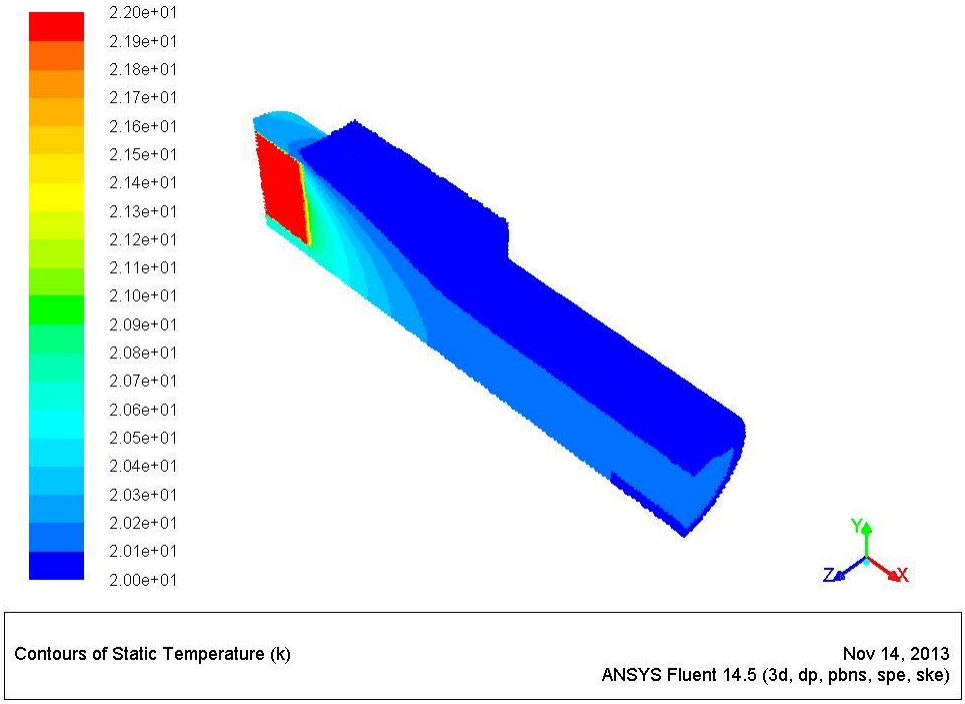

Figure 25: Copper Foam HX Temperature Profile for 22K/20K Temperature Differential and 1MPa System Pressure, 2 g/s flow, Re=30835, Re_K=2611

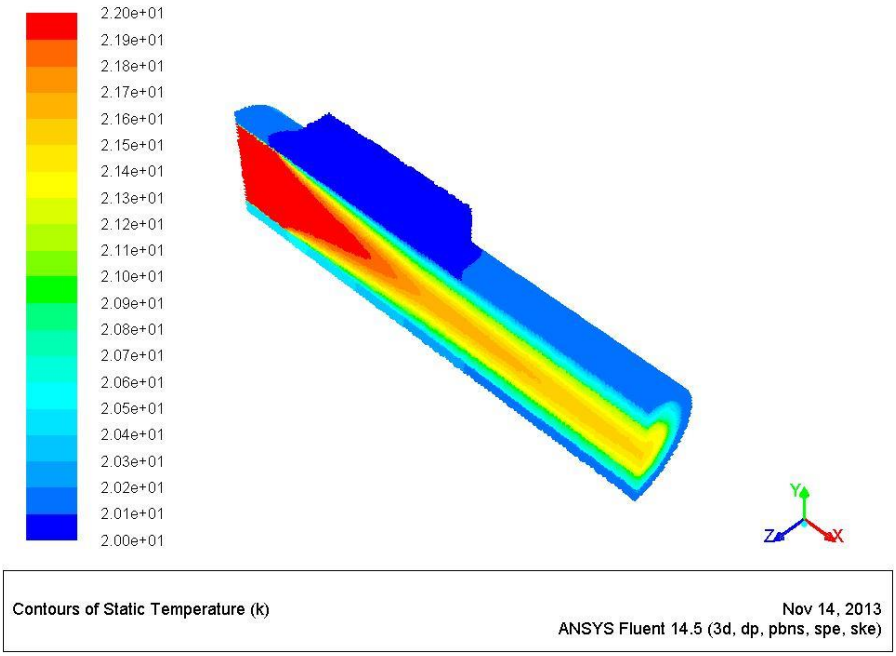

Figure 26: Aluminum HX Temperature Profile for 22K/20K Temperature Differential and 1MPa System Pressure, 2 g/s flow, Re=30835, Re_K=1633

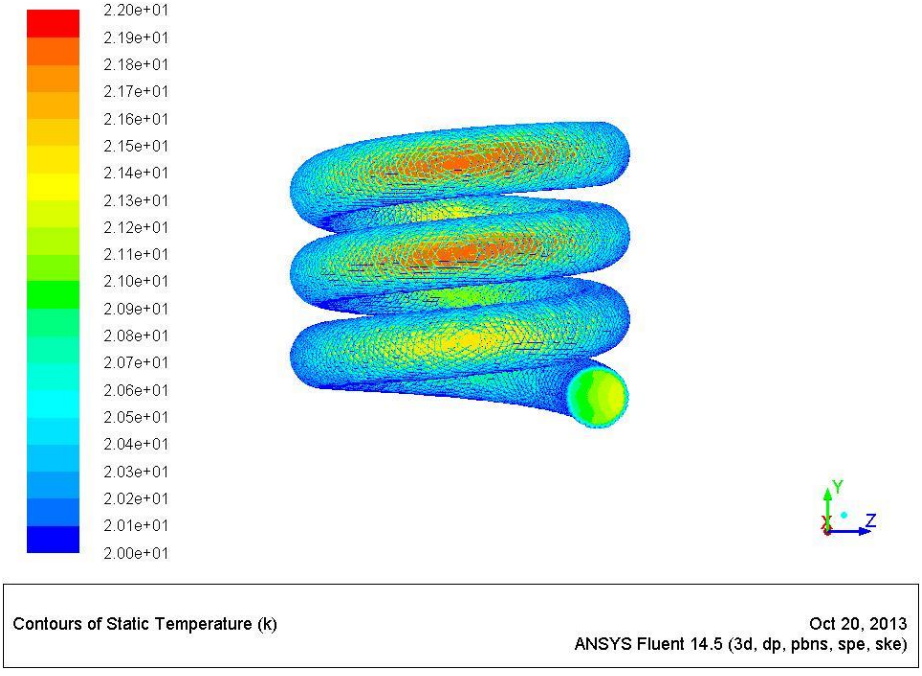

Figure 27: Helical HX Temperature Profile for 22K/20K Temperature Differential and 1MPa System Pressure, 2 g/s flow, Re=30835

4.1.3 Five grams per second case discussion

When the flow rate of the system was increased to five grams per second, system effectiveness again decreased for all heat exchangers studied. The effectiveness of the graphite and copper foam systems dropped nearly 15%; the helical system dropped approximately 9%, and the aluminum and copper systems dropped 8%.

As flow rate increased, the difference in performance between the graphite and copper foam heat exchangers increased. For 9 milligrams per second, the copper and graphite foam heat exchangers differed in effectiveness by only 2 or 3 percent. At 2 grams per second, this difference increased to 6 to 8 percent; and at 5 grams per second, the difference increased again to 9 to 12 percent. This trend for the gap in effectiveness to widen as flow rate increases can be attributed to the directional nation of heat conduction in the graphite foam. Room temperature experiments have shown that graphite foam is highly direction in heat conduction. Since the conduction of graphite foam in the direction of flow is roughly one quarter of the conduction perpendicular to the flow, the decreased residence time that results from higher mass flow rates results in a decrease in heat transfer effectiveness. The reduction in effectiveness for the copper foam heat exchanger is not as dramatic because the thermal conductivity is not directionally dependent.

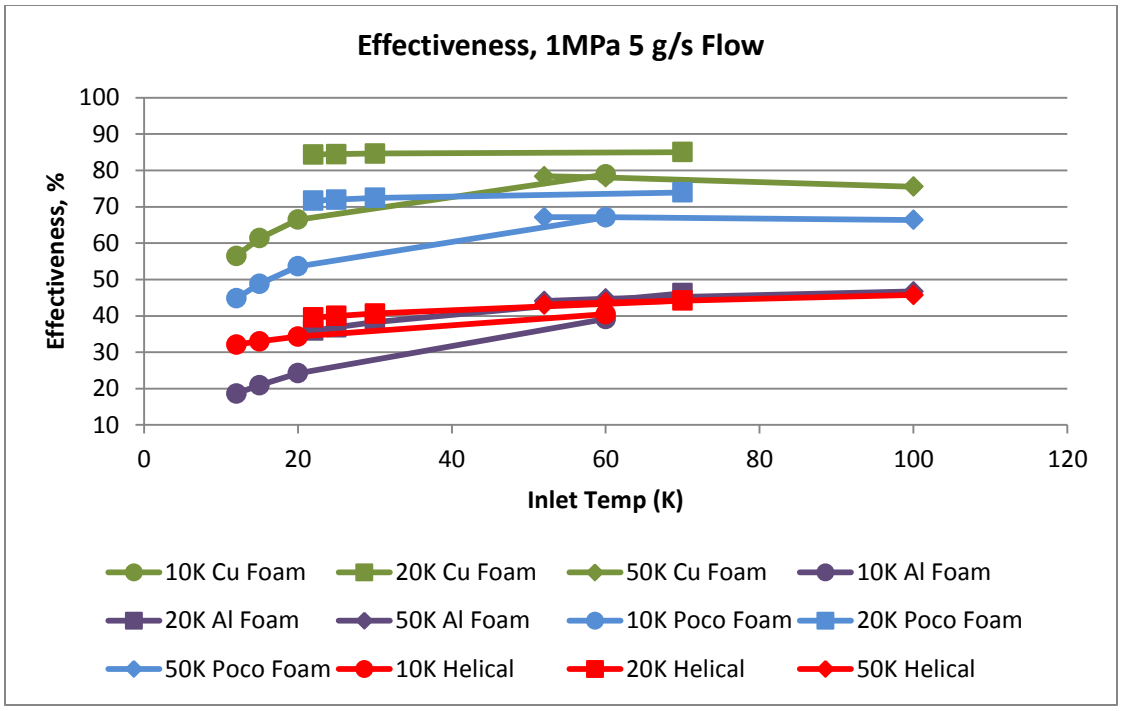

Figure 28: Heat exchanger effectiveness for 1MPa, 5 g/s flow

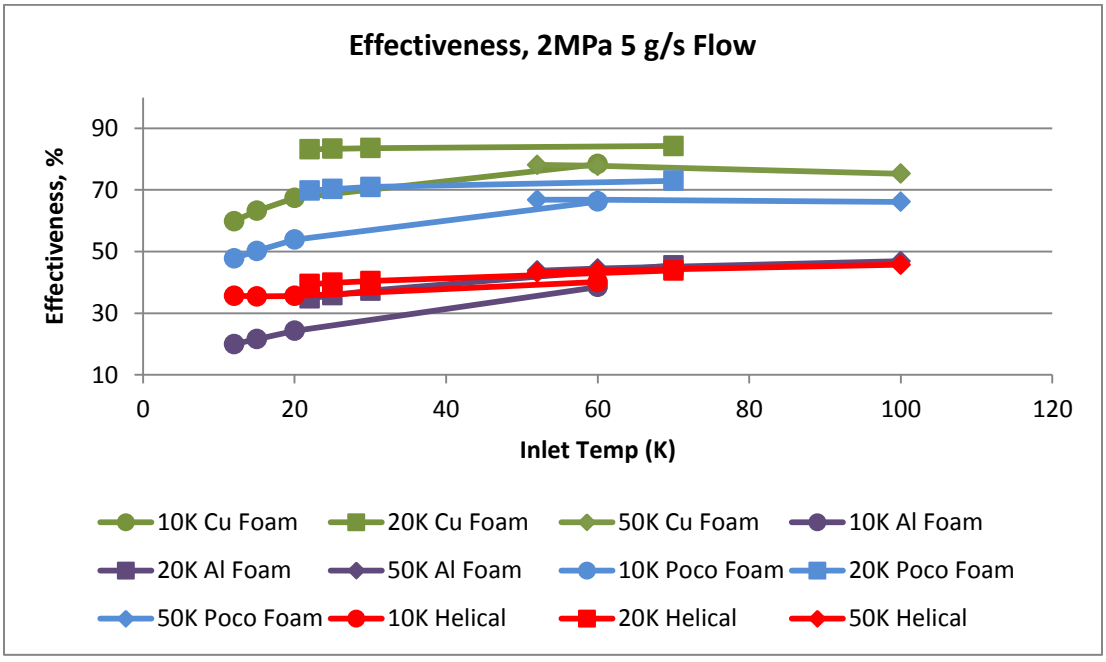

Figure 29: Heat exchanger effectiveness for 2MPa, 5 g/s flow

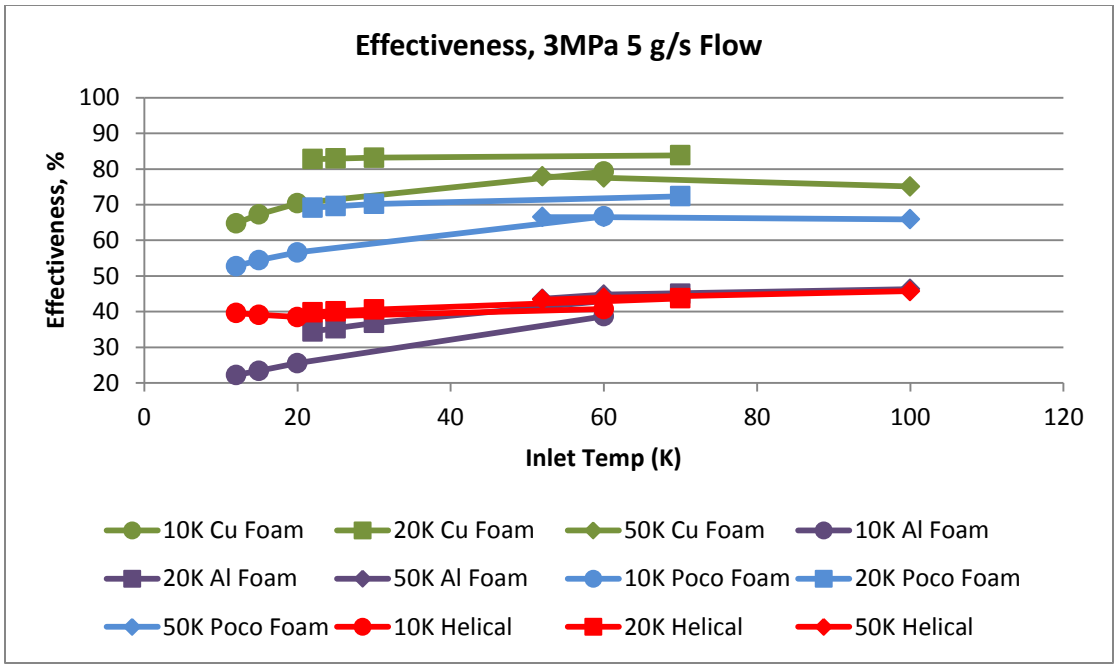

Figure 30: Heat exchanger effectiveness for 3MPa, 5 g/s flow

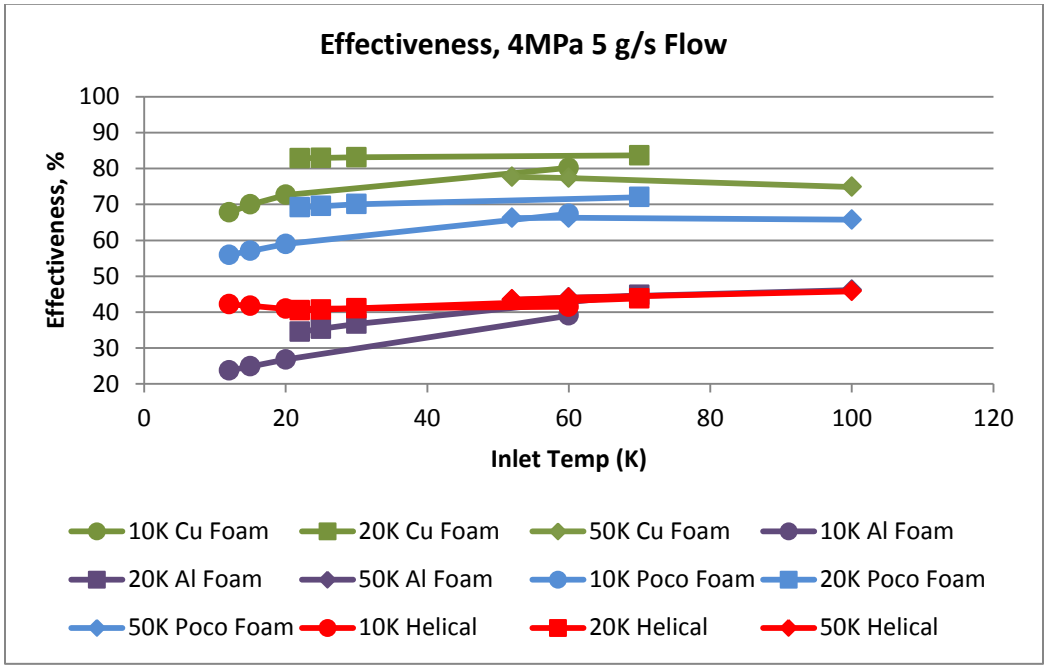

Figure 31: Heat exchanger effectiveness for 4MPa, 5 g/s flow

As noted in the 2 milligram per second flow case, the copper foam heat exchanger was much more effective at cooling the bulk of the working fluid than the graphite or aluminum foam models, as seen in the figure below. However, the effect that the decreased residence time in the foam element had on the temperature distribution can be easily observed.

The aluminum and graphite foams exhibited a decrease in the radial depth of effective cooling as compared to the 2 gram per second case. At 5 grams per second, in the aluminum foam model, only a thin film of fluid near the walls of the pipe is effectively cooled.

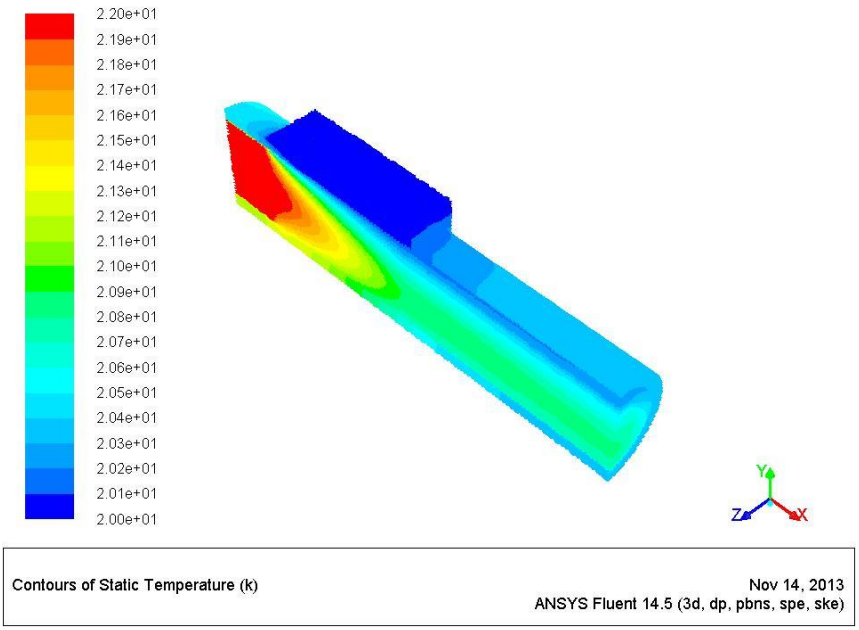

Figure 32: PocoFoam HX Temperature Profile for 22K/20K Temperature Differential and 1MPa System Pressure, 5 g/s flow, Re=77088, Re_K=130

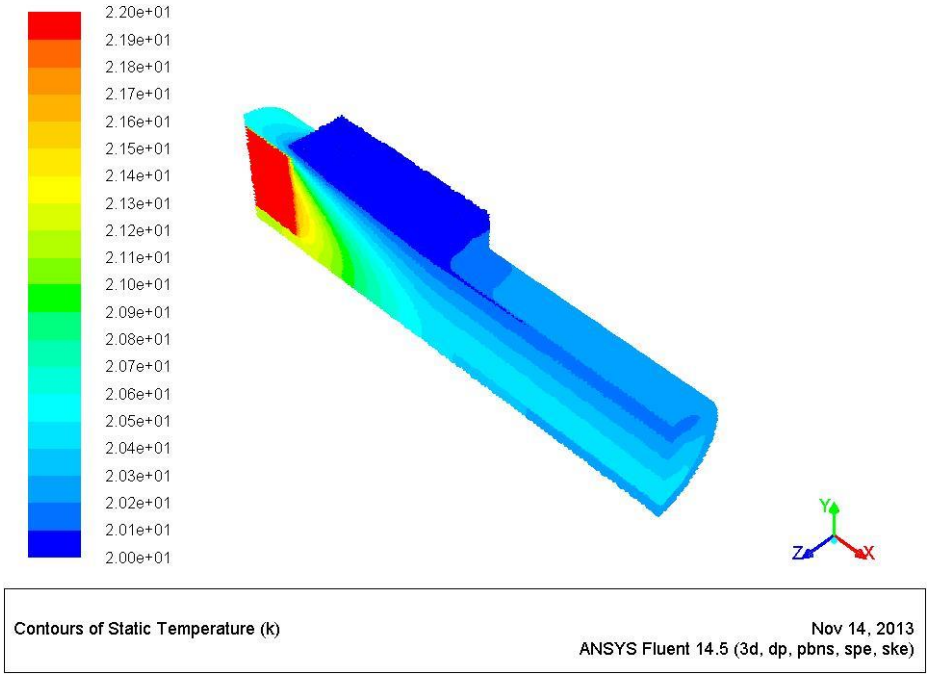

Figure 33: Copper Foam HX Temperature Profile for 22K/20K Temperature Differential and 1MPa System Pressure, 5 g/s flow, Re=77088, Re_K=2611

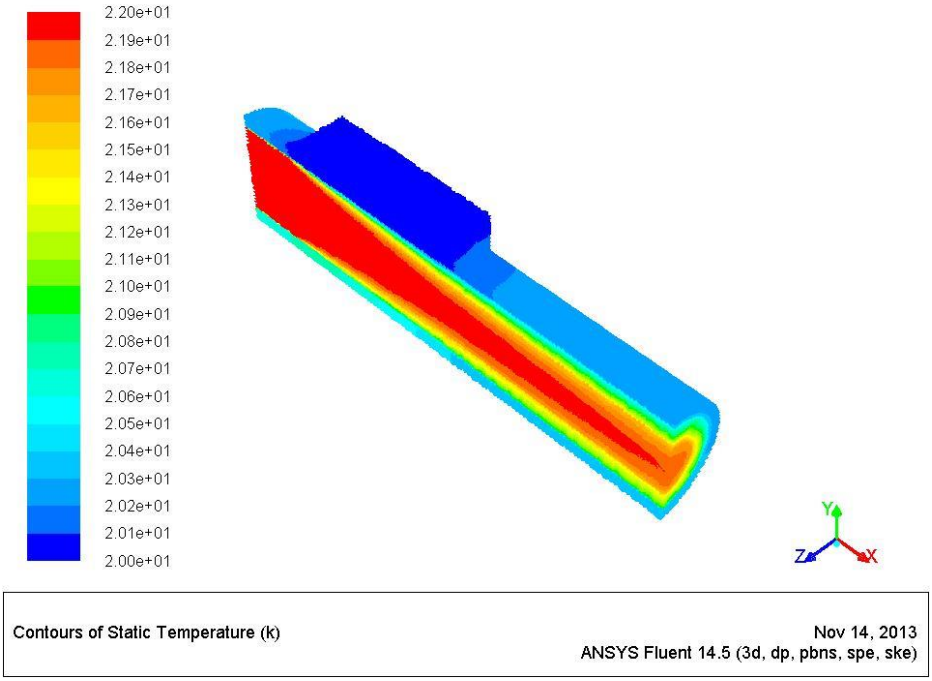

Figure 34: Aluminum Foam HX Temperature Profile for 22K/20K Temperature Differential and 1MPa System Pressure, 5 g/s flow, Re=77088, Re_K=1633

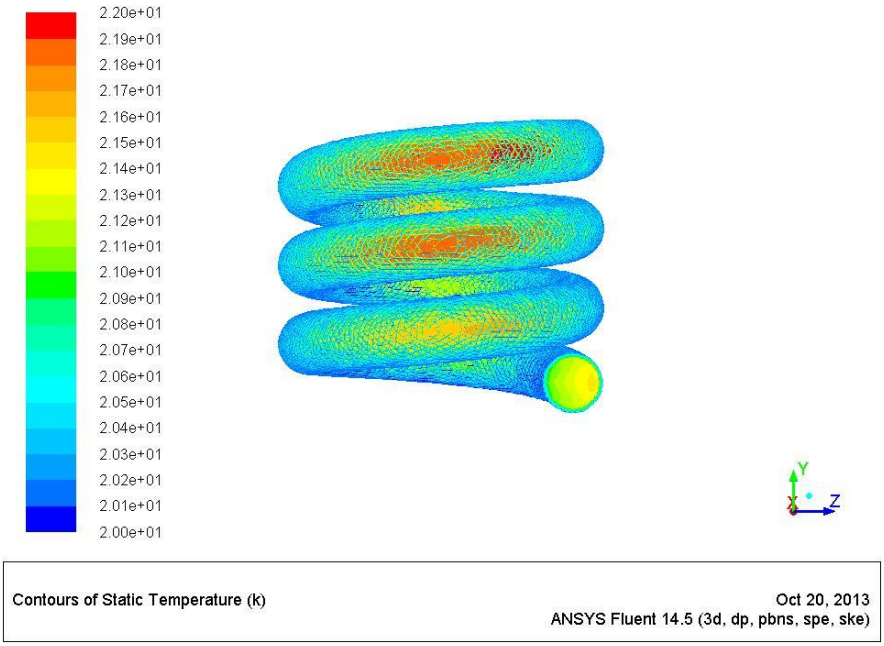

Figure 35: Helical HX Temperature Profile for 22K/20K Temperature Differential and 1MPa System Pressure, 5 g/s flow, Re=77088

4.2 System Pressure Drop and Weight

The graphite foam heat exchanger experienced the largest pressure drop of all the systems studied. However, aluminum and copper foam system pressure drops were only marginally lower than the graphite foam model. The smaller pressure drop for aluminum and copper foam models is attributed to the lower inertial and viscous flow resistance of these foams, as noted in Table 4. The following figures plot the calculated pressure drop for each system on a logarithmic plot versus inlet temperature.

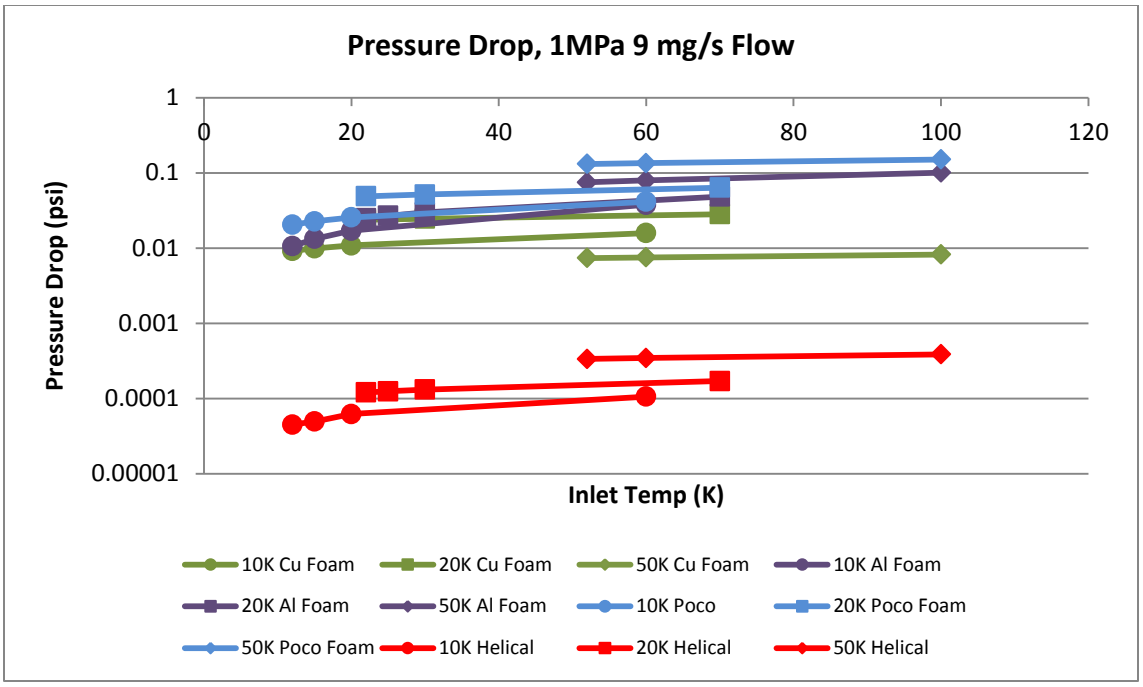

Figure 36: Heat exchanger pressure drop for 1MPa system pressure at 9 mg/s flow

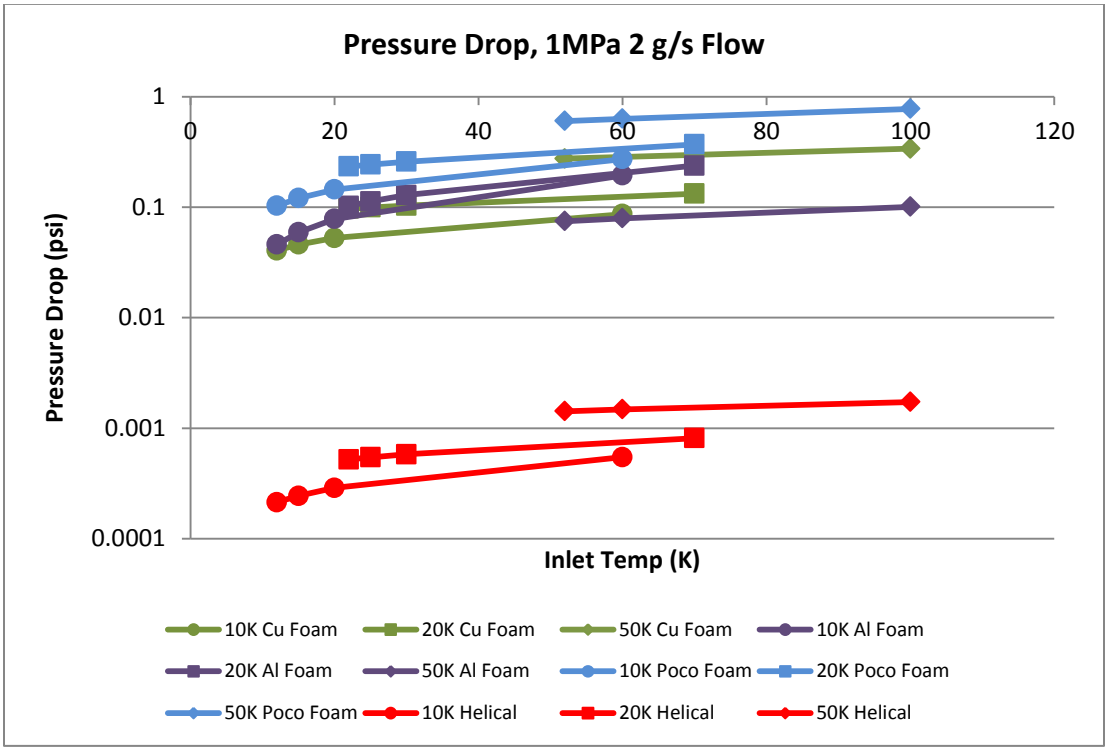

Figure 37: Heat exchanger pressure drop for 1MPa system pressure at 2 g/s flow

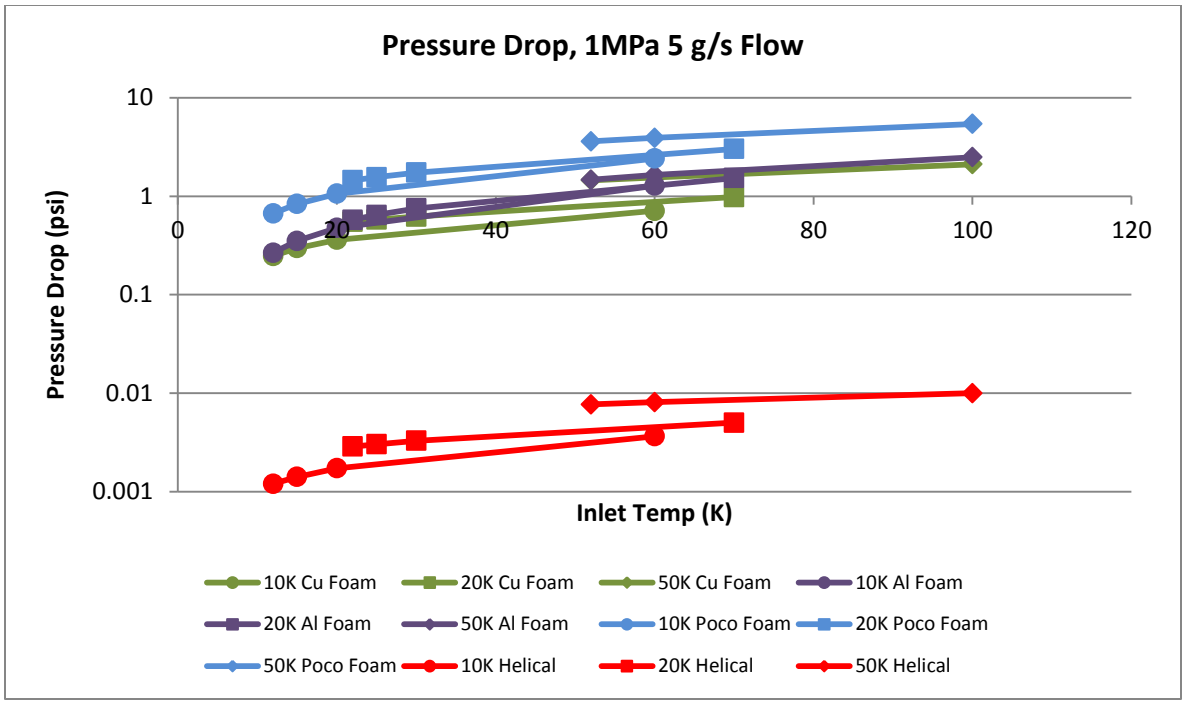

Figure 38: Heat exchanger pressure drop for 1MPa system pressure at 5 g/s flow

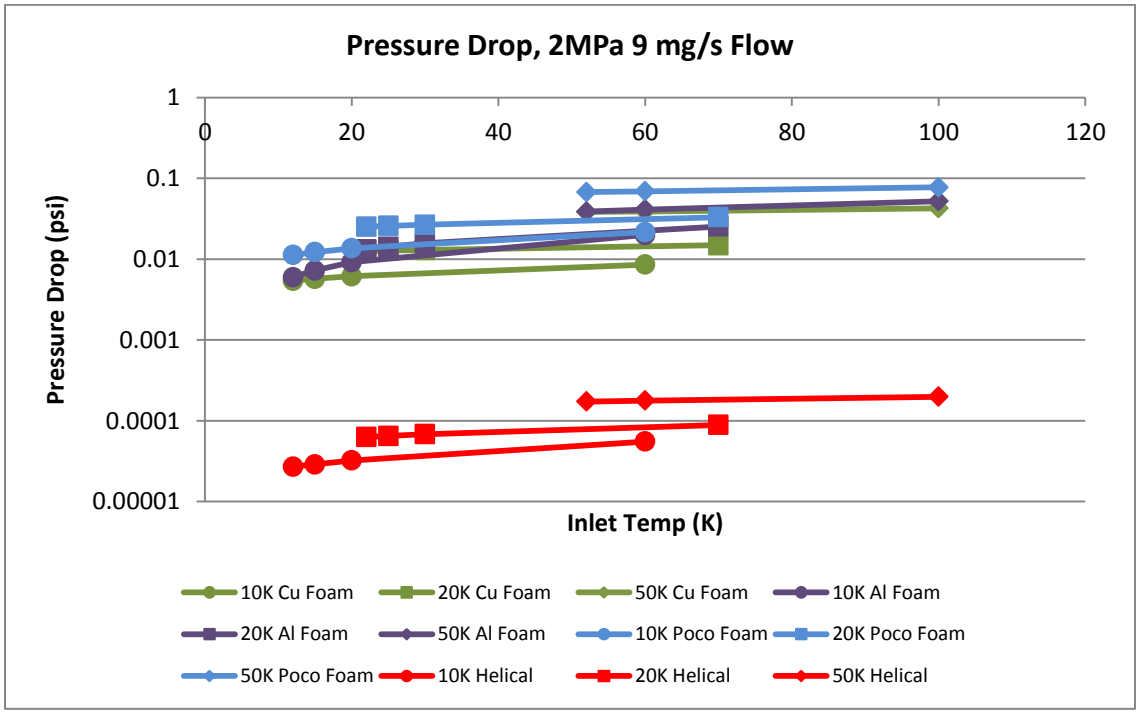

Figure 39: Heat exchanger pressure drop for 2MPa system pressure at 9 mg/s flow

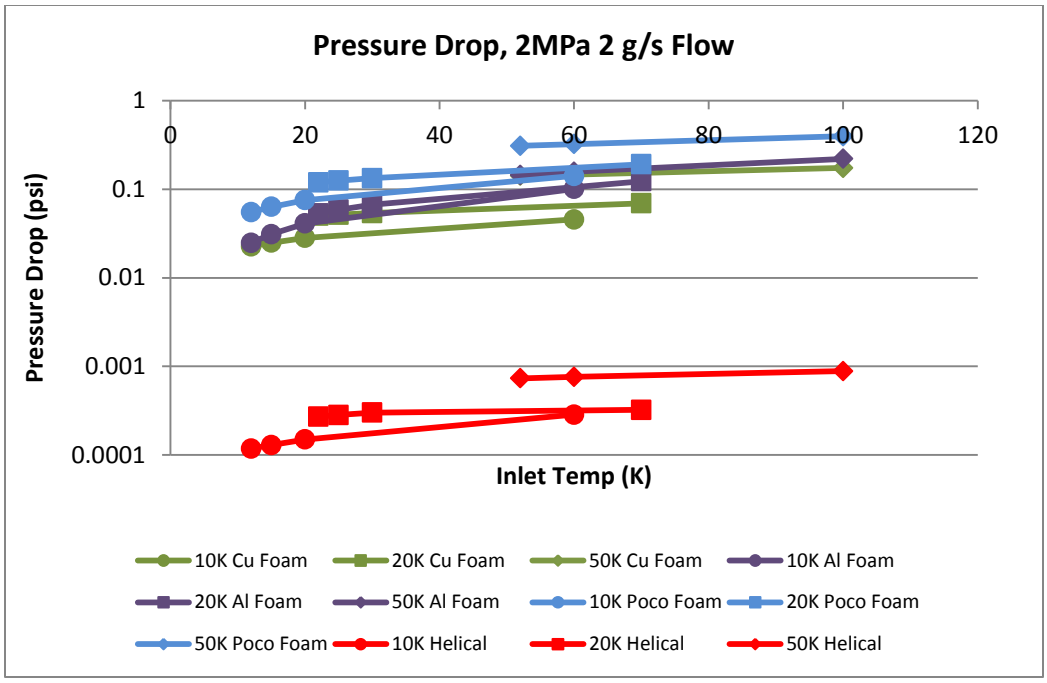

Figure 40: Heat exchanger pressure drop for 2MPa system pressure at 2 g/s flow

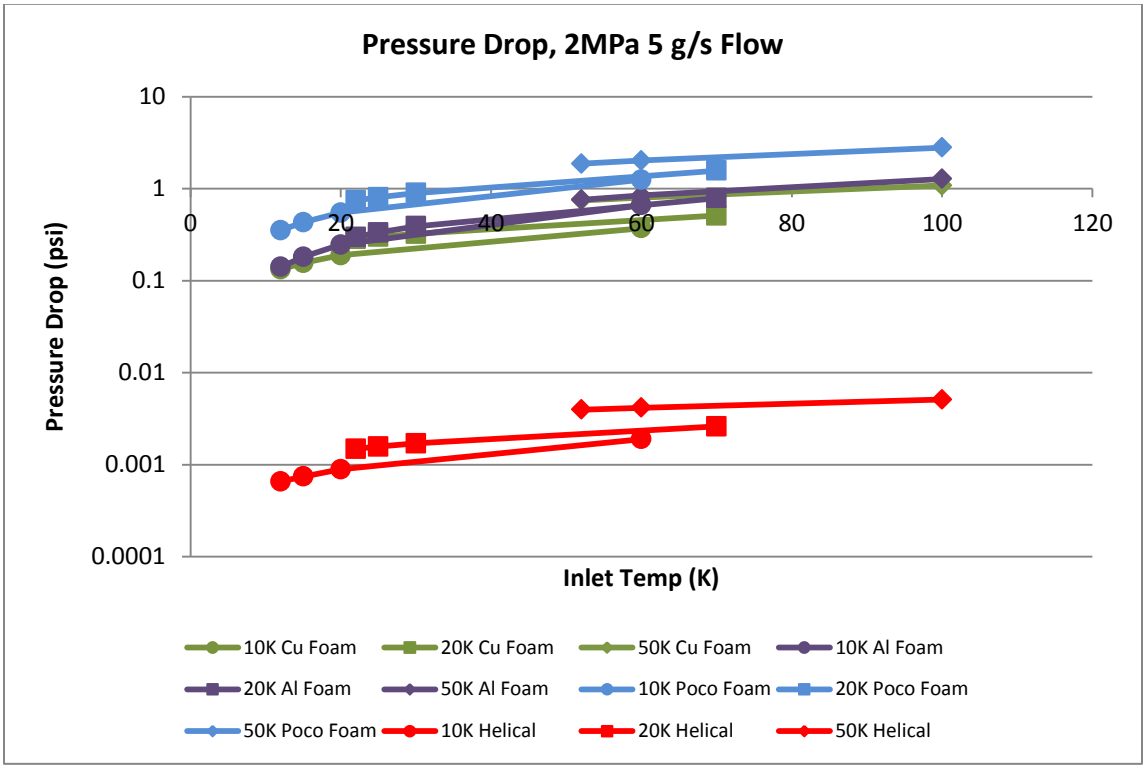

Figure 41: Heat exchanger pressure drop for 2MPa system at 5 g/s flow

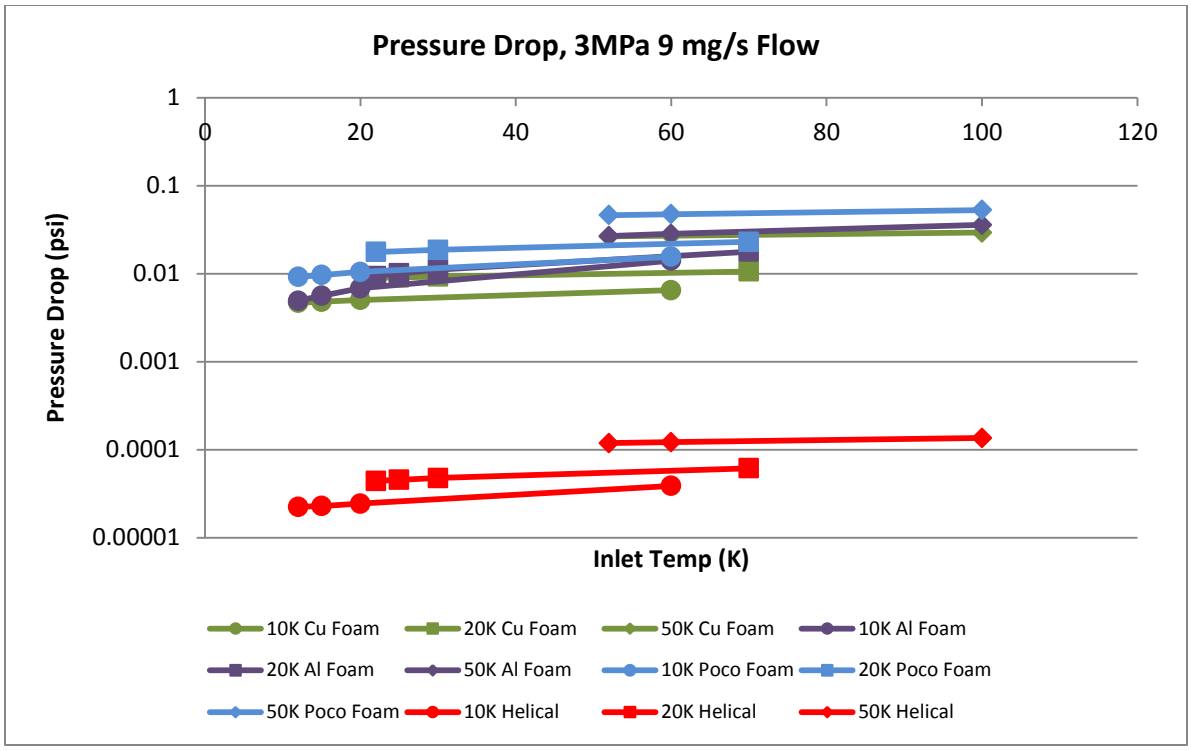

Figure 42: Heat exchanger pressure drop for 3MPa system pressure at 9 mg/s flow

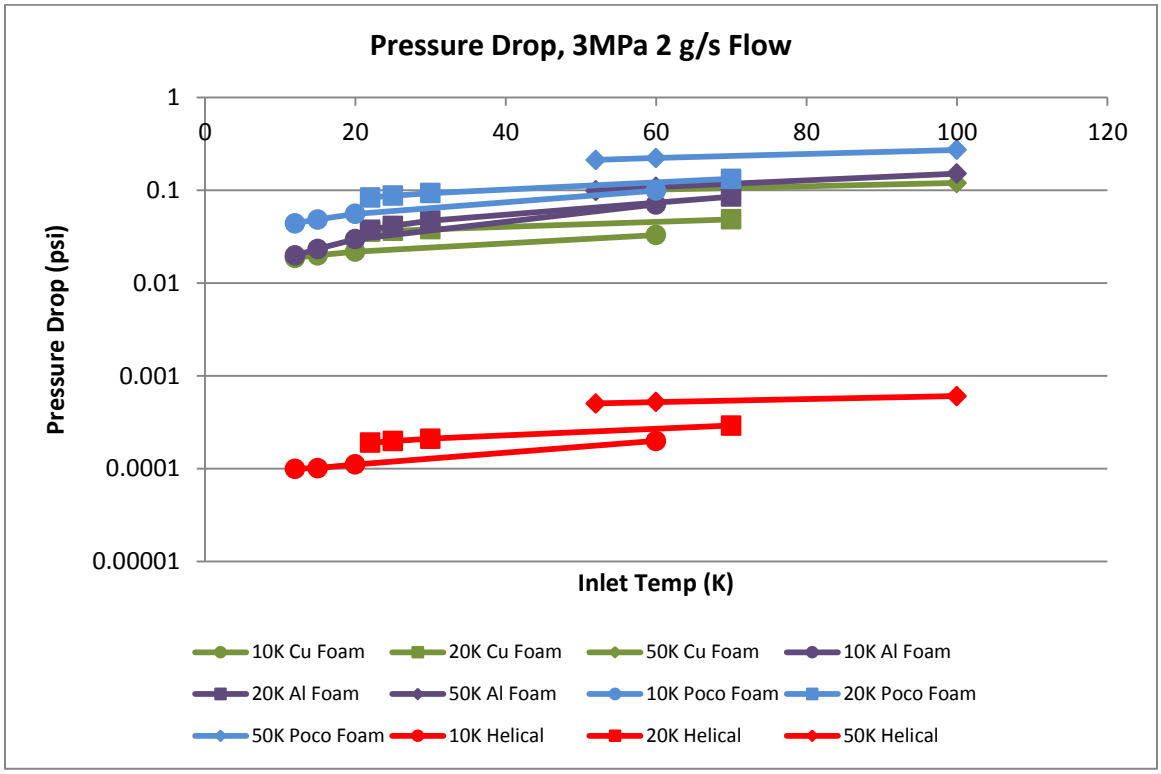

Figure 43: Heat exchanger pressure drop for 3MPa system pressure at 2 g/s flow

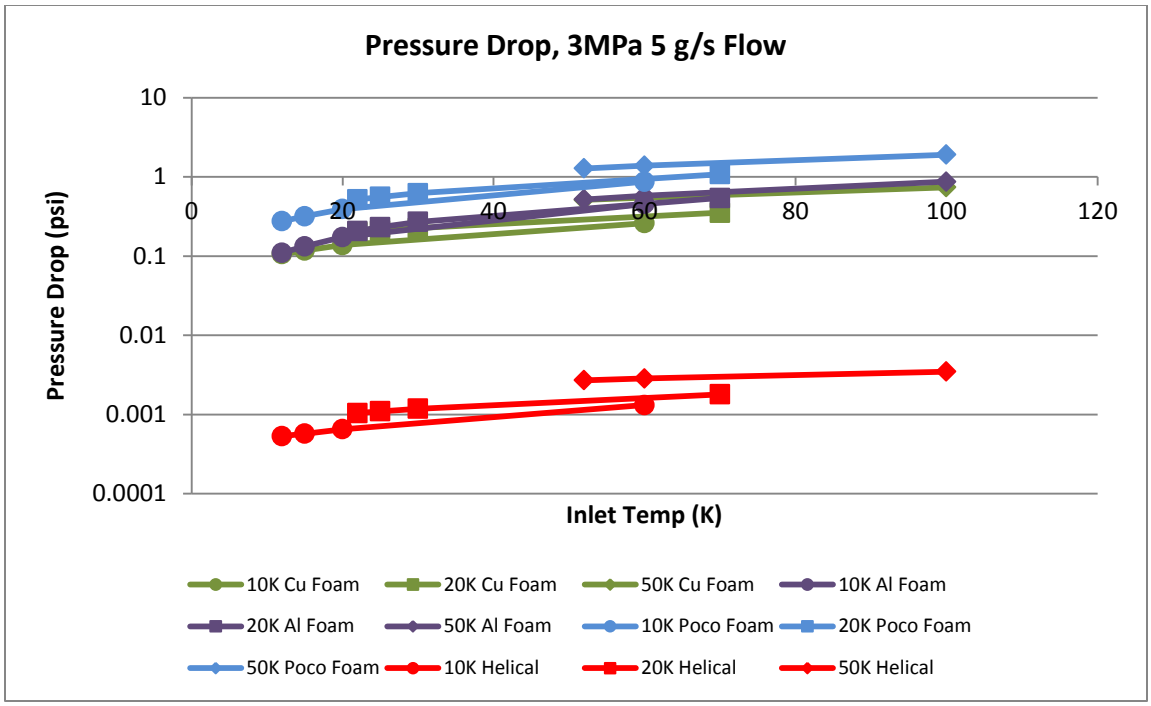

Figure 44: Heat exchanger pressure drop for 3MPa system pressure at 5 g/s flow

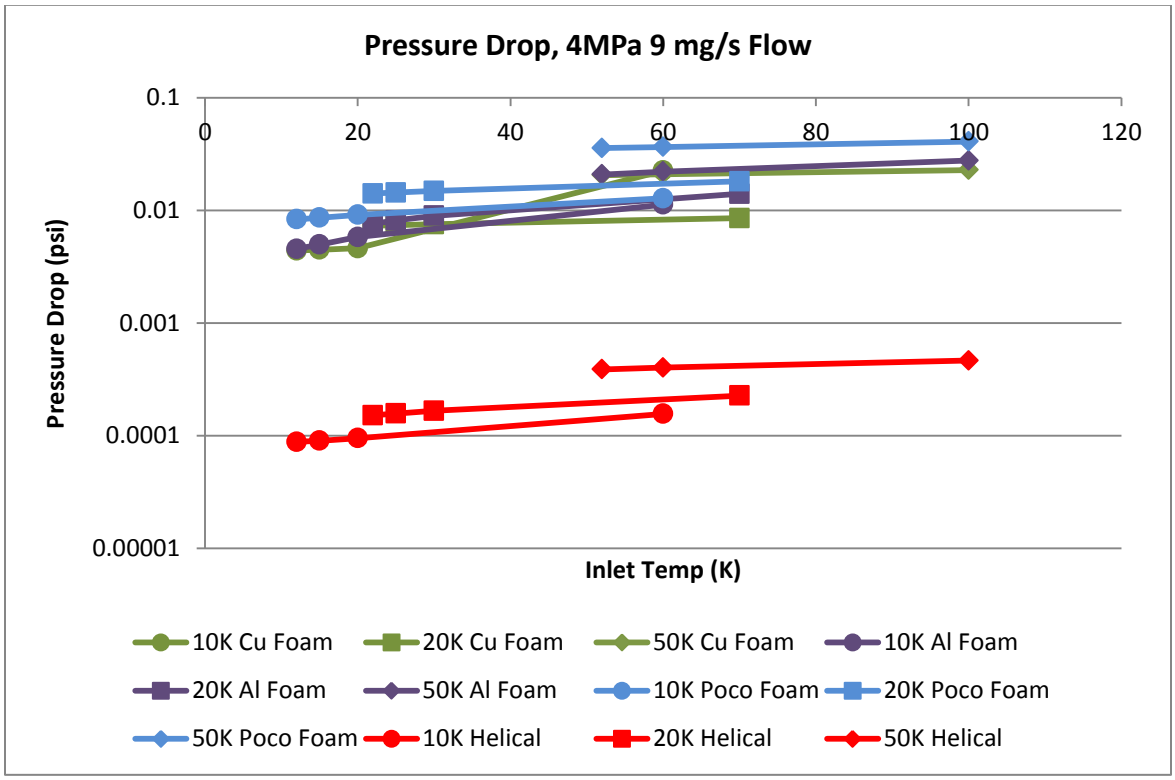

Figure 45: Heat exchanger pressure drop for 4MPa system pressure at 9 mg/s flow

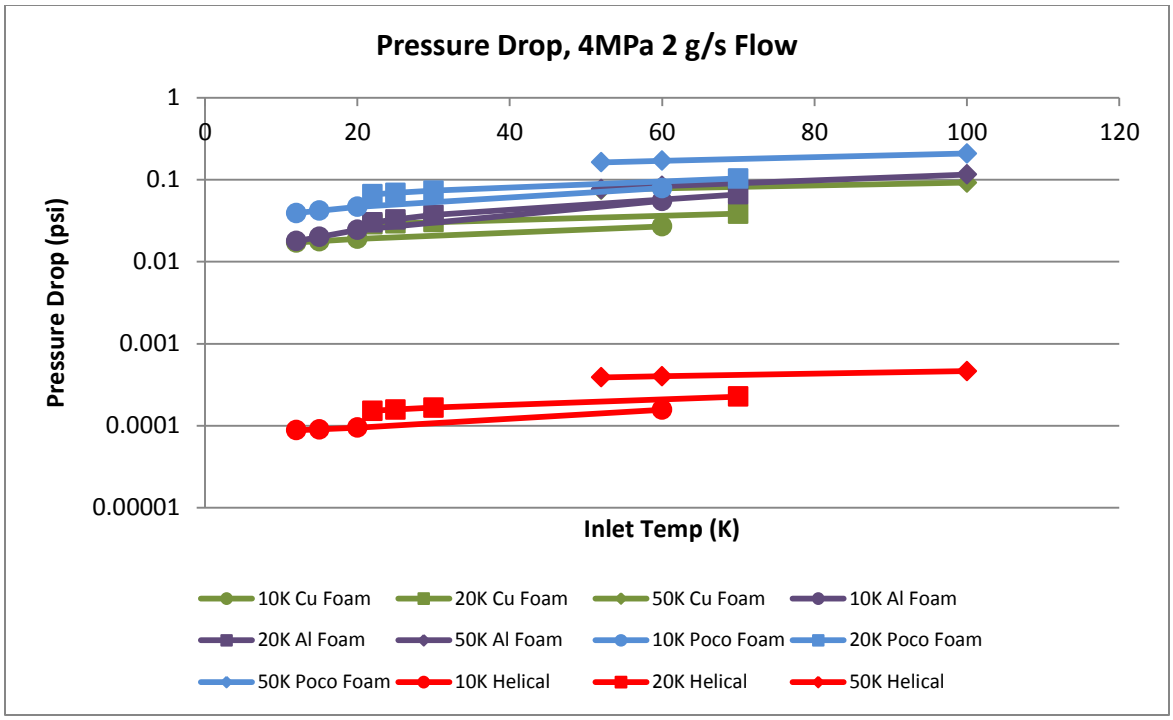

Figure 46: Heat exchanger pressure drop for 4MPa system pressure at 2 g/s flow

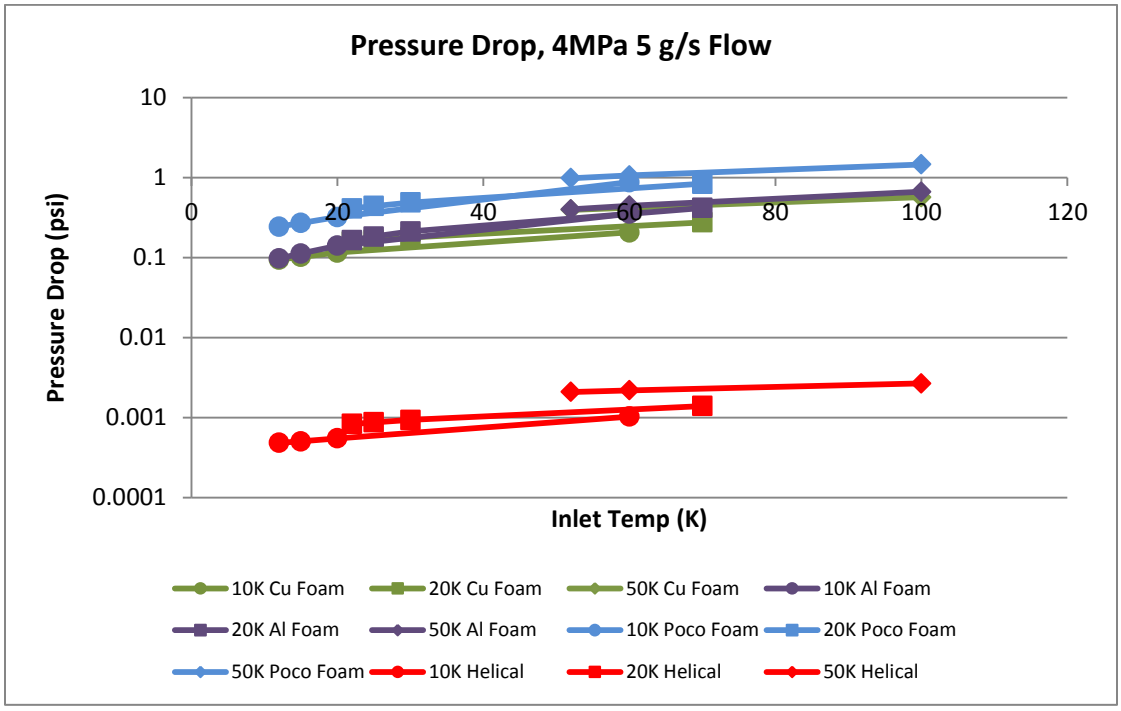

Figure 47: Heat exchanger pressure drop for 4MPa system pressure at 5 g/s flow

For the PocoFoam system, the greatest decrease in system differential pressure resulted from the increase of system pressure from one to two MPa. From one to two MPa, the pressure difference across the foam block dropped nearly 50%. From two to three MPa, the differential pressure only dropped by about 27%. Since the decrease in pressure differential diminishes as system pressure increases, cryogenic systems using graphite foam as a heat exchanger element would need to carefully balance the power requirements to maintain system pressure with the system effectiveness and pressure drop across the heat exchanger element.

For a better visualization of the tradeoff between pressure difference and effectiveness, these parameters were plotted against each other in the following figures.

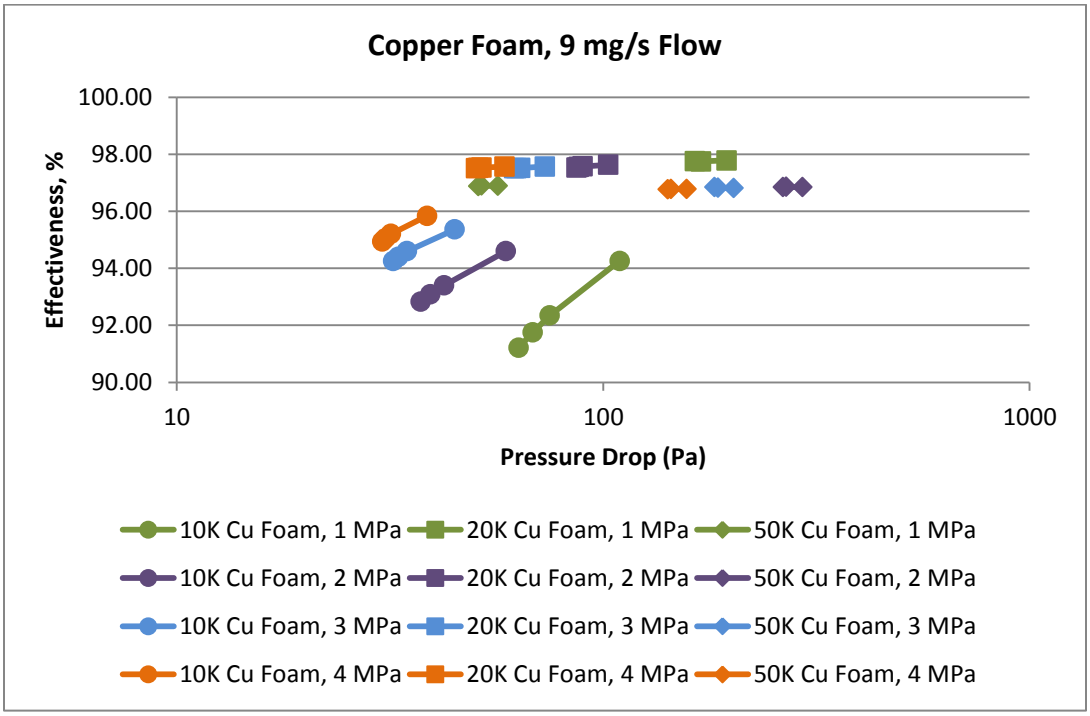

Figure 48: Effectiveness versus Pressure Drop for Copper Foam at 9 mg/s mass flow

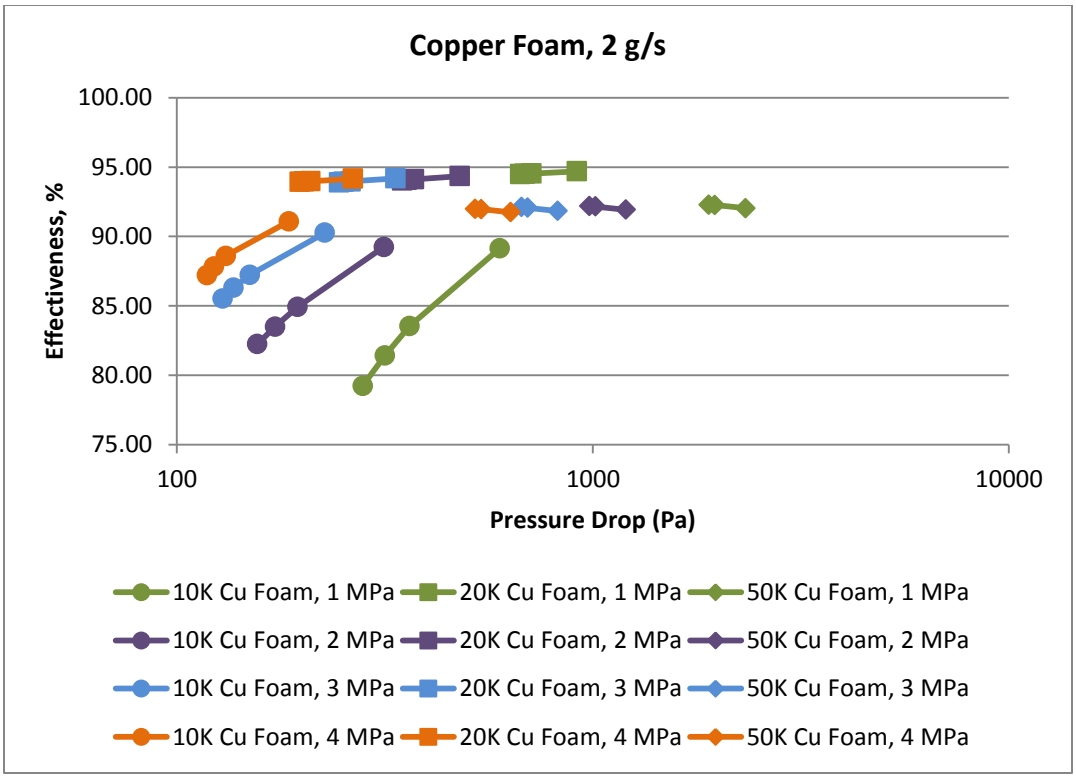

Figure 49: Effectiveness versus Pressure Drop for Copper Foam at 2 g/s mass flow

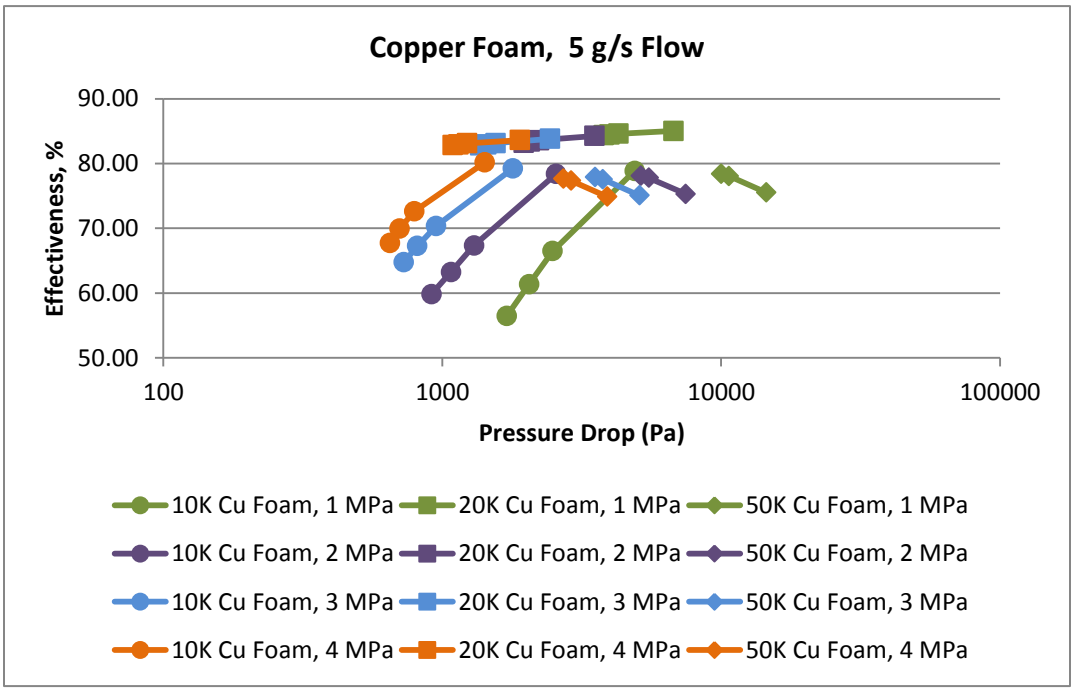

Figure 50: Effectiveness versus Pressure Drop for Copper Foam at 5 g/s mass flow

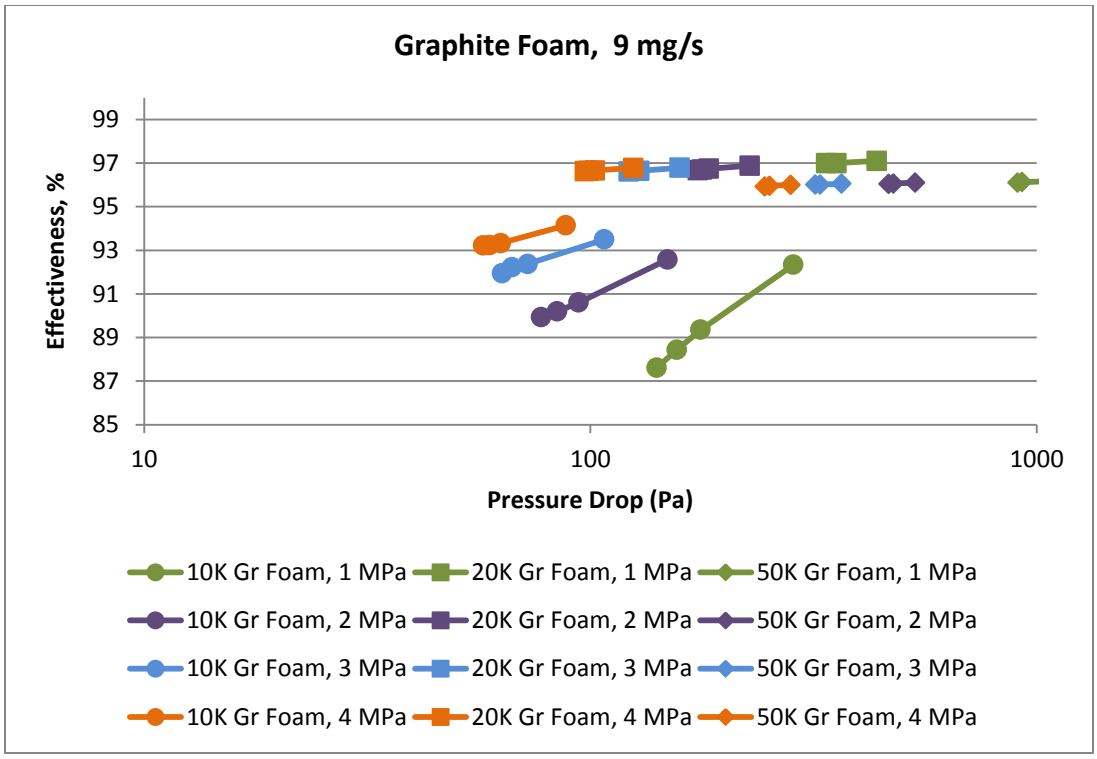

Figure 51: Effectiveness versus Pressure Drop for Graphite Foam at 9 mg/s mass flow

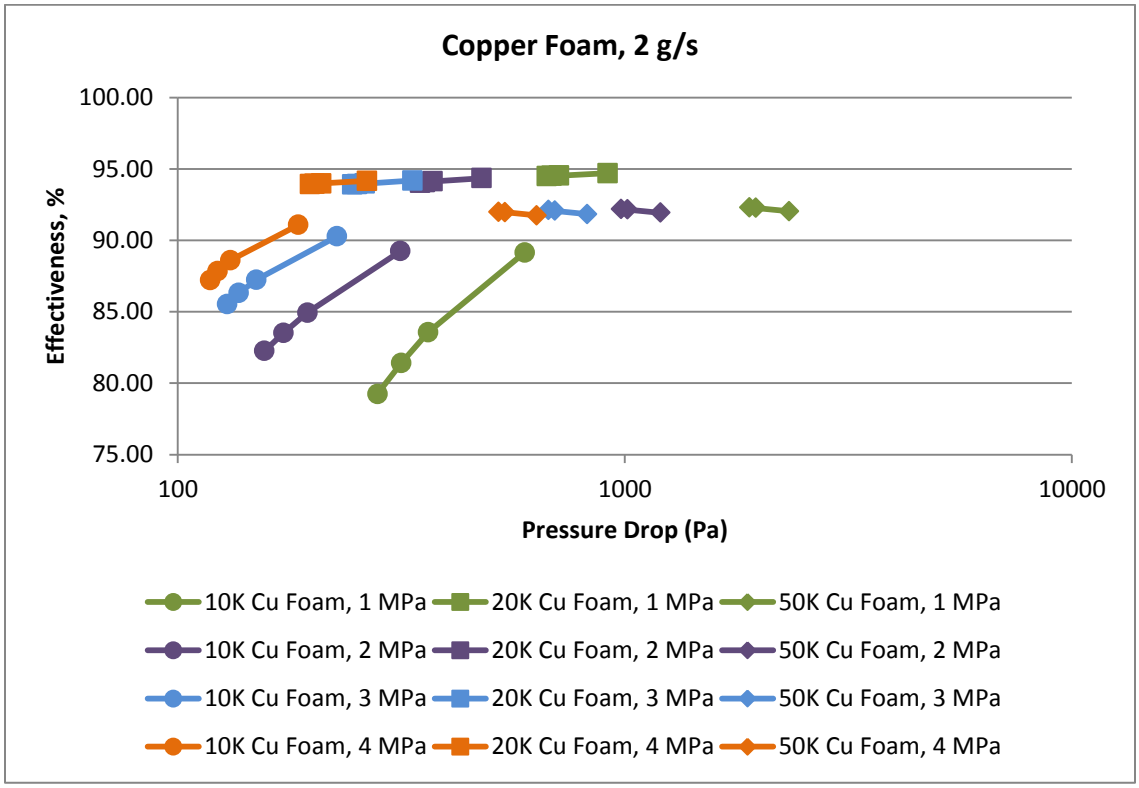

Figure 52: Effectiveness versus Pressure Drop for Graphite Foam at 2 g/s mass flow

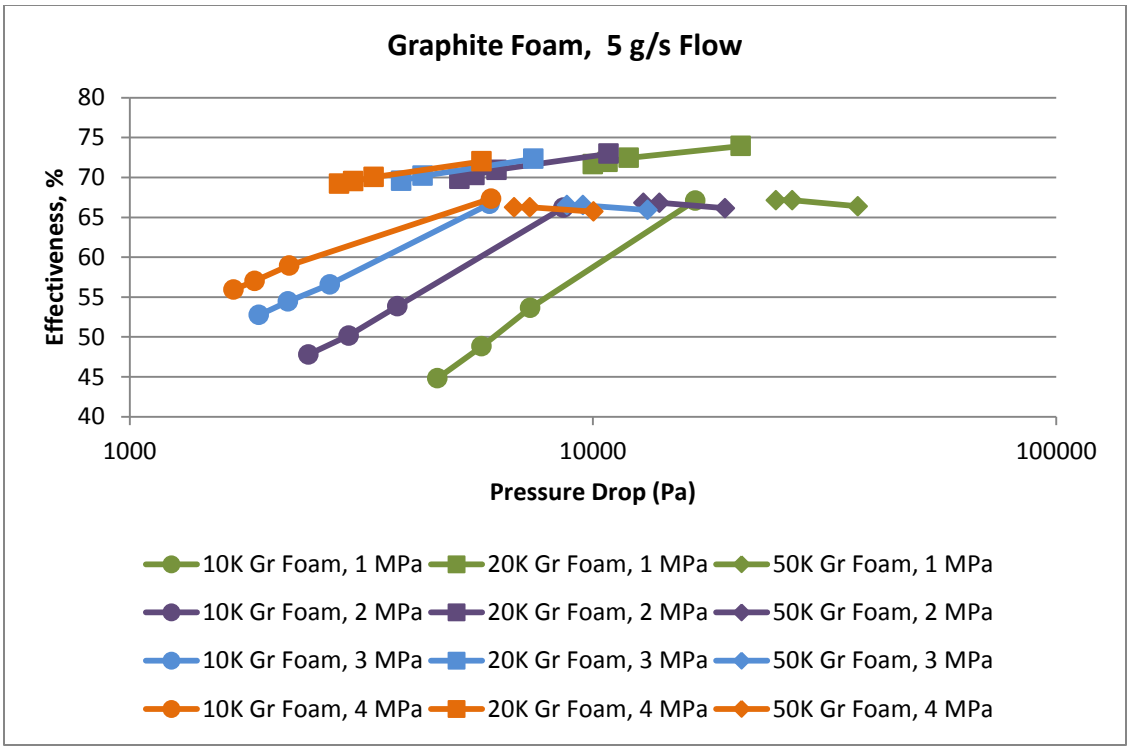

Figure 53: Effectiveness versus Pressure Drop for Graphite Foam at 5 g/s mass flow

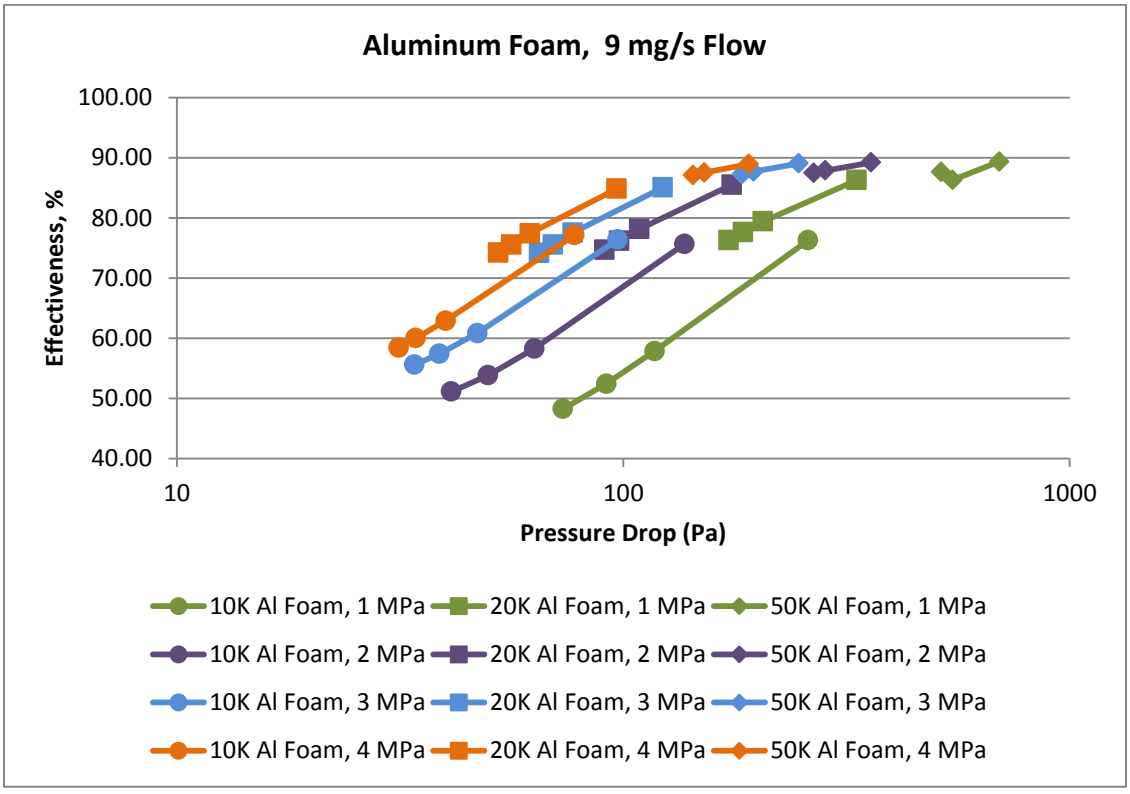

Figure 54: Effectiveness versus Pressure Drop for Aluminum Foam at 9 mg/s mass flow

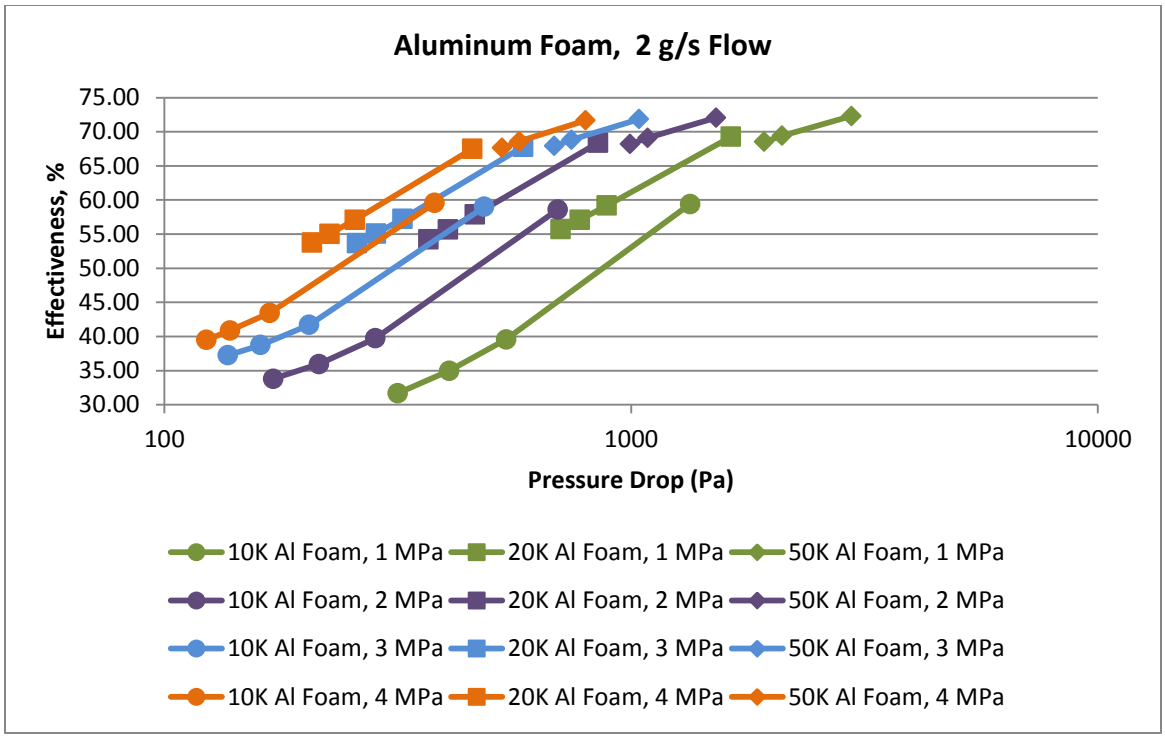

Figure 55: Effectiveness versus Pressure Drop for Aluminum Foam at 2 g/s mass flow

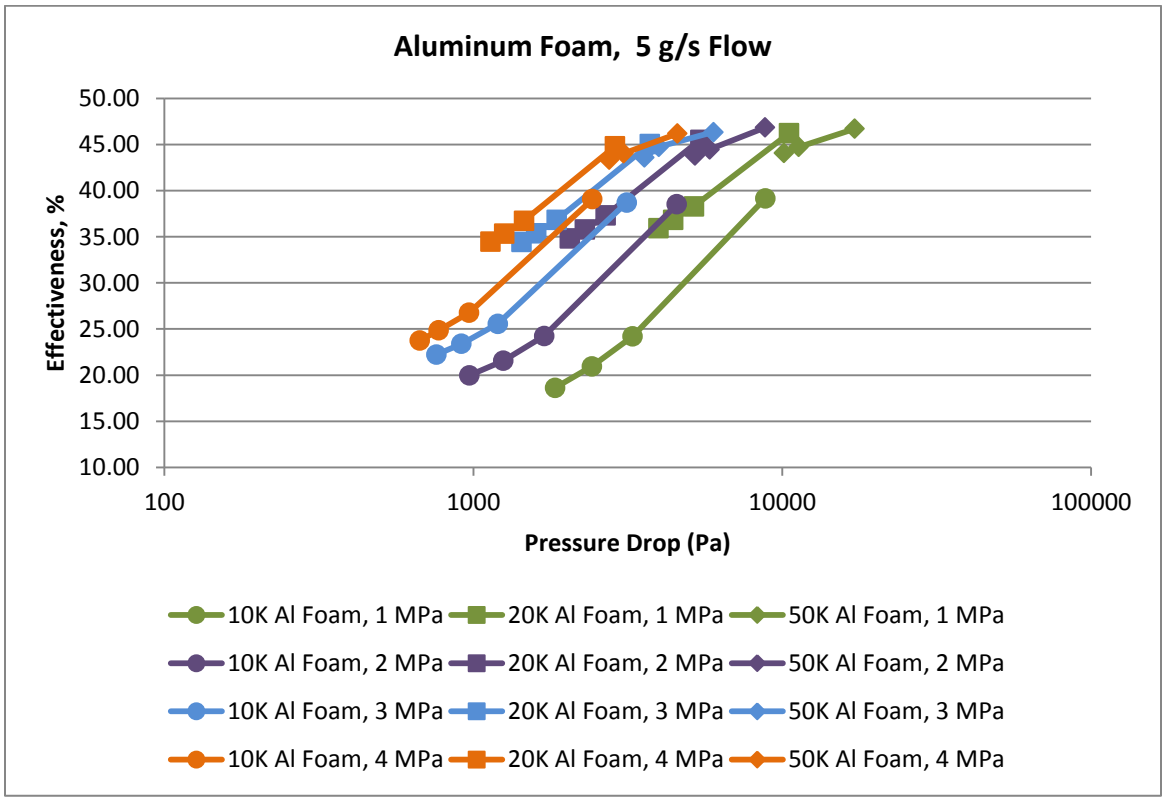

Figure 56: Effectiveness versus Pressure Drop for Aluminum Foam at 5 g/s mass flow

By plotting effectiveness versus pressure drop for each of the heat exchanger designs, the decrease in pressure difference across the foam element from 1 to 2 MPa can be clearly observed. By correlating the material properties of OFHC Copper and T-6061 Aluminum displayed in Figure 13 with Figures 48-56, it can be observed that the copper foam slopes become approximately horizontal for the 50 K cryocoolers. This flattened slope corresponds to the temperature range where the thermal conductivity of OFHC copper dramatically drops off. Likewise, the slope of the aluminum heat exchangers increases, corresponding with the increase of thermal conductivity of the material at the higher end of the temperature range studied. The change of slope for the graphite heat exchanger is attributed both to decreased residence time in the foam block, and the poor out-of-plane thermal conductivity of graphite foams.

The majority of literature sources that examine the pressure drop of a fluid crossing a foam heat exchanger element have involved experiments run near ambient pressure. The pressure drops reported in the figures above are significantly lower than many other studies, but this reduction can be attributed to the high system pressures examined. For comparison, a few additional cases were simulated at ambient pressure for the graphite foam model for comparison. The pressure drop results for ambient pressure through 4 MPa are reported below in Figure 57. Given these results, it is easy to see that the system pressure drop is dramatically reduced as the system pressure is increased from ambient to 1 MPa. However, the reduction of pressure drop is less pronounced as pressure is increased above 2 MPa. From these results, it is likely that system pressures between 1 and 2 MPa will yield the best balance of power required to maintain system pressure and pressure drop across the heat exchanger element.

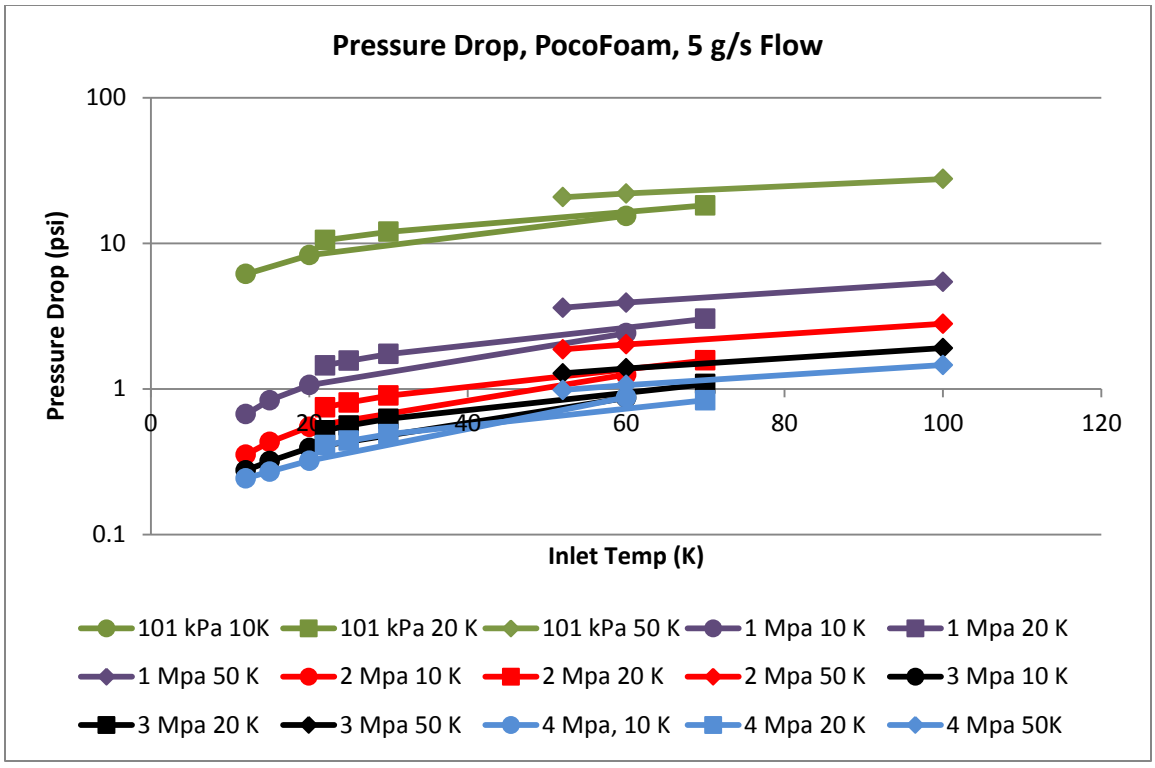

Figure 57: Pressure drop comparison for various system pressures for PocoFoam

All three foam heat exchangers simulated weighed significantly less than the helical heat exchanger. Using the material properties outlined in Tables 1 and 2 and the geometry of the simulated heat exchangers, the mass of each heat exchanger design was calculated, and the results are displayed in Table 10 below. The calculations for these values can be found in Appendix E. As indicated in Figure 3, it is anticipated that the superconductor cooling system used as motivation for this study would require several cryogenic coolers in series to maintain superconductor temperatures at acceptable levels over long spans of distance. Reduction of cryogenic heat exchanger weight can therefore result in significant savings in terms fuel used to transport such a system in mobile applications on land, sea, or in the air.

The metal foam and graphite foam heat exchangers in this simulation used 95 percent less OFHC copper, and the foam inserts for each foam design had very little mass. The graphite and copper foam inserts were calculated to have a mass of 3.6 and 21.6 grams, respectively, while the aluminum foam insert was calculated to have a mass of 6.5 grams. The total heat exchanger mass for the graphite foam, copper foam and aluminum foam heat exchangers were calculated to have masses of 96, 114, and 98.9 grams, respectively.

Table 10: Calculated Mass of Simulated Heat Exchangers

Heat Exchanger Design	Calculated heat sink and piping mass [g]	Calculated foam insert mass [g]	Calculated Total Mass [g]
Helical	2159	N/A	2159
Graphite Foam	92.4	3.6	96.0
Aluminum Foam	92.4	6.5	98.9
Copper Foam	92.4	21.6	114.0

4.3 Error and Comparison to Experimental Data

For the data above, two types of error must be considered. The first is numerical error. In this study, calculation error was tabulated by comparing the heat flux in Watts through the cryogenic cooler to the change in enthalpy in the Helium. The calculation error for each case is tabulated in the appendices, and was generally below 0.2% for all cases considered.

The second type of error to consider is the possible discrepancy between the simulation and experimental data obtained from a physical system. The timeframe of this study did not allow for experiments to be performed. Fortier [51] studied a similar foam heat exchanger system in his thesis. In his study, the discrepancy between the experimental and calculated model could result in a discrepancy in the outlet fluid temperature of several degrees Kelvin. Fortier concluded that much of the discrepancy was the result of uncertainty in the quantification of foam parameters. As discussed in Chapter 1, pore size, specific surface area, viscous resistance and inertial resistance are all difficult to quantify due to the random nature of the foam and the small pore size.

Although an experiment was not performed for this study, it can be argued that the largest uncertainty comes from the quantification of foam parameters for each of the three foam models. These values are approximated from data in the literature, which itself shows variation in material properties. There is also some error that results from the piecewise linear approximation for OFHC copper properties. Since the properties of this copper were approximated in this fashion, there will be some error in the exact heat transfer from the pipe to the foam and helium.

The results of this study also must be considered in the context of the limitations and uncertainty of available data. The properties for OFHC copper and 6061-T6 aluminum were calculated based on the base material properties at cryogenic tables multiplied by one minus the porosity. Experimental data would be valuable to verify the accuracy of this calculation.

There was no available data on graphite foam thermal conductivity at cryogenic temperature ranges. Both OFHC copper and 6061-T6 aluminum have highly non-linear

behavior for thermal conductivity and specific heat at cryogenic temperature ranges. If graphite foam exhibits a similar temperature dependency, the actual heat transfer effectiveness may vary from the results simulated in this study.

The pressure drop results for these models are based on the viscous and inertial flow coefficients of the foams. Since these terms are calculated based on parameters such as measured pore size, which is difficult to accurately quantify, there is room for error in the flow resistance coefficients. These uncertainties would be best addressed by running experiments and using the data to back-calculate more accurate values for the flow resistance parameters.

4.4 Observations and Conclusions

In this study an attempt was made to compare the performance of cryogenic heat exchangers made of porous structures of metal foams and graphite foam with the performance of a conventional heat exchanger based on a helical tube. The results show that larger heat conduction is very advantageous to the foams as it helps the diffusion of heat in the lateral direction. However, the helical coil enjoys the advantage of fluid mixing caused by the curvilinear streamlines that result from the helical geometry. Such macroscopic mixing is of course absent in the foams. The secondary flows that are typical for helical tubes are known to cause mixing in such tubes. The mixing of the fluid helps heat transfer in helical tube significantly. The simulations confirm this. As a result, comparison between the helical coil and foam heat exchangers is not straightforward and is far from monotonic.

For metal and graphite foams, which are essentially porous structures subject to the flow of a cryogenic gaseous coolant (helium), the effectiveness depends on the mass flow rate, inlet temperature and cold tip temperature. The effect of mass flow rate is particularly important, because as the residence time of the fluid in the porous structure is reduced, the thermal boundary layer that represents the extent of thermal penetration in the fluid and porous structure becomes thinner. This thinning of the thermal boundary layer evidently deteriorates the performance of the heat exchanger because much of the fluid passes through the heat exchanger without cooling. The effectiveness of helical heat exchangers is dependent on the same parameters, but such heat exchangers have significantly lower pressure drops. At high coolant velocities, the helical heat exchanger was more effective than any of the porous heat exchangers studied, but at lower coolant velocities, a heat exchanger using PocoFoam as a heat transfer element can be significantly more effective than the helical design.

For all foam heat exchangers and the helical heat exchanger, the highest effectiveness was achieved by systems with lower mass flow rates. At low mass flow rates, the copper and graphite foam heat exchangers had the highest effectiveness and lowest pressure drops of all the foam configurations studied.

The graphite and copper heat exchangers performed considerably better than the aluminum and helical heat exchangers. The simulations showed that at low flows, the effectiveness of copper and graphite foam heat exchangers differed by only 1 or 2 percent, but as flow rate increased, copper foam heat exchangers were over 10 percent more effective. This difference in performance is attributed to the comparatively poor out-of-plane conduction of the graphite foam and the decrease fluid residence time at higher flow rates.

Because of the changes in helium properties discussed in section 4.1.1, cryogenic coolers operating below 20 K should be operated at higher system pressures to take advantage of the favorable changes in helium properties at this temperature and pressure. Cryogenic cooling systems operating above 20 K did not show significant changes in effectiveness as system pressure was varied, however, for the metal foam systems, the system differential pressure decreased when the system operating pressure increased.

CHAPTER 5

5.1 Summary and Closing

In this study, the performance of four cryogenic heat exchanger designs was simulated using the ANSYS FLUENT CFD software. Cryogenic cooler temperatures of 10K, 20K and 50K were considered. Inlet temperatures 2K, 5K, 10K and 50K above the cryogenic cooler temperature simulated for each cryogenic cooler temperature. Each of these cases was simulated at system pressures of 1, 2, 3, and 4 MPa for mass flow rates of 9, 20 and 50 milligrams per second. In the preceding sections, several figures detail the system pressure drop and effectiveness of each of these cases. The mass of each system was also calculated and compared in section 4.2.

For the 9, 20 and 50 milligram per second mass flow rates, the copper foam heat exchanger was the most effective. At 9 milligrams per second, the copper foam heat exchanger was only 1 or 2 percent more effective than the graphite foam heat exchanger. However, as the flow rate increased to 5 grams per second, the copper foam heat exchanger was over 10 percent more effective than the graphite foam heat exchanger due to the low out-of-plane heat conduction of the graphite foam. In all cases considered, the aluminum foam and helical heat exchangers were significantly less effective than the graphite and copper foam designs.

In every simulated system condition, the helical heat exchanger had the lowest system pressure drop of the four simulated heat exchangers. The graphite foam heat exchanger always had the highest pressure drop of each of the systems considered due to its high inertial and viscous flow resistance. The aluminum and copper foam heat

exchangers had comparable pressure drop to the graphite foam heat exchanger, but were always lower.

Each of the three foam-based heat exchangers had approximately 95 percent less mass than the helical heat exchanger. Since the copper and graphite foam heat exchanger models exceeded the effectiveness of the helical heat exchanger, significant weight reductions and effectiveness improvements can be realized with copper and graphite foam heat exchanger designs in low mass flow rate conditions.

Optimally, the copper and graphite foam heat exchangers simulated above should be operated with low flow rates and low system pressures. At lower operating pressures and flow rates, the working fluid can be circulated through the system with less system input power. However, the results from this study need to be incorporated into a more macroscopic study of a superconductor cooling system. Low system flows may result in lower convective heat transfer from the superconductor, and the pressure drop across the foam element at low pressures may result in the need for booster fans in the cooling system to maintain system pressure.

5.2 Further Studies

Graphite and metal foams have been studied in a variety of applications at or above ambient temperature ranges, but little is known of the behaviors and properties of these foams at cryogenic temperatures. Further studies should include experiments designed to determine the thermal conductivity, Forchheimer and Darcy coefficients, and mechanical strength of copper, aluminum and graphite foams at cryogenic temperature ranges.

Existing literature largely studies metal and graphite foams used in heat exchange applications atmospheric pressure. Further study is needed to understand the effect of system pressure on pressure drop across a foam heat exchanger element.

The graphite and copper foam heat exchangers had significantly lower mass than the helical design, and were significantly more effective than the aluminum foam or helical models. However, the graphite foam heat exchanger had significantly higher pressure drops than the helical heat exchanger. Further studies could expand on the work of Lin et al [31] to examine the effect that geometric features such as grooves or holes incorporated into a graphite foam block would have on the balance of pressure drop reduction and subsequent effect on heat transfer effectiveness.

Further study should also examine the ability of graphite and metal foams to operate in high pressure cryogenic environments. This study did not consider the effect of temperature on the mechanical stability of the foam insert. Many authors have also discussed the limitations of various fixation methods such as brazes and epoxies. Future experimental studies would be valuable to determine whether which of the current mechanical attachment methods is best suited for cryogenic applications.

This study did not take mechanical attachment methods into account. As discussed in section 1.2.1, several methods including brazing, epoxy, and compression have been used as methods of attaching a metal or graphite foam to a heat sink. Experimental research data is needed to better understand which of these methods would be most suitable at cryogenic temperatures. Special mechanical attachment techniques may be needed to avoid thermal stress and degradation of the attachment method. Additionally, the thermal properties of the mechanical attachment may affect heat exchanger

performance. Depending on thermal conductivity and penetration of the attachment method into the foam, the effectiveness or flow characteristics may be altered.

APPENDIX A

PocoFoam Heat Exchanger Data

Table 11: 1MPa Data for PocoFoam Heat Exchanger

Flow	Inlet	Cryotip	In-enthalpy	out-enthalpy	cryo-enthalpy	effectiveness	Outlet temp	Pressure Drop	Cold tip	net enthalpy	Error
[kg/s]	[K]	[K]	[J/kg]	[J/kg]	[J/kg]	[%]	[K]	[psi]	[W]	[W]	[%]
0.001	12	10	54991	44692	40357	70.38	10.6	1.03E-01	-10.306	10.305	0.010
0.001	15	10	74487	49496	40357	73.22	11.2	1.21E-01	-25.038	25.034	0.016
0.001	20	10	104105	55480	40357	76.28	12.1	1.45E-01	-48.753	48.745	0.016
0.001	60	10	318548	82721	40357	84.77	16.3	2.72E-01	-236.540	236.490	0.021
0.001	22	20	115463	105146	104120	90.95	20.2	2.33E-01	-10.316	10.314	0.019
0.001	25	20	132190	106637	104120	91.03	20.4	2.43E-01	-25.552	25.546	0.023
0.001	30	20	159539	109018	104120	91.16	20.9	2.58E-01	-50.525	50.515	0.020
0.001	70	20	370873	126007	104120	91.80	23.9	3.70E-01	-245.080	245.010	0.029
0.001	52	50	276595	267264	266060	88.57	50.2	6.02E-01	-9.329	9.327	0.021
0.001	60	50	318596	272044	266060	88.61	51.1	6.31E-01	-46.547	46.536	0.024
0.001	100	50	527302	295875	266060	88.59	55.7	7.76E-01	-231.550	231.490	0.026
0.0025	12	10	54950	48411	40357	44.81	11.1	6.69E-01	-16.413	16.411	0.012
0.0025	15	10	74451	57807	40357	48.82	12.4	8.34E-01	-41.943	41.938	0.012
0.0025	20	10	104079	69905	40357	53.63	14.2	1.06E+00	-86.259	86.246	0.015
0.0025	60	10	318591	131922	40357	67.09	24.7	2.41E+00	-471.396	471.288	0.023
0.0025	22	20	115433	107328	104120	71.64	20.6	1.45E+00	-20.238	20.235	0.015
0.0025	25	20	132169	111986	104120	71.96	21.4	1.56E+00	-50.444	50.435	0.018
0.0025	30	20	159528	119385	104120	72.45	22.7	1.73E+00	-100.460	100.440	0.020
0.0025	70	20	370937	173650	104120	73.94	32.4	3.02E+00	-496.450	496.350	0.020
0.0025	52	50	276621	269531	266060	67.13	50.7	3.61E+00	-17.693	17.690	0.017
0.0025	60	50	318637	283340	266060	67.13	53.3	3.91E+00	-88.200	88.180	0.023
0.0025	100	50	527420	353944	266060	66.37	66.6	5.41E+00	-435.890	435.810	0.018
0.00045	12	10	54997	42171	40357	87.61	10.2	2.04E-02	-5.772	5.771	0.017
0.00045	15	10	74490	44305	40357	88.43	10.5	2.26E-02	-13.589	13.587	0.015
0.00045	20	10	104102	47142	40357	89.36	10.9	2.56E-02	-25.650	25.645	0.019
0.00045	60	10	318466	61664	40357	92.34	13.0	4.13E-02	-11.573	11.568	0.043
0.00045	22	20	115466	104461	104120	96.99	20.1	4.90E-02	-4.953	4.952	0.020
0.00045	30	20	159531	105783	104120	97.00	20.3	5.16E-02	-24.193	24.185	0.033
0.00045	70	20	370776	111858	104120	97.10	21.4	6.36E-02	-116.578	116.521	0.049
0.00045	52	50	276588	266471	266060	96.10	50.1	1.31E-01	-4.554	4.552	0.044
0.00045	60	50	318574	268097	266060	96.12	50.4	1.35E-01	-22.722	22.712	0.044
0.00045	100	50	527177	276090	266060	96.16	51.9	1.51E-01	-113.050	112.990	0.053

Table 12: Data for 2MPa PocoFoam Heat Exchanger

flow	Inlet	Cryotip	In-enthalpy	out-enthalpy	cryo-enthalpy	effectiveness	Outlet temp	Pressure Drop	Cold tip	net enthalpy	Error
	[K]	[K]	[J/kg]	[J/kg]	[J/kg]	[%]	[K]	[psi]	[W]	[W]	[%]
0.0025	12	10	48277	41842	34815	47.80	11.1	3.53E-01	-16.118	16.116	0.012
0.0025	15	10	68681	51690	34815	50.17	12.5	4.31E-01	-42.762	42.756	0.014
0.0025	20	10	100439	65098	34815	53.85	14.4	5.49E-01	-89.210	89.197	0.015
0.0025	60	10	320423	131332	34815	66.21	24.9	1.25E+00	-477.850	477.740	0.023
0.0025	22	20	112490	104083	100450	69.83	20.6	7.47E-01	-20.990	20.986	0.019
0.0025	25	20	130092	109254	100450	70.30	21.5	8.06E-01	-52.080	52.070	0.019
0.0025	30	20	158551	117332	100450	70.94	22.8	8.98E-01	-103.160	103.140	0.019
0.0025	70	20	373141	174174	100450	72.96	32.6	1.57E+00	-500.810	500.710	0.020
0.0025	52	50	278027	270894	267350	66.81	50.7	1.86E+00	-17.799	17.796	0.017
0.0025	60	50	320461	284977	267350	66.81	53.3	2.02E+00	-85.660	85.640	0.023
0.0025	100	50	530209	356373	267350	66.13	66.7	2.80E+00	-43.675	43.667	0.018
0.001	12	10	48283	38320	34815	73.98	10.5	5.52E-02	-9.964	9.962	0.020
0.001	15	10	68690	43158	34815	75.37	11.2	6.35E-02	-25.561	25.558	0.012
0.001	20	10	100446	49652	34815	77.39	12.2	7.55E-02	-50.905	50.897	0.016
0.001	60	10	320390	79032	34815	84.52	16.5	1.41E-01	-242.130	242.080	0.021
0.001	22	20	112500	101648	100450	90.06	20.2	1.20E-01	-10.849	10.847	0.018
0.001	25	20	130098	103353	100450	90.21	20.5	1.25E-01	-26.742	26.736	0.022
0.001	30	20	158552	106029	100450	90.40	20.9	1.33E-01	-52.526	52.515	0.021
0.001	70	20	373092	124356	100450	91.23	24.0	1.92E-01	-248.960	248.900	0.024
0.001	52	50	278011	268588	267350	88.39	50.2	3.09E-01	-9.421	9.419	0.021
0.001	60	50	320436	273494	267350	88.43	51.2	3.24E-01	-46.935	46.925	0.021
0.001	100	50	530126	297760	267350	88.43	55.7	3.98E-01	-232.490	232.420	0.030
0.00045	12	10	48283	36170	34815	89.94	10.2	1.13E-02	-5.451	5.450	0.018
0.00045	15	10	68688	38137	34815	90.19	10.5	1.22E-02	-13.751	13.748	0.022
0.00045	20	10	100440	40978	34815	90.61	10.9	1.36E-02	-26.771	26.765	0.022
0.00045	60	10	320306	56000	34815	92.58	13.1	2.16E-02	-119.100	119.050	0.042
0.00045	22	20	112500	100852	100450	96.66	20.1	2.52E-02	-5.243	5.241	0.038
0.00045	25	20	130094	101427	100450	96.70	20.2	2.58E-02	-12.903	12.899	0.031
0.00045	30	20	158542	102345	100450	96.74	20.3	2.67E-02	-25.295	25.287	0.032
0.00045	70	20	372995	108952	100450	96.88	21.4	3.30E-02	-118.890	118.830	0.050
0.00045	52	50	278006	267772	267350	96.04	50.1	6.76E-02	-4.607	4.605	0.043
0.00045	60	50	320416	269441	267350	96.06	50.4	6.92E-02	-22.946	22.936	0.044
0.00045	100	50	530005	277594	267350	96.10	51.9	7.75E-02	-113.650	113.580	0.062

Table 13: Data for 3MPa PocoFoam Heat Exchanger

flow	Inlet	Cryotip	In-enthalpy	out-enthalpy	cryo-enthalpy	effectiveness	Outlet temp	Pressure Drop	Cold tip	net enthalpy	Error
[kg/s]	[K]	[K]	[J/kg]	[J/kg]	[J/kg]	[%]	[K]	[psi]	[W]	[W]	[%]
0.001	12	10	47631	38676	36236	78.59	10.5	4.40E-02	-8.953	8.951	0.022
0.001	15	10	66564	42540	36236	79.21	11.1	4.83E-02	-24.032	24.029	0.012
0.001	20	10	98436	48467	36236	80.34	12.1	5.55E-02	-50.027	50.019	0.016
0.001	60	10	322282	77752	36236	85.49	16.6	9.93E-02	-245.20	245.14	0.024
0.001	22	20	110796	99709	98444	89.76	20.2	8.36E-02	-11.084	11.082	0.018
0.001	25	20	128886	101523	98444	89.89	20.5	8.72E-02	-27.359	27.353	0.022
0.001	30	20	158094	104369	98444	90.07	21.0	9.29E-02	-53.726	53.715	0.020
0.001	70	20	375333	123583	98444	90.92	24.1	1.33E-01	-251.98	251.91	0.028
0.001	52	50	279522	270016	268750	88.25	50.2	2.12E-01	-9.503	9.501	0.021
0.001	60	50	322329	275037	268750	88.27	51.2	2.22E-01	-47.285	47.274	0.023
0.001	100	50	532948	299705	268750	88.28	55.8	2.71E-01	-233.360	233.300	0.026
0.0025	12	10	47633	41621	36236	52.75	11.0	2.76E-01	-15.030	15.028	0.013
0.0025	15	10	66564	50055	36236	54.43	12.4	3.19E-01	-41.160	41.154	0.015
0.0025	20	10	98436	63239	36236	56.59	14.4	3.92E-01	-88.597	88.583	0.016
0.0025	60	10	322313	131556	36236	66.68	25.2	8.68E-01	-481.980	481.870	0.023
0.0025	22	20	110793	102253	98444	69.16	20.6	5.19E-01	-21.318	21.314	0.019
0.0025	25	20	128885	107702	98444	69.59	21.5	5.59E-01	-52.935	52.925	0.019
0.0025	30	20	158097	116214	98444	70.21	22.9	6.23E-01	-104.820	104.800	0.019
0.0025	70	20	375379	175046	98444	72.34	32.8	1.08E+00	-504.280	504.180	0.020
0.0025	52	50	279534	272360	268750	66.52	50.7	1.28E+00	-17.900	17.897	0.017
0.0025	60	50	322348	286693	268750	66.52	53.3	1.38E+00	-89.084	89.066	0.020
0.0025	100	50	533018	358836	268750	65.91	66.7	1.90E+00	-437.590	437.500	0.021
0.00045	12	10	47329	37129	36236	91.95	10.2	9.20E-03	-4.726	4.724	0.042
0.00045	15	10	66560	38596	36236	92.22	10.4	9.67E-03	-12.586	12.583	0.024
0.00045	20	10	98428	40980	36236	92.37	10.9	1.05E-02	-25.859	25.853	0.023
0.00045	60	10	322196	54832	36236	93.50	13.1	1.56E-02	-120.440	120.390	0.042
0.00045	22	20	110794	98863	98444	96.61	20.1	1.77E-02	-5.370	5.369	0.019
0.00045	30	20	158082	100444	98444	96.65	20.3	1.87E-02	-25.944	25.936	0.031
0.00045	70	20	375234	107352	98444	96.78	21.4	2.30E-02	-120.610	120.550	0.050
0.00045	52	50	279517	269179	268750	96.02	50.1	4.63E-02	-4.653	4.651	0.043
0.00045	60	50	322309	270887	268750	96.01	50.4	4.74E-02	-23.148	23.137	0.048
0.00045	100	50	532826	279185	268750	96.05	51.9	5.30E-02	-114.200	114.130	0.061

Table 14: Data for 4MPa PocoFoam Heat Exchanger

flow	Inlet	Cryotip	In-enthalpy	out-enthalpy	cryo-enthalpy	effectiveness	Outlet temp	Pressure Drop	Cold tip	net enthalpy	Error
[kg/s]	[K]	[K]	[J/kg]	[J/kg]	[J/kg]	[%]	[K]	[psi]	[W]	[W]	[%]
0.001	12	10	49606	41323	39393	81.10	10.4	3.92E-02	-8.280	8.279	0.012
0.001	15	10	69868	44483	39393	83.30	11.0	4.19E-02	-22.507	22.503	0.018
0.001	20	10	97953	49723	39393	82.36	12.0	4.67E-02	-48.260	48.252	0.017
0.001	60	10	324233	78140	39393	86.40	16.7	7.89E-02	-246.630	246.570	0.024
0.001	22	20	110314	99220	97961	89.81	20.2	6.64E-02	-11.092	11.089	0.027
0.001	25	20	128562	101050	97961	89.91	20.5	6.90E-02	-27.507	27.501	0.022
0.001	30	20	158185	103952	97961	90.05	21.0	7.33E-02	-54.232	54.221	0.020
0.001	70	20	377603	123642	97961	90.82	24.2	1.03E-01	-254.180	254.110	0.028
0.001	52	50	281135	271558	270260	88.06	50.2	1.63E-01	-9.574	9.572	0.021
0.001	60	50	324280	276680	270260	88.12	51.2	1.70E-01	-47.592	47.581	0.023
0.001	100	50	535766	301713	270260	88.15	55.8	2.08E-01	-23.417	23.410	0.030
0.0025	12	10	49610	43897	39393	55.92	10.9	2.43E-01	-14.273	14.271	0.014
0.0025	15	10	66990	51249	39393	57.04	12.3	2.70E-01	-39.413	39.407	0.015
0.0025	20	10	97957	63431	39393	58.95	14.4	3.20E-01	-86.696	86.682	0.016
0.0025	60	10	324263	132454	39393	67.33	25.4	8.75E-01	-484.340	484.230	0.023
0.0025	22	20	110315	101766	97961	69.20	20.6	4.11E-01	-21.339	21.335	0.019
0.0025	25	20	128564	107285	97961	69.53	21.5	4.40E-01	-53.168	53.158	0.019
0.0025	30	20	158189	115998	97961	70.05	22.9	4.88E-01	-105.570	105.550	0.019
0.0025	70	20	377646	176254	97961	72.01	32.9	8.35E-01	-506.900	506.800	0.020
0.0025	52	50	281145	273936	270260	66.23	50.7	9.81E-01	-17.988	17.985	0.017
0.0025	60	50	324297	288490	270260	66.26	53.4	1.06E+00	-89.456	89.441	0.017
0.0025	100	50	535830	361324	270260	65.71	66.8	1.46E+00	-438.360	438.280	0.018
0.00045	12	10	49603	40085	39393	93.22	10.1	8.34E-03	-4.284	4.282	0.047
0.00045	15	10	66982	41258	39393	93.24	10.4	8.62E-03	-11.578	11.575	0.026
0.00045	20	10	97944	43301	39393	93.33	10.8	9.14E-03	-24.596	24.589	0.028
0.00045	60	10	324144	56073	39393	94.14	13.1	1.28E-02	-120.733	120.681	0.043
0.00045	22	20	110312	98378	97961	96.62	20.1	1.41E-02	-5.371	5.370	0.019
0.00045	25	20	128556	98990	97961	96.64	20.2	1.44E-02	-13.308	13.304	0.030
0.00045	30	20	158172	99973	97961	96.66	20.3	1.48E-02	-26.196	26.187	0.034
0.00045	70	20	377502	106981	97961	96.77	21.5	1.81E-02	-121.801	121.741	0.049
0.00045	52	50	281130	270703	270260	95.92	50.1	3.57E-02	-4.694	4.692	0.043
0.00045	60	50	324260	272444	270260	95.96	50.4	3.65E-02	-23.325	23.315	0.043
0.00045	100	50	535643	280874	270260	96.00	52.0	4.08E-02	-114.710	114.640	0.061

APPENDIX B

Data for Aluminum Foam Heat Exchanger

Table 15: Data for 1MPa Aluminum Foam Heat Exchanger

flow	Inlet	Cryotip	In-enthalpy	out-enthalpy	cryo-enthalpy	Effectiveness	Outlet temp	Pressure Drop	Cold tip	net enthalpy	Error
[kg/s]	[K]	[K]	[J/kg]	[J/kg]	[J/kg]	[%]	[K]	[psi]	[W]	[W]	%
0.00045	12	10	54997	47933	40357	48.25	11.0	1.06E-02	-3.168	3.167	0.032
0.00045	15	10	74490	56598	40357	52.42	12.2	1.33E-02	-8.099	8.096	0.037
0.00045	20	10	104101	67219	40357	57.86	13.8	1.70E-02	-16.764	16.757	0.042
0.00045	60	10	318462	106341	40357	76.27	20.2	3.76E-02	-96.133	96.084	0.051
0.00045	22	20	115466	106811	104120	76.28	20.5	2.50E-02	-3.876	3.874	0.052
0.00045	25	20	132190	110407	104120	77.60	21.1	2.69E-02	-9.771	9.767	0.041
0.00045	30	20	159530	115525	104120	79.42	22.0	2.98E-02	-19.776	19.768	0.040
0.00045	70	20	370773	140754	104120	86.26	26.5	4.84E-02	-103.713	103.655	0.056
0.00045	52	50	276587	267361	266060	87.64	50.3	7.47E-02	-4.145	4.144	0.024
0.00045	60	50	318572	273249	266060	86.31	51.2	7.93E-02	-20.787	20.777	0.048
0.00045	100	50	527174	293886	266060	89.34	55.3	1.01E-01	-104.995	104.927	0.065
0.001	12	10	54995	50358	40357	31.68	11.3	4.59E-02	-4.627	4.625	0.043
0.001	15	10	74489	62556	40357	34.96	13.1	5.91E-02	-12.093	12.088	0.041
0.001	20	10	104105	78877	40357	39.57	15.7	7.83E-02	-25.794	25.784	0.039
0.001	60	10	318543	153321	40357	59.39	28.3	1.94E-01	-168.380	168.320	0.036
0.001	22	20	115466	109144	104120	55.72	20.9	1.02E-01	-6.270	6.267	0.048
0.001	25	20	132192	116163	104120	57.10	22.1	1.13E-01	-15.983	15.977	0.038
0.001	30	20	159538	126733	104120	59.20	24.0	1.29E-01	-32.893	32.881	0.036
0.001	70	20	370866	186083	104120	69.27	34.6	2.37E-01	-186.780	186.710	0.037
0.001	52	50	276592	269376	266060	68.52	50.6	2.80E-01	-7.176	7.174	0.028
0.001	60	50	318591	282126	266060	69.42	53.1	3.05E-01	-36.342	36.331	0.030
0.001	100	50	527290	338406	266060	72.31	63.7	4.30E-01	-189.320	189.250	0.037
0.0025	12	10	54979	52256	40357	18.62	11.6	2.67E-01	-6.780	6.776	0.059
0.0025	15	10	74475	67328	40357	20.95	13.9	3.51E-01	-18.106	18.097	0.050
0.0025	20	10	104095	88662	40357	24.21	17.3	4.76E-01	-39.653	39.635	0.045
0.0025	60	10	318570	209634	40357	39.16	38.5	1.28E+00	-283.770	283.640	0.046
0.0025	22	20	115454	111383	104120	35.92	21.3	5.77E-01	-10.070	10.065	0.050
0.0025	25	20	132183	121845	104120	36.84	23.1	6.44E-01	-25.814	25.802	0.046
0.0025	30	20	159535	138313	104120	38.30	26.1	7.51E-01	-53.567	53.543	0.045
0.0025	70	20	370907	247593	104120	46.22	45.8	1.53E+00	-318.030	317.910	0.038
0.0025	52	50	276601	271955	266060	44.08	51.1	1.47E+00	-11.489	11.485	0.035
0.0025	60	50	318608	295111	266060	44.72	55.5	1.64E+00	-58.491	58.471	0.034
0.0025	100	50	527358	405344	266060	46.70	76.3	2.49E+00	-309.197	309.097	0.032

Table 16: Data for 2MPa Aluminum Heat Exchanger

flow	Inlet	Cryotip	In-enthalpy	out-enthalpy	cryo-enthalpy	effectiveness	Outlet temp	Pressure Drop	Cold tip	net enthalpy	Error
[kg/s]	[K]	[K]	[J/kg]	[J/kg]	[J/kg]	[%]	[K]	[psi]	[W]	[W]	%
0.00045	12	10	48282	41396	34815	51.13	11.0	5.97E-03	-3.076	3.074	0.039
0.00045	15	10	68687	50449	34815	53.84	12.3	7.22E-03	-8.226	8.223	0.036
0.00045	20	10	100438	62194	34815	58.28	14.0	9.16E-03	-17.361	17.354	0.040
0.00045	60	10	320302	104269	34815	75.67	20.4	1.99E-02	-97.940	97.889	0.052
0.00045	22	20	112500	103496	100450	74.72	20.5	1.32E-02	-4.029	4.028	0.025
0.00045	25	20	130094	107511	100450	76.18	21.2	1.42E-02	-10.127	10.122	0.049
0.00045	30	20	158541	113142	100450	78.15	22.1	1.57E-02	-20.399	20.391	0.039
0.00045	70	20	372991	139957	100450	85.50	26.7	2.54E-02	-105.080	105.020	0.057
0.00045	52	50	278006	268689	267350	87.43	50.3	3.87E-02	-4.185	4.184	0.045
0.00045	60	50	320415	273788	267350	87.87	51.2	4.11E-02	-20.956	20.946	0.048
0.00045	100	50	530002	295747	267350	89.19	55.4	5.21E-02	-105.427	105.358	0.065
0.001	12	10	48283	43730	34815	33.81	11.3	2.48E-02	-4.517	4.515	0.044
0.001	15	10	68689	56510	34815	35.95	13.2	3.11E-02	-12.292	12.287	0.041
0.001	20	10	100445	74375	34815	39.72	15.8	4.10E-02	-26.637	26.627	0.038
0.001	60	10	320384	153033	34815	58.60	28.5	1.01E-01	-170.660	170.590	0.041
0.001	22	20	112501	105965	100450	54.24	20.9	5.33E-02	-6.478	6.475	0.046
0.001	25	20	130098	113585	100450	55.70	22.2	5.87E-02	-16.462	16.456	0.036
0.001	30	20	158551	124919	100450	57.89	24.1	6.71E-02	-33.727	33.715	0.036
0.001	70	20	373085	186673	100450	68.37	34.8	1.23E-01	-188.454	188.382	0.038
0.001	52	50	278010	270741	267350	68.19	50.6	1.44E-01	-7.227	7.225	0.028
0.001	60	50	320433	283750	267350	69.10	53.1	1.57E-01	-36.555	36.543	0.033
0.001	100	50	530118	340740	267350	72.07	63.8	2.21E-01	-189.800	189.730	0.037
0.0025	12	10	48281	45591	34815	19.98	11.6	1.41E-01	-6.661	6.657	0.060
0.0025	15	10	68686	61385	34815	21.56	13.9	1.81E-01	-18.430	18.421	0.049
0.0025	20	10	100443	84527	34815	24.25	17.4	2.46E-01	-40.869	40.850	0.046
0.0025	60	10	320409	210433	34815	38.51	38.7	6.61E-01	-286.500	286.370	0.045
0.0025	22	20	112497	108302	100450	34.82	21.3	2.98E-01	-10.369	10.364	0.048
0.0025	25	20	130096	119483	100450	35.80	23.2	3.33E-01	-26.491	26.479	0.045
0.0025	30	20	158552	136871	100450	37.32	26.2	3.90E-01	-54.723	54.699	0.044
0.0025	70	20	373123	249036	100450	45.51	45.9	7.88E-01	-319.950	319.830	0.038
0.0025	52	50	278016	273343	267350	43.81	51.1	7.57E-01	-11.551	11.547	0.035
0.0025	60	50	320445	296841	267350	44.46	55.6	8.45E-01	-17.975	17.945	0.167
0.0025	100	50	527344	405567	267350	46.84	76.3	1.28E+00	-309.630	308.380	0.404

Table 17: Data for 3MPa Aluminum Foam Heat Exchanger

flow	Inlet	Cryotip	In-enthalpy	out-enthalpy	cryo-enthalpy	effectiveness	Outlet temp	Pressure Drop	Cold tip	net enthalpy	Error
[kg/s]	[K]	[K]	[J/kg]	[J/kg]	[J/kg]	[%]	[K]	[psi]	[W]	[W]	%
0.00045	12	10	47628	41294	36236	55.60	10.9	34.023	-2.82	2.82	0.035
0.00045	15	10	66559	49151	36236	57.40	12.2	38.703	-7.81	7.81	0.038
0.00045	20	10	98426	60596	36236	60.82	14	47.097	-17.09	17.08	0.041
0.00045	60	10	322191	103803	36236	76.37	20.7	97.173	-98.94	98.89	0.054
0.00045	22	20	110794	101636	98444	74.15	20.5	64.757	-4.10	4.10	0.049
0.00045	25	20	128880	105879	98444	75.57	21.2	69.603	-10.31	10.31	0.039
0.00045	30	20	158081	111839	98444	77.53	22.2	77.02	-20.77	20.77	0.039
0.00045	70	20	375230	139823	98444	85.05	26.8	122.617	-106.15	106.09	0.057
0.00045	52	50	279517	270121	268750	87.26	50.3	184.596	-4.22	4.22	0.047
0.00045	60	50	322308	275341	268750	87.69	51.2	195.75	-21.11	21.10	0.052
0.00045	100	50	532823	297667	268750	89.04	55.4	247.003	-105.83	105.76	0.066
0.001	12	10	47630	43387	36236	37.23	11.3	136.72	-4.19	4.19	0.048
0.001	15	10	66563	54813	36236	38.74	13.1	160.76	-11.76	11.76	0.051
0.001	20	10	98434	72496	36236	41.70	15.9	204.24	-26.34	26.33	0.042
0.001	60	10	322276	153497	36236	59.00	28.8	484.478	-172.05	171.99	0.035
0.001	22	20	110796	104164	98444	53.69	20.9	258.98	-6.57	6.57	0.030
0.001	25	20	128885	112114	98444	55.09	22.2	284.26	-16.71	16.70	0.042
0.001	30	20	158093	123947	98444	57.24	24.2	323.938	-34.23	34.22	0.038
0.001	70	20	375327	187596	98444	67.80	34.9	587.09	-189.77	189.70	0.037
0.001	52	50	279521	272206	268750	67.91	50.6	684.34	-7.27	7.27	0.028
0.001	60	50	322326	285448	268750	68.83	53.1	745.846	-36.75	36.73	0.033
0.001	100	50	532940	343099	268750	71.85	63.8	1039.68	-190.25	190.18	0.037
0.0025	12	10	47631	45097	36236	22.23	11.6	760.25	-6.24	6.24	0.048
0.0025	15	10	66563	59466	36236	23.40	13.9	916.37	-17.78	17.77	0.056
0.0025	20	10	98435	82534	36236	25.56	17.4	1200.2	-40.59	40.57	0.049
0.0025	60	10	322301	211558	36236	38.71	38.8	3139.08	-288.34	288.20	0.049
0.0025	22	20	110795	106543	98444	34.42	21.3	1433.96	-10.50	10.50	0.048
0.0025	25	20	128885	118122	98444	35.35	23.2	1599.55	-26.84	26.83	0.048
0.0025	30	20	158095	136120	98444	36.83	26.2	1863.65	-55.42	55.40	0.045
0.0025	70	20	375363	250633	98444	45.04	46	3727.49	-321.47	321.35	0.037
0.0025	52	50	279525	274830	268750	43.57	51.1	3578.96	-11.61	11.60	0.034
0.0025	60	50	322336	298358	268750	44.74	55.6	3986.2	-58.97	58.95	0.034
0.0025	100	50	532993	410564	268750	46.33	76.4	5990.77	-310.04	309.93	0.033

Table 18: Data for 4MPa Aluminum Foam Heat Exchanger

Flow	Inlet	Cryotip	In-enthalpy	out-enthalpy	cryo-enthalpy	effectiveness	Outlet temp	Pressure Drop	Cold tip	net enthalpy	Error
[kg/s]	[K]	[K]	[J/kg]	[J/kg]	[J/kg]	[%]	[K]	[psi]	[W]	[W]	%
0.00045	12	10	49603	43636	39393	58.44	10.9	31.418	-2.66	2.65	0.038
0.00045	15	10	66981	50429	39393	60.00	12.2	34.282	-7.40	7.40	0.054
0.00045	20	10	97942	61107	39393	62.91	14	39.99	-16.58	16.57	0.048
0.00045	60	10	324140	104491	39393	77.14	20.9	77.666	-99.41	99.36	0.054
0.00045	22	20	110312	101146	97961	74.21	20.5	52.481	-4.10	4.10	0.049
0.00045	25	20	128555	105447	97961	75.53	21.2	56.107	-10.36	10.35	0.048
0.00045	30	20	158171	111560	97961	77.41	22.2	61.742	-20.93	20.92	0.043
0.00045	70	20	377497	140324	97961	84.85	26.9	96.658	-106.93	106.86	0.065
0.00045	52	50	281130	271666	270260	87.07	50.3	143.4	-4.25	4.25	0.047
0.00045	60	50	324259	276993	270260	87.53	51.3	151.93	-21.24	21.23	0.047
0.00045	100	50	535640	299654	270260	88.92	55.5	190.94	-106.20	106.13	0.066
0.001	12	10	49605	45571	39393	39.50	11.2	123.05	-3.97	3.97	0.050
0.001	15	10	66985	55708	39393	40.87	13.1	138.26	-11.23	11.22	0.045
0.001	20	10	97951	72507	39393	43.45	15.8	168.257	-25.67	25.66	0.043
0.001	60	10	324227	154576	39393	59.56	29	379.48	-172.77	172.71	0.035
0.001	22	20	110314	103674	97961	53.75	20.9	207.27	-6.57	6.57	0.046
0.001	25	20	128561	111716	97961	55.05	22.2	226.11	-16.77	16.76	0.042
0.001	30	20	158183	123800	97961	57.09	24.2	256.11	-34.44	34.42	0.038
0.001	70	20	377596	188848	97961	67.50	35.1	456.65	-190.75	190.67	0.042
0.001	52	50	281134	273780	270260	67.63	50.7	529.13	-7.31	7.31	0.030
0.001	60	50	324278	287228	270260	68.59	53.2	575.92	-36.91	36.90	0.033
0.001	100	50	535759	345488	270260	71.67	63.9	798.64	-190.65	190.59	0.031
0.0025	12	10	49607	47181	39393	23.75	11.6	672.125	-5.96	5.96	0.067
0.0025	15	10	66988	60129	39393	24.86	13.8	772.64	-17.07	17.06	0.053
0.0025	20	10	97954	82275	39393	26.77	17.4	969.63	-39.76	39.74	0.053
0.0025	60	10	324252	212979	39393	39.06	38.9	2430.38	-289.38	289.25	0.045
0.0025	22	20	110315	106055	97961	34.48	21.3	1137.53	-10.51	10.50	0.057
0.0025	25	20	128563	117749	97961	35.34	23.2	1260.61	-26.93	26.92	0.048
0.0025	30	20	158186	136062	97961	36.74	26.2	1459.6	-55.72	55.70	0.047
0.0025	70	20	377633	252383	97961	44.78	46.1	2874.17	-322.60	322.48	0.038
0.0025	52	50	281138	276422	270260	43.35	51.1	2757.3	-11.65	11.65	0.034
0.0025	60	50	324287	300501	270260	44.03	55.6	3066.05	-59.17	59.15	0.035
0.0025	100	50	535810	413192	270260	46.18	76.4	4580.46	-310.41	310.31	0.032

APPENDIX C

Data for Copper Foam Heat Exchanger

Table 19: Data for 1MPa Copper Foam Heat Exchanger

flow	Inlet	Cryotip	In-enthalpy	out-enthalpy	cryo-enthalpy	effectiveness	Outlet temp	Pressure Drop	Cold tip	net enthalpy	Error
[kg/s]	[K]	[K]	[J/kg]	[J/kg]	[J/kg]	[%]	[K]	[psi]	[W]	[W]	%
0.00045	12	10	54997	41643	40357	91.22	10.2	63	-6.01	6.01	0.018
0.00045	15	10	74490	43171	40357	91.76	10.4	68	-14.39	14.39	0.019
0.00045	20	10	104101	45238	40357	92.34	10.6	75	-26.50	26.50	0.024
0.00045	60	10	318459	56330	40357	94.26	12.2	109	-118.09	118.04	0.043
0.00045	22	20	115466	104374	104120	97.76	20.0	164	-4.99	4.99	0.030
0.00045	30	20	159531	105369	104120	97.75	20.2	170	-24.38	24.37	0.034
0.00045	70	20	370772	110035	104120	97.78	21.0	195	-117.39	117.34	0.050
0.00045	52	50	276587	266388	266060	96.88	50.1	51	-4.59	4.59	0.041
0.00045	60	50	318571	267688	266060	96.90	50.3	52	-22.91	22.90	0.045
0.00045	100	50	527166	274182	266060	96.89	51.5	57	-113.91	113.84	0.062
0.001	12	10	54996	43396	40357	79.24	10.4	280	-11.60	11.60	0.017
0.001	15	10	74490	46700	40357	81.42	10.8	316	-27.82	27.82	0.015
0.001	20	10	104106	50841	40357	83.55	11.4	363	-53.35	53.34	0.017
0.001	60	10	318543	70566	40357	89.14	14.3	597	-248.47	248.42	0.023
0.001	22	20	115466	104744	104120	94.50	20.1	669	-10.72	10.72	0.019
0.001	25	20	132193	105662	104120	94.51	20.3	686	-26.53	26.53	0.019
0.001	30	20	159540	107151	104120	94.53	20.5	712	-52.40	52.39	0.021
0.001	70	20	370868	118265	104120	94.70	22.5	915	-252.75	252.68	0.027
0.001	52	50	276592	266872	266060	92.29	50.2	1899	-9.72	9.72	0.023
0.001	60	50	318591	270121	266060	92.27	50.8	1965	-48.48	48.46	0.023
0.001	100	50	527289	286861	266060	92.04	53.9	2330	-240.55	240.49	0.028
0.0025	12	10	54981	46725	40357	56.46	10.8	1704	-20.69	20.69	0.013
0.0025	15	10	74479	53539	40357	61.37	11.8	2048	-52.60	52.59	0.013
0.0025	20	10	104100	61724	40357	66.48	13.0	2489	-106.52	106.51	0.013
0.0025	60	10	318570	99205	40357	78.85	19.0	4902	-550.90	550.81	0.017
0.0025	22	20	115455	105893	104120	84.36	20.3	3791	-23.91	23.90	0.017
0.0025	25	20	132186	108483	104120	84.45	20.8	3982	-59.27	59.26	0.015
0.0025	30	20	159538	112645	104120	84.62	21.5	4289	-117.30	117.28	0.015
0.0025	70	20	370908	144071	104120	85.03	27.1	6756	-568.52	568.42	0.017
0.0025	52	50	276601	268339	266060	78.38	50.4	9995	-20.65	20.64	0.015
0.0025	60	50	318608	277589	266060	78.06	52.2	10669	-102.57	102.55	0.017
0.0025	100	50	527356	330008	266060	75.53	62.1	14531	-495.16	495.07	0.017

Table 20: Data for 2MPa Copper Foam Heat Exchanger

flow	Inlet	Cryotip	In-enthalpy	out-enthalpy	cryo-enthalpy	effectiveness	Outlet temp	Pressure Drop	Cold tip	net enthalpy	Error
		[K]	[J/kg]	[J/kg]	[J/kg]	[%]	[K]	[psi]	[W]	[W]	%
0.00045	12	10	48282	35781	34815	92.83	10.1	37	-5.63	5.62	0.021
0.00045	15	10	68687	37158	34815	93.08	10.4	39	-14.19	14.19	0.021
0.00045	20	10	100438	39149	34815	93.40	10.7	42	-27.59	27.58	0.025
0.00045	60	10	320298	50233	34815	94.60	12.3	59	-121.65	121.60	0.044
0.00045	22	20	112500	100748	100450	97.53	20.0	87	-5.29	5.29	0.030
0.00045	25	20	130094	101174	100450	97.56	20.1	88	-13.02	13.01	0.031
0.00045	30	20	158541	101860	100450	97.57	20.2	89	-25.51	25.51	0.035
0.00045	70	20	372990	106908	100450	97.63	21.1	103	-119.80	119.74	0.050
0.00045	52	50	278005	267686	267350	96.85	50.1	264	-4.65	4.64	0.043
0.00045	60	50	320414	269018	267350	96.86	50.3	269	-23.14	23.13	0.045
0.00045	100	50	529994	275631	267350	96.85	51.6	293	-114.53	114.46	0.063
0.001	12	10	48283	37205	34815	82.25	10.4	156	-11.08	11.08	0.018
0.001	15	10	68690	40403	34815	83.50	10.8	172	-28.30	28.30	0.018
0.001	20	10	100446	44708	34815	84.93	11.5	195	-55.80	55.79	0.016
0.001	60	10	320385	65521	34815	89.25	14.5	315	-255.37	255.31	0.023
0.001	22	20	112501	101170	100450	94.03	20.1	348	-11.33	11.33	0.018
0.001	25	20	130099	102207	100450	94.07	20.3	357	-27.90	27.89	0.022
0.001	30	20	158552	103864	100450	94.12	20.6	371	-54.70	54.69	0.022
0.001	70	20	373088	115845	100450	94.35	22.6	478	-257.39	257.33	0.027
0.001	52	50	278010	268183	267350	92.19	50.2	981	-9.83	9.82	0.020
0.001	60	50	320433	271513	267350	92.16	50.8	1014	-48.93	48.91	0.022
0.001	100	50	530118	288558	267350	91.93	54.0	1200	-241.68	241.62	0.029
0.0025	12	10	48282	40225	34815	59.83	10.8	915	-20.16	20.15	0.015
0.0025	15	10	68688	47265	34815	63.25	11.8	1075	-53.74	53.74	0.011
0.0025	20	10	100446	56244	34815	67.35	13.1	1301	-111.06	111.04	0.014
0.0025	60	10	320413	96573	34815	78.38	19.2	2559	-562.35	562.26	0.016
0.0025	22	20	112498	102476	100450	83.18	20.3	1958	-25.05	25.05	0.012
0.0025	25	20	130098	105382	100450	83.36	20.8	2062	-61.80	61.80	0.015
0.0025	30	20	158554	109978	100450	83.60	21.6	2227	-121.52	121.50	0.015
0.0025	70	20	373128	143364	100450	84.26	27.2	3513	-575.93	575.84	0.016
0.0025	52	50	278016	269685	267350	78.11	50.4	5155	-20.82	20.82	0.014
0.0025	60	50	320445	279141	267350	77.79	52.2	5501	-103.28	103.26	0.019
0.0025	100	50	530177	332292	267350	75.29	62.1	7470	-496.48	496.40	0.017

Table 21: Data for 3MPa Copper Foam Heat Exchanger

flow	Inlet	Cryotip	In-enthalpy	out-enthalpy	cryo-enthalpy	effectiveness	Outlet temp	Pressure Drop	Cold tip	net enthalpy	Error
		[K]	[J/kg]	[J/kg]	[J/kg]	[%]	[K]	[psi]	[W]	[W]	%
0.00045	12	10	47628	36890	36236	94.26	10.1	32	-4.83	4.83	0.029
0.00045	15	10	66559	37933	36236	94.40	10.3	33	-12.88	12.88	0.031
0.00045	20	10	98426	39595	36236	94.60	10.6	35	-26.48	26.47	0.026
0.00045	60	10	322188	49491	36236	95.36	12.3	45	-122.80	122.75	0.044
0.00045	22	20	110794	98752	98444	97.51	20.0	62	-5.42	5.42	0.030
0.00045	25	20	128881	99201	98444	97.51	20.1	63	-13.36	13.36	0.030
0.00045	30	20	158082	99924	98444	97.52	20.2	64	-26.18	26.17	0.034
0.00045	70	20	375230	105175	98444	97.57	21.1	73	-121.59	121.53	0.050
0.00045	52	50	279517	269090	268750	96.84	50.1	183	-4.69	4.69	0.043
0.00045	60	50	322307	270451	268750	96.82	50.3	186	-23.34	23.33	0.047
0.00045	100	50	532815	277173	268750	96.81	51.6	202	-115.11	115.04	0.063
0.001	12	10	47630	37884	36236	85.54	10.3	129	-9.74	9.74	0.021
0.001	15	10	66563	40388	36236	86.31	10.8	137	-26.18	26.17	0.019
0.001	20	10	98435	44171	36236	87.24	11.4	150	-54.29	54.28	0.018
0.001	60	10	322278	64054	36236	90.27	14.6	227	-258.61	258.55	0.023
0.001	22	20	110796	99197	98444	93.90	20.1	246	-11.60	11.60	0.017
0.001	25	20	128886	100291	98444	93.93	20.3	252	-28.60	28.59	0.021
0.001	30	20	158094	102040	98444	93.97	20.6	262	-56.06	56.05	0.021
0.001	70	20	375330	114538	98444	94.19	22.6	335	-260.95	260.88	0.027
0.001	52	50	279521	269600	268750	92.11	50.2	674	-9.92	9.92	0.022
0.001	60	50	322326	273002	268750	92.06	50.8	697	-49.33	49.32	0.024
0.001	100	50	532941	290327	268750	91.83	54.0	823	-242.74	242.67	0.029
0.0025	12	10	47631	40250	36236	64.77	10.7	728	-18.45	18.45	0.016
0.0025	15	10	66564	46165	36236	67.26	11.7	813	-51.07	51.07	0.014
0.0025	20	10	98437	54669	36236	70.37	13.1	951	-109.75	109.74	0.009
0.0025	60	10	322306	95606	36236	79.25	19.4	1794	-569.33	569.24	0.016
0.0025	22	20	110796	100571	98444	82.78	20.3	1369	-25.56	25.56	0.016
0.0025	25	20	128887	103640	98444	82.93	20.8	1441	-63.13	63.12	0.014
0.0025	30	20	158098	108495	98444	83.15	21.6	1554	-124.08	124.07	0.008
0.0025	70	20	375370	143266	98444	83.81	27.4	2433	-581.83	581.73	0.016
0.0025	52	50	279526	271132	268750	77.90	50.4	3534	-20.98	20.97	0.014
0.0025	60	50	322337	280776	268750	77.56	52.2	3768	-103.92	103.90	0.019
0.0025	100	50	532997	334610	268750	75.08	62.2	5096	-497.73	497.64	0.017

Table 22: Data for 4MPa Copper Foam Heat Exchanger

flow	Inlet	Cryotip	In-enthalpy	out-enthalpy	cryo-enthalpy	effectiveness	Outlet temp	Pressure Drop	Cold tip	net enthalpy	Error
		[K]	[J/kg]	[J/kg]	[J/kg]	[%]	[K]	[psi]	[W]	[W]	%
0.00045	12	10	49602	39910	39393	94.94	10.1	30	-4.36	4.36	0.023
0.00045	15	10	66981	40759	39393	95.05	10.3	31	-11.80	11.80	0.034
0.00045	20	10	97942	42199	39393	95.21	10.6	32	-25.09	25.08	0.028
0.00045	60	10	324137	51233	39393	95.84	12.3	39	-122.88	122.82	0.046
0.00045	22	20	110312	98268	97961	97.51	20.0	50	-5.42	5.42	0.031
0.00045	25	20	128556	98719	97961	97.52	20.1	51	-13.43	13.43	0.030
0.00045	30	20	158171	99449	97961	97.53	20.2	52	-26.43	26.42	0.034
0.00045	70	20	377498	104756	97961	97.57	21.1	59	-122.80	122.74	0.051
0.00045	52	50	281130	270611	270260	96.77	50.1	142	-4.74	4.73	0.042
0.00045	60	50	324258	271997	270260	96.78	50.3	144	-23.53	23.52	0.047
0.00045	100	50	535633	278817	270260	96.78	51.6	157	-115.64	115.57	0.064
0.001	12	10	49605	40700	39393	87.20	10.3	118	-8.90	8.90	0.011
0.001	15	10	66986	42750	39393	87.83	10.7	123	-24.24	24.23	0.021
0.001	20	10	97952	46067	39393	88.60	11.3	131	-51.90	51.89	0.019
0.001	60	10	324229	64788	39393	91.08	14.6	186	-259.72	259.66	0.023
0.001	22	20	110314	98710	97961	93.94	20.1	197	-11.61	11.60	0.017
0.001	25	20	128562	99811	97961	93.95	20.3	202	-28.75	28.75	0.021
0.001	30	20	158184	101584	97961	93.98	20.6	209	-56.61	56.60	0.021
0.001	70	20	377600	114291	97961	94.16	22.6	265	-263.46	263.39	0.027
0.001	52	50	281134	271131	270260	91.99	50.2	522	-10.00	10.00	0.030
0.001	60	50	324278	274598	270260	91.97	50.8	539	-49.69	49.67	0.024
0.001	100	50	535760	292176	270260	91.75	54.0	635	-243.71	243.64	0.029
0.0025	12	10	49607	42689	39393	67.73	10.7	650	-17.28	17.28	0.017
0.0025	15	10	66988	47688	39393	69.94	11.6	703	-48.27	48.27	0.015
0.0025	20	10	97956	55426	39393	72.62	13.0	795	-106.51	106.50	0.009
0.0025	60	10	324258	95913	39393	80.16	19.5	1419	-573.11	573.01	0.017
0.0025	22	20	110315	100081	97961	82.84	20.3	1090	-25.58	25.58	0.016
0.0025	25	20	128564	103180	97961	82.95	20.8	1143	-63.47	63.46	0.014
0.0025	30	20	158189	108131	97961	83.11	21.6	1228	-125.22	125.20	0.016
0.0025	70	20	377640	143754	97961	83.63	27.5	1897	-586.27	586.17	0.017
0.0025	52	50	281139	272691	270260	77.65	50.4	2723	-21.11	21.11	0.019
0.0025	60	50	324288	282502	270260	77.34	52.3	2902	-104.48	104.46	0.019
0.0025	100	50	535814	336963	270260	74.88	62.2	3907	-498.88	498.80	0.016

APPENDIX D

Data for Helical Heat Exchanger

Table 23: Data for 1MPa Helical Heat Exchanger

flow	Inlet	Cryotip	In-enthalpy	out-enthalpy	cryo-enthalpy	effectiveness	Outlet temp	pressure drop	Cold tip	net enthalpy	Error
[kg/s]	[K]	[K]	[J/kg]	[J/kg]	[J/kg]	[%]	[K]	[psi]	[W]	[W]	[%]
0.0009	12	10	54996	47754	40357	49.47	11.0	4.51E-05	-6.279	6.275	0.0653
0.0009	15	10	74486	57211	40357	50.62	12.4	4.95E-05	-14.986	14.976	0.0647
0.0009	20	10	104080	72133	40357	50.13	14.8	6.22E-05	-28.053	28.023	0.1059
0.0009	60	10	318410	158740	40357	57.42	30.5	1.06E-04	-141.040	140.870	0.1205
0.0009	22	20	115460	109130	104120	55.82	20.9	1.21E-04	-5.578	5.572	0.1076
0.0009	25	20	132180	116370	104120	56.34	13.9	1.25E-04	-13.933	13.918	0.1077
0.0009	30	20	159520	127840	104120	57.18	24.3	1.32E-04	-27.910	27.879	0.1111
0.0009	70	20	370740	206500	104120	61.60	39.4	1.71E-04	-144.960	144.780	0.1242
0.0009	52	50	276580	270050	266060	62.07	50.8	3.36E-04	-5.768	5.761	0.1144
0.0009	60	50	318560	285610	266060	62.76	53.8	3.46E-04	-29.114	29.081	0.1133
0.0009	100	50	527120	356400	266060	65.39	67.8	3.86E-04	-150.960	150.760	0.1325
0.002	12	10	54994	49143	40357	39.97	11.2	2.14E-04	-11.366	11.354	0.1056
0.002	15	10	74483	60498	40357	40.98	12.9	2.44E-04	-27.154	27.126	0.1031
0.002	20	10	103090	77012	40357	41.57	15.5	2.89E-04	-52.594	52.540	0.1027
0.002	60	10	318448	181410	40357	49.28	34.7	5.48E-04	-237.737	237.438	0.1258
0.002	22	20	115465	110038	104120	47.84	21.1	5.23E-04	-10.582	10.571	0.1030
0.002	25	20	132185	118620	104120	48.33	22.6	5.45E-04	-26.446	26.418	0.1059
0.002	30	20	159522	132319	104120	49.10	25.2	5.81E-04	-53.022	52.964	0.1081
0.002	70	20	370777	228759	104120	53.26	43.6	8.13E-04	-277.298	276.984	0.1132
0.002	52	50	276585	271016	266060	52.91	51.0	1.43E-03	-10.889	10.877	0.1102
0.002	60	50	318568	290427	266060	53.59	54.8	1.48E-03	-55.023	54.962	0.1109
0.002	100	50	527194	380659	266060	56.11	72.5	1.73E-03	-286.535	286.209	0.1138
0.005	12	10	54995	50295	40357	32.11	11.4	1.21E-03	-22.697	22.673	0.1031
0.005	15	10	74485	63230	40357	32.98	13.3	1.42E-03	-54.329	54.273	0.1038
0.005	20	10	104093	82227	40357	34.31	16.4	1.73E-03	-105.610	105.499	0.1051
0.005	60	10	318475	205954	40357	40.46	39.3	3.66E-03	-54.648	54.589	0.1080
0.005	22	20	115465	110977	104120	39.56	21.2	2.88E-03	-21.766	21.742	0.1070
0.005	25	20	132187	120968	104120	39.97	23.0	3.04E-03	-54.392	54.333	0.1076
0.005	30	20	159526	137019	104120	40.62	26.0	3.29E-03	-109.084	108.966	0.1082
0.005	70	20	370802	252902	104120	44.21	48.2	5.03E-03	-572.504	571.877	0.1095
0.005	52	50	276583	272048	266060	43.10	51.2	7.70E-03	-22.055	22.031	0.1088
0.005	60	50	318570	295642	266060	43.66	55.7	8.11E-03	-111.476	111.355	0.1078
0.005	100	50	527219	407747	266060	45.75	77.7	9.99E-03	-580.721	580.089	0.1088

Table 24: Data for 2MPa Helical Heat Exchanger

flow	Inlet	Cryotip	In-enthalpy	out-enthalpy	cryo-enthalpy	effectiveness	Outlet temp	pressure drop	Cold tip	net enthalpy	Error
		[K]	[J/kg]	[J/kg]	[J/kg]	[%]	[K]	[psi]	[W]	[W]	[%]
0.0009	12	10	48278	41217	34815	52.45	11.0	2.70E-05	-6.210	6.204	0.1031
0.0009	15	10	68677	50999	34815	52.21	12.5	2.89E-05	-15.532	15.516	0.1024
0.0009	20	10	100419	66036	34815	52.41	14.7	3.23E-05	-30.195	30.163	0.1043
0.0009	60	10	320255	156674	34815	57.31	30.3	5.55E-05	-144.453	144.284	0.1170
0.0009	22	20	112497	105768	100450	55.86	20.9	6.28E-05	-5.929	5.922	0.1080
0.0009	25	20	130087	113386	100450	56.35	22.2	6.49E-05	-14.715	14.699	0.1087
0.0009	30	20	158527	125366	100450	57.10	24.3	6.83E-05	-29.216	29.184	0.1102
0.0009	70	20	372960	205957	100450	61.28	39.2	8.89E-05	-147.385	147.209	0.1194
0.0009	52	50	278003	271369	267350	62.27	50.8	1.73E-04	-5.861	5.854	0.1143
0.0009	60	50	320405	287012	267350	62.94	53.8	1.78E-04	-29.508	29.474	0.1159
0.0009	100	50	529950	358050	267350	65.46	67.7	1.98E-04	-1.520	1.518	0.1329
0.002	12	10	48279	42306	34815	44.36	11.2	1.18E-04	-11.626	11.614	0.1024
0.002	15	10	68679	53733	34815	44.14	12.9	1.29E-04	-29.049	29.019	0.1033
0.002	20	10	100426	71353	34815	44.31	15.5	1.49E-04	-56.476	56.418	0.1027
0.002	60	10	320291	180306	34815	49.04	34.6	2.85E-04	-273.431	273.128	0.1108
0.002	22	20	112498	106736	100450	47.83	21.1	2.71E-04	-11.238	11.226	0.1068
0.002	25	20	130089	115782	100450	48.27	22.6	2.83E-04	-27.898	27.868	0.1065
0.002	30	20	158533	130100	100450	48.95	25.1	3.01E-04	-55.422	55.363	0.1070
0.002	70	20	372998	228821	100450	52.90	43.5	3.23E-03	-281.493	281.177	0.1125
0.002	52	50	278004	272347	267350	53.10	51.0	7.34E-04	-11.062	11.050	0.1094
0.002	60	50	320412	291903	267350	53.73	54.7	7.62E-04	-55.747	55.685	0.1098
0.002	100	50	530026	382553	267350	56.14	72.4	8.84E-04	-288.387	288.059	0.1136
0.005	12	10	48281	43484	34815	35.62	11.3	6.59E-04	-23.206	23.181	0.1043
0.005	15	10	68682	56684	34815	35.43	13.3	7.43E-04	-57.963	57.903	0.1035
0.005	20	10	100431	77062	34815	35.61	16.4	8.93E-04	-112.874	112.758	0.1028
0.005	60	10	320321	205731	34815	40.14	39.2	1.90E-04	-556.401	555.801	0.1078
0.005	22	20	112499	107744	100450	39.46	21.2	1.49E-03	-23.065	23.040	0.1067
0.005	25	20	130092	118286	100450	39.83	23.0	1.57E-03	-57.244	57.183	0.1066
0.005	30	20	158538	135070	100450	40.40	26.0	1.70E-03	-113.744	113.622	0.1073
0.005	70	20	373028	253558	100450	43.83	48.1	2.60E-03	-580.074	579.442	0.1090
0.005	52	50	278005	273400	267350	43.22	51.2	3.96E-03	-22.392	22.368	0.1072
0.005	60	50	320417	297207	267350	43.74	55.7	4.16E-03	-112.856	112.735	0.1072
0.005	100	50	530060	409908	267350	45.74	77.7	5.11E-03	-584.044	583.410	0.1086

Table 25: Data for 3MPa Helical Heat Exchanger

flow	Inlet	Cryotip	In-enthalpy	out-enthalpy	cryo-enthalpy	effectiveness	Outlet temp	pressure drop	Cold tip	net enthalpy	Error
		[K]	[J/kg]	[J/kg]	[J/kg]	[%]	[K]	[psi]	[W]	[W]	[%]
0.0009	12	10	47625	41022	36236	57.98	10.9	2.24E-05	-5.820	5.814	0.1100
0.0009	15	10	66549	49178	36236	57.31	12.3	2.30E-05	-15.293	15.277	0.1066
0.0009	20	10	98408	63282	36236	56.50	14.6	2.44E-05	-30.881	30.848	0.1056
0.0009	60	10	322146	155080	36236	58.43	30.1	3.88E-05	-147.495	147.323	0.1166
0.0009	22	20	110791	103820	98444	56.46	20.9	4.42E-05	-6.144	6.138	0.1074
0.0009	25	20	128873	111569	98444	56.87	22.2	4.56E-05	-15.250	15.234	0.1082
0.0009	30	20	158068	123786	98444	57.50	24.3	4.78E-05	-30.211	30.177	0.1096
0.0009	70	20	375201	205553	98444	61.30	39.1	6.16E-05	-149.716	149.538	0.1189
0.0009	52	50	278514	272779	268750	58.74	50.8	1.19E-04	-5.951	5.944	0.1143
0.0009	60	50	322298	288466	268750	63.18	53.8	1.22E-04	-29.899	29.864	0.1161
0.0009	100	50	532772	359640	268750	65.57	67.6	1.36E-04	-153.116	152.911	0.1339
0.002	12	10	47626	42027	36236	49.16	11.1	9.97E-05	-10.920	10.908	0.1071
0.002	15	10	66552	51824	36236	48.58	12.7	1.01E-04	-28.681	28.651	0.1049
0.002	20	10	98414	68669	36236	47.84	15.5	1.11E-04	-57.835	57.775	0.1036
0.002	60	10	322183	179500	36236	49.90	34.4	1.99E-04	-278.638	278.331	0.1102
0.002	22	20	110792	104825	98444	48.32	21.1	1.90E-04	-11.642	11.630	0.1057
0.002	25	20	128876	114060	98444	48.69	22.6	1.98E-04	-288.964	288.657	0.1062
0.002	30	20	158074	128703	98444	49.26	25.1	2.10E-04	-57.265	57.203	0.1067
0.002	70	20	375240	228969	98444	52.84	43.4	2.92E-04	-285.571	285.251	0.1121
0.002	52	50	279515	273773	268750	53.34	51.0	5.03E-04	-11.230	11.218	0.1095
0.002	60	50	322305	293431	268750	53.91	54.7	5.22E-04	-56.467	56.405	0.1100
0.002	100	50	532850	384393	268750	56.21	72.4	6.04E-04	-290.329	289.999	0.1137
0.005	12	10	47627	43118	36236	39.58	11.3	5.35E-04	-21.862	21.838	0.1075
0.005	15	10	66555	54701	36236	39.10	13.2	5.73E-04	-57.371	57.311	0.1051
0.005	20	10	98419	74500	36236	38.47	16.4	6.52E-04	-115.619	115.499	0.1038
0.005	60	10	322214	205694	36236	40.74	39.1	1.32E-03	-565.663	565.055	0.1075
0.005	22	20	110793	105876	98444	39.82	21.2	1.04E-03	-23.860	23.835	0.1060
0.005	25	20	128879	116671	98444	40.11	23.0	1.10E-03	-59.208	59.145	0.1062
0.005	30	20	158080	133876	98444	40.59	26.0	1.19E-03	-117.336	117.211	0.1065
0.005	70	20	375272	254266	98444	43.71	48.0	1.80E-03	-587.503	586.866	0.1084
0.005	52	50	279517	274846	268750	43.38	51.2	2.71E-03	-22.716	22.692	0.1079
0.005	60	50	322311	298822	268750	43.85	55.7	2.85E-03	-114.223	114.101	0.1068
0.005	100	50	532886	412025	268750	45.76	77.6	3.49E-03	-587.521	586.884	0.1084

Table 26: Data for 4MPa Helical Heat Exchanger

flow	Inlet	Cryotip	In-enthalpy	out-enthalpy	cryo-enthalpy	effectiveness	Outlet temp	pressure drop	Cold tip	net enthalpy	Error
		[K]	[J/kg]	[J/kg]	[J/kg]	[%]	[K]	[psi]	[W]	[W]	[%]
0.0009	12	10	49599	43320	39393	61.52	10.8	2.06E-05	-5.543	5.537	0.1137
0.0009	15	10	66972	50166	39393	60.94	12.2	2.07E-05	-14.821	14.805	0.1080
0.0009	20	10	97924	62892	39393	59.85	14.4	2.12E-05	-30.843	30.810	0.1080
0.0009	60	10	324096	154108	39393	59.71	29.9	3.09E-05	-150.034	149.860	0.1160
0.0009	22	20	110309	103218	97961	57.43	20.9	3.54E-05	-6.252	6.245	0.1088
0.0009	25	20	128548	110892	97961	57.72	22.2	3.64E-05	-15.566	15.549	0.1092
0.0009	30	20	158158	123113	97961	58.22	24.2	3.79E-05	-30.892	30.859	0.1065
0.0009	70	20	377469	205439	97961	61.55	38.9	4.81E-05	-151.819	151.639	0.1186
0.0009	52	50	281128	274299	270260	62.84	50.8	9.16E-05	-6.034	6.027	0.1148
0.0009	60	50	324250	290008	270260	63.42	53.8	9.41E-05	-30.265	30.230	0.1160
0.0009	100	50	535589	361240	270260	65.71	67.5	1.04E-04	-154.204	153.997	0.1342
0.002	12	10	49601	44268	39393	52.24	11.0	8.84E-05	-10.417	10.405	0.1104
0.002	15	10	66975	52697	39393	51.77	12.6	9.02E-05	-27.853	27.822	0.1081
0.002	20	10	97931	68206	39393	50.78	15.3	9.50E-05	-57.871	57.810	0.1052
0.002	60	10	324133	179130	39393	50.92	34.3	1.57E-04	-283.107	282.797	0.1095
0.002	22	20	110310	104242	97961	49.14	21.0	1.52E-04	-118.442	118.317	0.1055
0.002	25	20	128551	113437	97961	49.41	22.6	1.57E-04	-29.490	29.459	0.1051
0.002	30	20	158164	128148	97961	49.86	25.1	1.66E-04	-58.539	58.477	0.1059
0.002	70	20	377510	229324	97961	53.01	43.2	2.27E-04	-289.304	288.981	0.1116
0.002	52	50	281129	275308	270260	53.56	51.0	3.88E-04	-113.846	113.721	0.1098
0.002	60	50	324258	295041	270260	54.11	54.7	4.02E-04	-57.142	57.079	0.1103
0.002	100	50	535670	386237	270260	56.30	72.3	4.64E-04	-292.259	291.928	0.1133
0.005	12	10	49602	45300	39393	42.14	11.2	4.84E-04	-20.887	20.864	0.1101
0.005	15	10	66978	55462	39393	41.75	13.1	5.04E-04	-55.829	55.769	0.1075
0.005	20	10	97937	73995	39393	40.90	16.3	5.50E-04	-115.854	115.732	0.1053
0.005	60	10	324166	205949	39393	41.51	39.0	1.03E-03	-573.805	573.191	0.1070
0.005	22	20	110311	105315	97961	40.45	21.2	8.32E-04	-24.253	24.227	0.1072
0.005	25	20	128554	116111	97961	40.67	23.0	8.71E-04	-60.374	60.310	0.1061
0.005	30	20	158170	133457	97961	41.05	25.9	9.34E-04	-119.837	119.710	0.1060
0.005	70	20	377543	255117	97961	43.79	47.9	1.39E-03	-594.382	593.739	0.1082
0.005	52	50	281130	276400	270260	43.51	51.2	2.09E-03	-23.013	22.988	0.1078
0.005	60	50	324264	300514	270260	43.98	55.7	2.19E-03	-115.505	115.381	0.1074
0.005	100	50	535706	414139	270260	45.80	77.5	2.67E-03	-590.988	590.347	0.1085

APPENDIX E

Heat Exchanger Mass Calculations

E.1 Mass and Volume of Foam Heat Exchangers

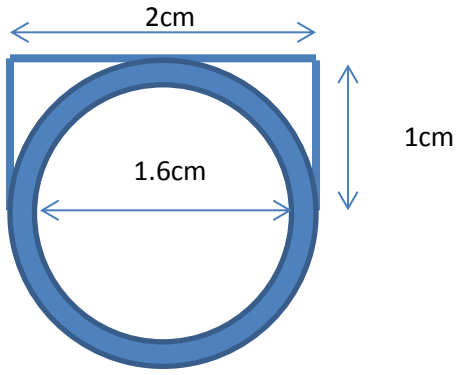

Figure 58: Dimensions of Foam HX Systems

E.1.1 Pipe Volume

$$V_{pipe} = \pi l(R^2 - r^2)$$
$$l = 8cm$$
$$R = 1cm$$
$$r = 0.8cm$$
$$V_{pipe} = 8\pi\left(1^2 - 0.8^2\right) = 9.048cm^3$$

E.1.2 Foam Volume

$$V_{foam} = \pi r^2 l_{foam}$$
$$r = 0.8cm$$
$$l_{foam} = 3cm$$
$$V_{foam} = 3\pi(0.8^2) = 6.032cm^3$$

E.1.3 Heat Sink Volume

$$V_{heatsink} = lwh - 0.5l\pi R^2$$
$$w = 2cm$$
$$h = 1cm$$
$$l = 3cm$$
$$R = 1cm$$
$$V_{heatsink} = (3)(1)(2) - 0.5(3)(1^2)\pi = 1.288cm^2$$

E.1.4 Copper Foam Heat Exchanger Mass

$$M_{Cu} = (V_{pipe} + V_{heatsink})\rho_{pipe} + V_{foam}\rho_{CuFoam}$$
$$\rho_{pipe} = 8941\,{kg}/{m^3} = 8.941\,{g}/{cm^3}$$
$$\rho_{CuFoam} = (1-\varepsilon)\rho = (1-0.6)8940\,{kg}/{m^3} = 3.576\,{g}/{cm^3}$$
$$M_{Cu} = (9.048 + 1.288)(8.941) + (6.032)(3.576) = 114g$$

E.1.5 Aluminum Foam Heat Exchanger Mass

$$M_{Al} = (V_{pipe} + V_{heatsink})\rho_{pipe} + V_{foam}\rho_{AlFoam}$$
$$\rho_{pipe} = 8941\,{kg}/{m^3} = 8.941\,{g}/{cm^3}$$
$$\rho_{AlFoam} = (1-\varepsilon)\rho = (1-0.6)2700\,{kg}/{m^3} = 1.08\,{g}/{cm^3}$$
$$M_{Al} = (9.048 + 1.288)(8.941) + (6.032)(1.08) = 98.9g$$

E.1.6 PocoFoam Heat Exchanger Mass

$$M_{Poco} = (V_{pipe} + V_{heatsink})\rho_{pipe} + V_{foam}\rho_{PocoFoam}$$

$$\rho_{pipe} = 8941\,{kg}/{m^3} = 8.941\,{g}/{cm^3}$$

$$\rho_{PocoFoam} = 602\,{kg}/{m^3} = 0.602\,{g}/{cm^3}$$

$$M_{Poco} = (9.048 + 1.288)(8.941) + (6.032)(0.602) = 96.0g$$

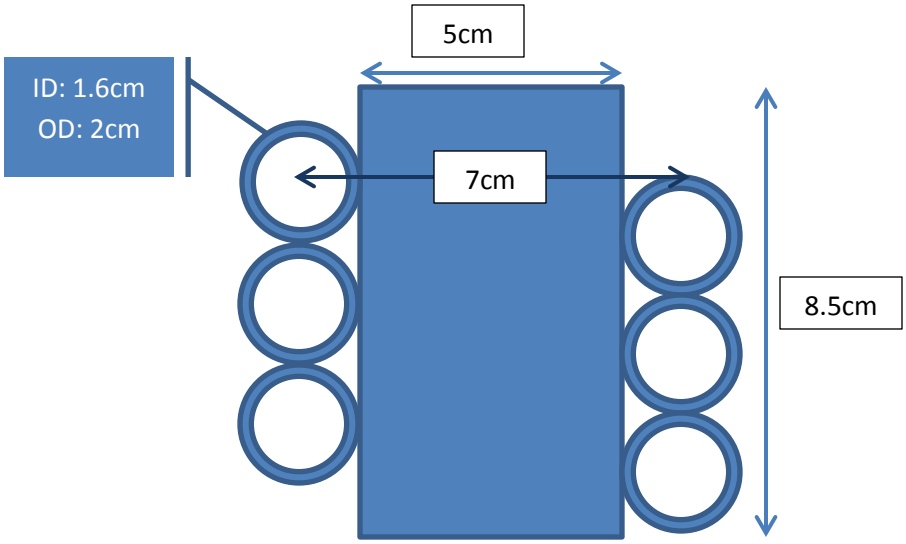

Figure 59: Dimensions of Helical Heat Exchanger

E.2.1 Length of Piping in Helical Heat Exchanger

$l = 2\pi r_1 n$

$r_1 = 3.5cm$

$n = 3turns$

$l = 2\pi(3.5)(3) = 65.97cm$

E.2.2 Volume of Piping in Helical Heat Exchangers

$V_{pipe} = \pi l(R^2 - r^2)$

$R = 1cm$

$r = 0.8cm$

$l = 65.97cm$

$V_{pipe} = \pi(66.97)(1)(0.8) = 165.81cm^3$

E.2.3 Volume of Heat Sink in Helical Heat Exchanger System

$$V_{heatsink} = \pi R_2^2 h$$
$$R_2 = 2.5cm$$
$$h = 8.5cm$$
$$V_{heatsink} = \pi(2.5^2)(8.5) = 166.90cm^3$$

E.2.4 Mass of Helical Heat Exchanger

$$M_{helical} = (V_{pipe} + V_{heatsink})\rho_{pipe}$$
$$\rho_{pipe} = 8941 \, kg/m^3 = 8.941 \, g/cm^3$$
$$M_{helical} = (74.61 + 165.81)(8.941) = 2149g = 2.2kg$$

APPENDIX F

Summary of Cases and Reynolds Number Calculations

Table 27: Summary of cases and Reynolds number calculations for 2MPa, 9 mg/s flow

Inlet Temperature [K]	Cryogenic cooler temperature [K]	Re in open pipe	Re_K for PocoFoam	Re_K for Copper Foam	Re_K for Aluminum Foam
12	10	14820	565	11356	7102
15	10	14504	416	8362	5230
20	10	13304	270	5439	3401
60	10	7707	51	1029	644
22	20	12816	234	4711	2946
25	20	12133	193	3885	2429
30	20	11142	147	2951	1845
70	20	7057	40	810	506
52	50	8349	64	1282	802
55	50	8262	63	1273	796
60	50	7707	51	1029	644
100	50	5720	23	465	291

Table 28: Summary of cases and Reynolds number calculations for 2MPa, 2 g/s flow

Inlet Temperature [K]	Cryogenic cooler temperature [K]	Re in open pipe	Re_K for PocoFoam	Re_K for Copper Foam	Re_K for Aluminum Foam
12	10	32933	565	11356	7102
15	10	32231	416	8362	5230
20	10	29563	270	5439	3401
60	10	17126	51	1029	644
22	20	28480	234	4711	2946
25	20	26962	193	3885	2429
30	20	24760	147	2951	1845
70	20	15683	40	810	506
52	50	18554	64	1282	802
55	50	18359	63	1273	796
60	50	17126	51	1029	644
100	50	12712	23	465	291

Table 29: Summary of cases and Reynolds number calculations for 2MPa, 5 g/s flow

Inlet Temperature [K]	Cryogenic cooler temperature [K]	Re in open pipe	Re_K for PocoFoam	Re_K for Copper Foam	Re_K for Aluminum Foam
12	10	82331	565	11356	7102
15	10	80577	416	8362	5230
20	10	73909	270	5439	3401
60	10	42815	51	1029	644
22	20	71199	234	4711	2946
25	20	67404	193	3885	2429
30	20	61899	147	2951	1845
70	20	39207	40	810	506
52	50	46386	64	1282	802
55	50	45898	63	1273	796
60	50	42815	51	1029	644
100	50	31780	23	465	291

Table 30: Summary of cases and Reynolds number calculations for 3MPa, 9 mg/s flow

Inlet Temperature [K]	Cryogenic cooler temperature [K]	Re in open pipe	Re_K for PocoFoam	Re_K for Copper Foam	Re_K for Aluminum Foam
12	10	12721	633	12725	7958
15	10	12909	516	10372	6486
20	10	12283	359	7227	4520
60	10	7543	74	1479	925
22	20	11941	315	6343	3967
25	20	11424	264	5304	3317
30	20	10618	203	4090	2558
70	20	6931	58	1173	734
52	50	8141	91	1831	1145
55	50	7904	84	1685	1054
60	50	7543	74	1479	925
100	50	5652	34	680	425

Table 31: Summary of cases and Reynolds number calculations for 3MPa, 2 g/s flow

Inlet Temperature [K]	Cryogenic cooler temperature [K]	Re in open pipe	Re_K for PocoFoam	Re_K for Copper Foam	Re_K for Aluminum Foam
12	10	28268	633	12725	7958
15	10	28686	516	10372	6486
20	10	27296	359	7227	4520
60	10	16762	74	1479	925
22	20	26536	315	6343	3967
25	20	25387	264	5304	3317
30	20	23596	203	4090	2558
70	20	15402	58	1173	734
52	50	18092	91	1831	1145
55	50	17563	84	1685	1054
60	50	16762	74	1479	925
100	50	12559	34	680	425

Table 32: Summary of cases and Reynolds number calculations for 3MPa, 5 g/s flow

Inlet Temperature [K]	Cryogenic cooler temperature [K]	Re in open pipe	Re_K for PocoFoam	Re_K for Copper Foam	Re_K for Aluminum Foam
12	10	70670	633	12725	7958
15	10	71714	516	10372	6486
20	10	68239	359	7227	4520
60	10	41905	74	1479	925
22	20	66341	315	6343	3967
25	20	63467	264	5304	3317
30	20	58991	203	4090	2558
70	20	38506	58	1173	734
52	50	45230	91	1831	1145
55	50	43908	84	1685	1054
60	50	41905	74	1479	925
100	50	31398	34	680	425

Table 33: Summary of cases and Reynolds number calculations for 4MPa, 9 mg/s flow

Inlet Temperature [K]	Cryogenic cooler temperature [K]	Re in open pipe	Re_K for PocoFoam	Re_K for Copper Foam	Re_K for Aluminum Foam
12	10	11265	644	12952	8100
15	10	11684	564	11346	7096
20	10	11437	422	8486	5307
60	10	7390	94	1893	1184
22	20	11203	376	7563	4730
25	20	10813	179	3608	2257
30	20	10156	251	5042	3154
70	20	6812	75	1509	944
52	50	7948	116	2330	1457
55	50	7727	107	2148	1343
60	50	7390	94	1893	1184
100	50	5586	44	883	553

Table 34: Summary of cases and Reynolds number calculations for 4MPa, 2 g/s flow

Inlet Temperature [K]	Cryogenic cooler temperature [K]	Re in open pipe	Re_K for PocoFoam	Re_K for Copper Foam	Re_K for Aluminum Foam
12	10	25034	644	12952	8100
15	10	25965	564	11346	7096
20	10	25415	422	8486	5307
60	10	16421	94	1893	1184
22	20	24897	376	7563	4730
25	20	24030	179	3608	2257
30	20	22569	251	5042	3154
70	20	15137	75	1509	944
52	50	17662	116	2330	1457
55	50	17171	107	2148	1343
60	50	16421	94	1893	1184
100	50	12413	44	883	553

Table 35: Summary of cases and Reynolds number calculations for 4MPa, 5 g/s flow

Inlet Temperature [K]	Cryogenic cooler temperature [K]	Re in open pipe	Re_K for PocoFoam	Re_K for Copper Foam	Re_K for Aluminum Foam
12	10	62586	644	12952	8100
15	10	64912	564	11346	7096
20	10	63537	422	8486	5307
60	10	41053	94	1893	1184
22	20	62242	376	7563	4730
25	20	60074	179	3608	2257
30	20	56422	251	5042	3154
70	20	37843	75	1509	944
52	50	44156	116	2330	1457
55	50	42927	107	2148	1343
60	50	41053	94	1893	1184
100	50	31033	44	883	553

REFERENCES

[1] Iris Technology and The Georgia Institute of Technology, SBIR Phase I Proposal for: Lightweight Efficient Cryogenic Gas Heat Exchanger.

[2] Poco Graphite, Inc, "PocoGraphite Thermal Management Material," Poco Graphite, Inc, Decatur, TX, 2008.

[3] R. J. Englar and K. P. Burdges, "Vehicle Heat Exchanger System and Method for a Vehicle That Augments and Modifies Aerodynamic Forces". United States Patent US 6179077 B1, 30 January 2001.

[4] P. T. Garrity, J. F. Klausner and R. Mei, "Performance of Aluminum and Carbon Foams for Air Side Heat Transfer Augmentation," *Journal of Heat Transfer,* vol. 132, pp. 1-9, 2010.

[5] W. Lin, J. Yuan and B. Sunden, "Review on graphite foam as thermal material for heat exchangers," in *Energy End-Use Efficiency Issues*, Linkoping, Sweden, 2011.

[6] M. D. Haskell, "Thermal Resistancce Comparison of Graphite Foam, Aluminum, and Copper Heat Sinks," 2006.

[7] X. Han, C. T'Joen, Q. Wang, A. Sommers, Y. Park and A. Jacobi, "A Review of Metal Foam and Metal Matrix Composites for Heat Exchangers and Heat Sinks," *Heat Transfer Engineering,* pp. 991-1009, 2012.

[8] M. F. Ashby, A. Evans, N. A. Fleck, L. J. Gibson, J. W. Hutchinson and H. N. G. Wadley, Metal foams: a design guide, Boston: Butterworth-Heinemann, 2000.

[9] D. P. Haack, K. R. Butcher, R. Kim and T. J. Lu, "Novel lightweight metal foam heat exchanger," in *Proceedings of 2001 ASME International Mechanical Engineering Congress and Exposition*, New York, 2001.

[10] Z. Dai, K. Nawaz, Y. G. Park, J. Bock and A. M. Jacobi, "Correcting and extending the Boomsma-Poulikakos effective thermal conductivity model for three-dimensional, fluid-saturated metal foams," *International Communications in Heat and Mass Transfer,* vol. 37, no. 6, pp. 575-580, 2010.

[11] S. R. Howard and P. S. Korinko, "Vacuum Furnace Brazing Open Cell Reticulated Foam to Stainless Steel Tubing," in *Proceedings of the 2nd International Brazing and Soldering Conference*, San Diego, 2003.

[12] H. R. Salimi Jazi, J. Mostaghimi, S. Chandra, L. Pershin and L. Coyle, "Spray formed, metal-foam heat exchangers for high temperature applications," *Journal of Thermal Science and Engineering Applications,* vol. 1, pp. 031008-031014, 2009.

[13] A. F. Bastowros and A. G. Evans, "Characterization of open cell aluminum alloy foams as heat sinks for high power electronic devices," in *Proceedings of the ASME Conference on CAE/CAD and thermal management issues in electronic systems*, Dallas, 1997.

[14] K. C. Leong, H. Y. Li, L. W. Jin and J. C. Chai, "Numerical and experiemental study of forced convection in graphite foams of different configurations," *Applied Thermal Engineering,* vol. 30, pp. 520-532, 2010.

[15] N. C. Gallego and J. W. Klett, "Carbon foams for thermal mangement," *Carbon,* vol. 41, pp. 1461-1466, 2003.

[16] Y. L. Jamin and A. A. Mohammad, "Enhanced heat transfer using porous carbon foam in cross flow - Par I: Forced convection," *Journal of Heat Transfer,* vol. 129, pp. 735-742, 2007.

[17] A. Straatman, N. Gallego, B. Thompson and H. Hangan, "Thermal characterization of porous carbon foam - convection in parallel flow," *International Journal of Heat and Mass Transfer,* pp. 1991-1998, 2006.

[18] C. T'Joen, P. De Jaeger, H. Huisseune, S. Van Heerzele, N. Vorst and M. De Paepe, "Thermohydraulic study of a single row heat exchanger, consisting of metal foam covered round tubes," *Internaltional Journal of Heat and Mass Transfer,* vol. 53, pp. 3262-3274, 2010.

[19] E. N. Schmierer and A. Razani, "Self consistend open-celled metal foam model for thermal applications," *Journal of Heat Transfer,* vol. 131, pp. 1194-1203, 2006.

[20] B. Ozma, B. Leyda and B. Benson, "Thermal applications of open-cell metal foams," *Materials and Manufacturing Processes,* vol. 19, pp. 839-862, 2004.

[21] A. Bhattacharya, V. V. Calmidi and R. L. Mahajan, "Thermophysical properties of high porosity metal foams," *Internaltional Journal of Heat and Mass Transfer,* vol. 24, pp. 1017-1031, 2002.

[22] P. Du Plessis, A. Montillet, J. Comiti and J. Legrand, "Pressure drop prediction for flow through high porosity metallic foams," *Chemical Engineering Science,* vol. 57, pp. 3545-3553, 1994.

[23] M. Kaviany, Principles of Heat Transfer in Porous Media, New York: Springer, 1995.

[24] K. Boomsma and D. Poulikakos, "On the effective thermal conductivity of a three dimensionally structured fluid saturated metal foam," *International Journal of Heat and Mass Transfer,* vol. 44, pp. 827-836, 2001.

[25] T. J. Lu, H. A. Stone and M. F. Ashby, "Heat Transfer in Metal Foams," *Acta Meterialia,* vol. 46, pp. 3619-3635, 1998.

[26] I. Ghosh, "Heat Tranfers correlation for high-porosity open cell foam," *International Journal of Heat and Mass Transfer,* vol. 52, pp. 1488-1494, 2009.

[27] Y. W. Kwon, R. E. Cooke and C. Park, "Representative unit cell models for open cell metal foams with or without elastic filler," *Material Science and Engineering,* vol. 343, pp. 63-70, 2002.

[28] R. Singh and H. S. Kasana, "Computational aspects of effective thermal conductivity of highly porous metal foams," *Applied Thermal Engineering,* vol. 24, pp. 1841-1849, 2004.

[29] A. G. Straatman, N. C. Gallego, Q. Yu and B. E. Thompson, "Characterization of Porous Carbon Foam as a Material for Compact Recuperators," *Journal of Engineering for Gas Turbines and Power,* pp. 326-330, 2007.

[30] J. Kuang, T. Kim, M. Xu and T. Lu, "Ultralightweight Compact Heat Sinks With Metal Foams Under Axial Fan Flow Impingement," *Heat Transfer Engineering,* pp. 642-650, 2011.

[31] Y. Lin, J. Du, W. Wu and L. Chow, "Experimental Study on Heat Transfer and Pressure Drop of Recuperative Heat Exchangeers Using Carbon Foam," *Journal of Heat Transfer,* 2010.

[32] J. Song, Q. Guo, Y. Zhong, X. Gao, Z. Feng, Z. Fan, J. Shi and L. Liu, "Thermophysical properties of high-density graphite foams and their paraffin composites," *New Carbon Materials,* pp. 27-34, 2012.

[33] P. Elayiaraja, S. Harish, L. Wilson, A. Bensely and D. M. Lal, "Experimental investigation on pressure drop and heat transfer characteristics of copper metal foam heat sink," *Experimental Heat Transfer,* vol. 23, pp. 185-195, 2010.

[34] A. A. Sertkaya, K. Altinisik and K. Dincer, "Experimental investigation of thermal performance of aluminum finned heat exchangers and open-cell aluminum foam heat exchangers," *Experimental Thermal and Fluid Science,* vol. 36, pp. 86-92, 2012.

[35] J. Klett and B. Conway, "Thermal management solutions utilizing high thermal conductivity graphite foams".

[36] S. Mancin, C. Zilio, A. Diani and L. Rossetto, "Experimental air heat transfer and pressure

drop through copper foams," *Experimental Thermal and Fluid Science,* vol. 36, pp. 224-232, 2012.

[37] W. Lu, C. Y. Zhao and S. A. Tassou, "Thermal analysis on metal-foam filled heat exchangers. Part I: Metal-foam filled pipes," *International Journal of Heat and Mass Transfer,* vol. 49, pp. 2751-2761, 2006.

[38] P. M. Kamath, C. Balaji and S. Venkateshan, "Convection heat transfer from aluminium and copper foams in a vertical channel - An experimental study," *International Journal of Thermal Sciences,* vol. 64, pp. 1-10, 2012.

[39] C. Y. Zhao, W. Lu and S. A. Tassou, "Thermal analysis on metal-foam filled heat exchangers. Part II: Tube heat exchangers," *International Journal of Heat and Mass Transfer,* vol. 49, pp. 2762-2770, 2006.

[40] J. Pacio and C. Dorao, "A review on heat exchanger thermal hycraulic models for cryogenic applications," *Cryogenics,* pp. 366-379, 2011.

[41] T. W. Adams, "Microporouaphite Foam and Process for Producing Same". United States Patent US 2005/0281730 A1, 22 December 2005.

[42] NIST, "NIST," [Online]. Available: http://cryogenics.nist.gov/MPropsMAY/OFHC%20Copper/OFHC_Copper_rev.htm#sh. [Accessed 20 February 2013].

[43] NIST, "Cryogenic Material Properties: 6061-T6 Aluminum UNS A96061," [Online]. Available: http://cryogenics.nist.gov/MPropsMAY/6061%20Aluminum/6061_T6Aluminum_rev.htm. [Accessed 15 November 2013].

[44] ERG Aerospace Corporation, "Physical Characteristics of Duocel Aluminum Foam".

[45] ERG Aerospace Corporation, "Characteristics of Duocel Copper Foam".

[46] ANSYS, Inc., "ANSYS Fluent User's Guide," ANSYS, Inc., Canonsburg, 2012.

[47] ANSYS, Inc., ANSYS Fluent Theory Guide, Canonsburg, PA: ANSYS, Inc., 2012.

[48] D. Poulikakos and K. Boomsma, "The Effects of Compression and Pore Size Variations on the Liquid Flow Characteristics in Metal Foams," *Journal of Fluids Engineering,* vol. 124, no. March 2002, pp. 263-272, 2002.

[49] D. R. Munson and D. F. Young, Fundamentals of Fluid Mechanics, Ames, IA: John Wiley & Sons, Inc., 2002.

[50] NIST, "Thermophysical Properties of Helium," [Online]. Available: http://webbook.nist.gov/cgi/fluid.cgi?ID=C7440597&Action=Page. [Accessed November 2013].

[51] C. R. Fortier, "Modeling of a Porous Metal Foam Cryogenic Counter Flow Heat Exchanger," Clemson University, Clemson, SC, 2010.